POLITECNICO DI TORINO

**Corso di Laurea Magistrale
in Ingegneria Civile**

Tesi di Laurea Magistrale

Physical and mechanical characterization of ornamental stone for numerical modeling of the quarry exploitation activities. The case of Cava Lorgino (Northern Italy).

Relatori:

prof. Maria Rita Migliazza

prof. Federico Vagnon

prof. Maria Teresa Carriero

Candidato:

Diego Eduardo Cevallos Carbajal

A.A. 2022-2023

DEDICATION

{Here writes the dedication. It cannot be more than one page}

ACKNOWLEDGEMENTS

{Here writes the dedication. It cannot be more than one page}

LIST OF CONTENTS

LIST OF TABLES

LIST OF FIGURES

ABSTRACT

This master's thesis focuses on the determination of physical and mechanical parameters of ornamental stone from Cava Lorgino in Northern Italy, with a primary objective of creating a numerical modeling for quarry exploitation activities. Four distinct types of metamorphic rock exploited in the quarry and defined here as classic, blue, brown, and black marble, were analyzed by measurement and laboratory tests to define the physical and mechanical properties of the rock. Since this type of rock shows an anisotropic features two different analysis directions were considered: parallel (verso) and orthogonal (contro) to the foliation plane. With this aim specimen with different shape and directions (cubic, prismatic, and cylindrical) were collected to carry out a range of physical measurements and mechanical laboratory tests. These tests included ultrasonic pulse velocity (UPV) measurements to determine shear and compression wave velocity, subsequently enabling the calculation of elastic-dynamic parameters like Young's modulus, shear modulus, bulk modulus, and Poisson's ratio. Furthermore, uniaxial, triaxial compression and 4-point bending tests, were performed on the two considered directions to evaluate the mechanical properties.

The laboratory results were processed to identify the maximum compressive and tensile strength of each material and the anisotropic features, useful for numerical modeling. The intact rock strength parameters were obtained considering both the Hoek and Brown and Mohr-Coulomb criteria. The results showed different deformability and strength, as well as anisotropic behavior for each considered metamorphic rock.

Subsequently, a numerical model of the quarry was developed in the UDEC software, a Distinct Element Method (DEM) tool, to analyze quarry stability conditions. The numerical simulations were carried out to consider the variability of the physical and mechanical properties of the rock in order to take into account the heterogeneous nature of the quarry, including mixed zones of different rock types.

The outcomes of the UDEC software simulations provided valuable insights into the stability conditions of the quarry, identifying potential failure zones and enhancing the understanding of quarry exploitation activities in the context of ornamental stone extraction.

1   INTRODUCTION

The excavation of marble quarries is a complex work that demands a deep understanding of the geological, mechanical, and structural aspects that govern the stability and safety of these operations. This thesis will determine, model and analyze a quarry named Cava Lorgino, situated in the North-West region of Crevoladossola, Italy, owned by Palissandro Marmi SRL. The primary goal of this work is to determine the state of stresses and maximum displacements that are developed during the various stages of excavation within this geological context. To achieve this objective, a comprehensive methodology was adopted. It started with the extraction of a series of specimens in prismatic, cubic and cylindrical configurations, each representing distinct types of the quarry's geological materials. Subsequently, these specimens were characterized and tested in the laboratory, in this last there were performed both non-destructive and destructive tests.

The non-destructive tests involved the measurement of wave propagation, executed through Pundit, a specialized wave processor. This instrument allowed to determine the dynamic mechanical parameters of the material and was conducted for both prismatic and cylindrical specimens. Following this, the destructive testing phase was performed, with uniaxial and triaxial compression tests performed on the cylindrical specimens, and a 4-point bending test executed on the prismatic specimens. Through these tests it was determined the material's maximum resistance to compression and tension, parameters that would serve as critical inputs for the subsequent numerical modeling of the quarry and for the determination of the mechanical parameters of the material. The material parameters determined by laboratory tests were further processed and analyzed using two established methodologies, the Hoek & Brown and Mohr-Coulomb linearization. These techniques allowed the determination of mechanical parameters for the intact rock in both its elastic and plastic states of the material.

Once these parameters were determined, a numerical model was built within the UDEC software. UDEC, a Distinct Element Method (DEM) resolution software, offers a dynamic and powerful approach to simulate the complexities of quarry excavation. The software represents the quarry as an assembly of rigid or deformable blocks (in this work deformable blocks were modelled), with the motion equation employed to iteratively balance forces until achieve convergence. By doing so, it reveals the state of stresses and the maximum displacements experienced during the stages studied. These stages cover the full range of quarry excavation, from the initial phases to the present-day operations and extend to the depth aimed to excavate for in this specific region of the quarry.

In chapter 1, it's defined the theoretical framework that involves the work, providing understandings into the principles and theories shaping this research. Chapter 2 offers a comprehensive specification of Cava Lorgino, describing its geological and the mineralogical composition of the materials found on it. Chapter 3 presents the results of both the laboratory and numerical model, while the final chapter discuss and analyze the implications of the findings and their relevance to the broader context of quarry excavation and stability.

2 THEORETICAL FRAMEWORK

2.1 LABORATORY TESTS

This chapter describes the laboratory tests that were performed in order to characterize the constituent materials of the Cava Lorgino in Northern Italy. Specifically, all the specimens were characterized and tested in the laboratory, in this last there were performed both non-destructive and destructive tests.

2.1.1 NON-DESTRUCTIVE TESTS

Non-destructive tests are employed in rock mechanics in order to estimate mechanical parameters of the rock, the advantage of applying these kinds of tests is that any disturbance is not induced in the rock specimen during all the phases of the tests. There are six non-destructive methods: eddy-current, liquid penetrant, radiographic, magnetic-particle, visual testing and ultrasonic. (Ahmed et al., 2023)

The ultrasonic velocity test measures two kind of waves propagated through the specimen: shear (S waves) and compression (P waves). This test is conducted by passing a pulse of ultrasonic through specimen to be tested and measuring the time taken by pulse to get through the material. This process is made by a system of a pulse generator that works together with a software which process the travel time of the wave and the length of the specimen in order to get the P and S waves. Once the velocity values of P and S waves are determined it is possible to calculate dynamic properties of the rock sample such as bulk modulus (K), shear modulus (G), elastic modulus (E) and Poisson's ratio (v). (Wille, n.d.).

2.1.1.1 Pulse unit utilized

The specifications of the pulse generator and the process to calculate the dynamic properties of the rock are specified in ASTM D2845-00, this standard describes the validity, apparatus, test specimens, procedure and calculation of all the parameters and results. In general, this method is valid for both isotropic and anisotropic rocks (but there is a limit in the degree of anisotropy that is specified). The testing apparatus must have (Figure 1):

- An electronic pulse generator with a maximum voltage output,
- Transducers: which are the responsible to convert electrical pulses in mechanical pulses and vice versa,
- A preamplifier: which is required in the case of a low voltage output by the receiver transducer,
- the display and timing unit: which are important in order to know the voltage applied and the voltage output, also it must display the waveforms in real time.
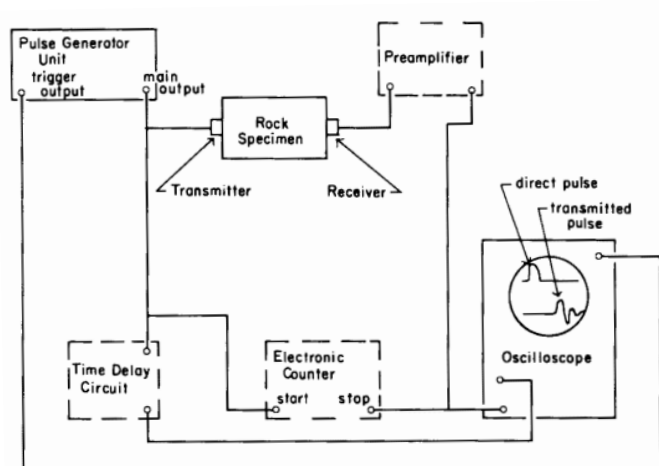
Figure 1: Schematic Diagram of Typical Apparatus(ASTM, 1995a)

The unit used to perform the measures of the pulse velocities was Pundit Lab from proceq, made in Switzerland. This unit complies with the following standards: EN 12504-4 (Europe), ASTM C597-02 (North America), BS 1881 Part 203 (UK), ISO1920-7:2004 (International), IS13311 (India), CECS21 (China). This unit is composed by display unit, power/transmission data cables, 2 transducers of 54kHz with their respective 1.5m cables, 1 calibration rod and 1 viscous couplant.

Figure 2: Pundit Lab.

Before each measure the unit must be zeroed using the calibration rod and the couplant; this process is mandatory every time that the unit is turned on or when several measures had been taken, in order to avoid errors. In order to do this the couplant is placed on each transducer and place in the opposite faces of the calibration rod, this kind of arrangement of the transducers is called direct, then a measure is performed and the time displayed in microseconds (µs) must be the same that is marked on the rod (25.4 µs). Direct arrangement ensures the maximum signal transmission between the transducers.
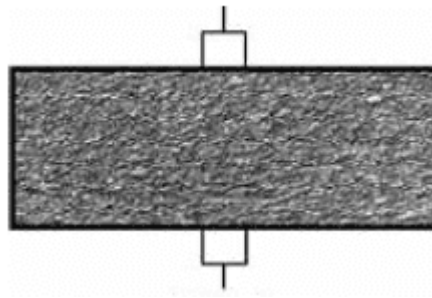
Figure 3: Direct arrangement of the transducers.

In order to perform the measures for the specimens the path length between the transducers must be measured previously, then the same process for zeroing the unit is performed for each rock specimen. In the software there is an option that allows to see the wave in real time and it's called live mode, here the waveform can be checked whether its form is right or not before recording the corresponding measures, here also the path length of the must be written in meters, this allows to the software to calculate the pulse velocity automatically.
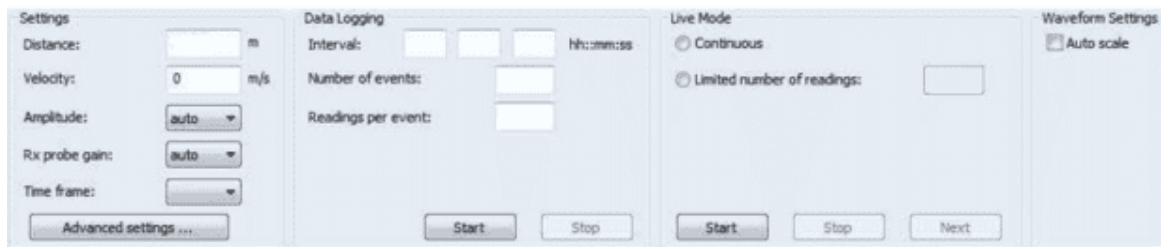
Figure 4: Software menu displayed for wave measurement.

Based on the type of the wave, the user will pick the first arrival of the wave manually in order to calculate the shear and compression waves, a minimum of 5 measures must be performed, in this work there were performed a total of 15 measures: 5 measures for shear waves, 5 measures for compression waves and 5 measures for shear waves by rotating 90 degrees one of the transducers, this last procedure was performed in order to determine the degree of anisotropy of the rock in order to check with the standard whether ultrasonic equations can be used or not.

Figure 5: Measurement of the cubic specimen.

Figure 6: Example of picking the shear and compression waves in the software.

2.1.1.2 Determination of the pulse velocities and of the elastic constants of the rock specimens

To determine the pulse velocities and ultrasonic elastic constants of rocks (which later will be defined in this chapter), all processes and calculations were conducted following the ASTM D 2485-00 standard. Evaluating the rock properties by means of pulse velocities is useful as an approach of the static properties of the rock, it should be emphasized that the quality of the results mainly depends on the personnel performing the test and the equipment's quality.

In accordance with the ASTM D2485 standard, there is no minimum dimensions of the specimens, however is specified in point 7.2 that the ratio between the length of pulse-travel distance and the minimum lateral dimension do not exceed 5. Test specimens dimensions and limits are also defined in the standard and shall not be vary 0.1mm for each 20mm of width (ASTM, 1995a).

First the test specimen must be measured in order to calculate its volume, also its mass must be measured; these two values will let to calculate the density of the specimen is required to calculate the ultrasonic elastic constants (that will be later defined).

$$\rho = \frac{m}{V} \tag{1}$$

Where:

ρ: Density [kg/m^3]

m: Mass [kg]

V: Volume [m^3]

Then the pulse-travel time must be determined, this is done by picking the first arrival of the pulse to the receiver, this is done by checking the wave form graphics in the software. Is relatively easy to pick the 1st arrival of the pulse that for the compression wave determination; in the case of the shear-wave some factors such as vibration of the transducers

may affect the determination of the arrival time, however, by changing the output voltage and the frequency of the pulse generator it's possible to have a better shape of the wave form graphics, therefore, the shear-waves can be defined easier.

In this way, the propagation velocities of compression and shear waves, V_p and V_s are calculated as:

$$Vp = \frac{L_p}{T_p} \tag{2}$$

$$Vs = \frac{L_s}{T_s} \tag{3}$$

Where:

V: Pulse propagation [m/s]

L: pulse-travel distance [m]

T: effective pulse-travel time [s]

Once the velocity values of P and S waves are determined it is possible to calculate dynamic properties of the rock sample such as elastic modulus (E), shear modulus (G), Poisson's ratio (ν) and bulk modulus (K).

$$E = \frac{[\rho * Vs^2(3Vp^2 - 4Vs^2)]}{Vp^2 - Vs^2} \quad [Pa] \tag{4}$$

$$G = \rho * Vs^2 \quad [Pa] \tag{5}$$

$$\nu = \frac{Vp^2 - 2Vs^2}{2(Vp^2 - Vs^2)} \quad [-] \tag{6}$$

$$K = \rho * \frac{(3Vp^2 - 4Vs^2)}{3} \quad [Pa] \tag{7}$$

2.1.2 DESTRUCTIVE TESTS

Destructive testing is a method that consists in analyzing the point at which a material fails in order to determine the physical properties of the material such as hardness, toughness, strength and flexibility. This method also analyzes the response of the material to an applied load which is progressively increased, in order to define the kind of failure that the material will have in site. Destructive tests are performed in certified laboratories under the aligns stated by the corresponding standards of each test (SA, 2018). All the destructive tests were performed by a certified laboratory called gdtest, this laboratory is located in Torino and is certified by the Ministry of Infrastructure and Transport of Italy.

2.1.2.1   Uniaxial compressive test

The uniaxial compressive test (UCT), or unconfined compression test, is a fundamental laboratory experiment used to assess the mechanical properties of rocks under compressive loads. In this test, a cylindrical or cubical rock specimen is subjected to axial compression along a single axis, in general the vertical one. The applied force gradually increases until the specimen fails, often by fracturing or crushing. The UCT provides critical information about the material's strength, deformation characteristics, stress-strain behavior, and failure mode under uniaxial stress conditions. This test is used to determine the stability of rock formations, design structures, predict the behavior of soil layers, and other asses. (Ahmed et al., 2023)
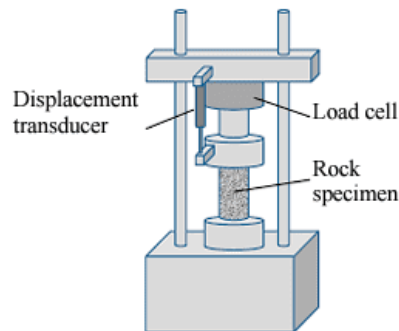
Figure 7: Conventional Rock Uniaxial testing machine. (Ahmed et al., 2023)

This test was executed following the standard ASTM D2938-95 "Standard Test Method for Unconfined Compressive Strength of Intact Rock Core Specimens".

The test apparatus is equipped with:

• Loading device: The loading device consist in two steel plates that apply a load in a constant rate, this load must be applied in a way that increases constantly and the failure is reached between 2 and 15 minutes. This rate must not deviate more than 10% of the specified one.

• Platens: Two steel plates are used to transmit the load from the loading device to the specimen, these plates must not exceed more than 1.10 times the diameter of the specimen and the thickness must be at least 0.5 times specimen diameter.

• Spherical seating: One of the plates must be rigid and the other one should be seated to a spherical seating, which should not exceed 2 times the specimen diameter. The spherical seating shall be lubricated in order to ensure free movement. The center of the spherical seating must exactly coincide with the center of the plate (also with the center of the specimen when it's placed), this spherical seating will ensure that both plates are in contact with both faces of the specimen.

Figure 8: Loading device uniaxial compressive test.

The test includes the following steps:

- Check that the spherical seating is free to rotate before placing the specimen.
- Place the lower plate in the base of the loading device and clean the surface.
- Place the specimen aligning its center with the center of the lower plate.
- Place the upper plate and align with the specimen, apply a little load of 100N in order to check if the plates are correctly aligned and the specimen is correctly placed.
- Place strain gauges or extensometers in the case that deformations are aimed to be determined.
- Start the axial load application by a constant rate, the failure (as it was mentioned before) must be reached between 2 and 15 minutes.

The maximum applied load of the test specimen must be recorded, the dimensions of the specimen previously taken must be used to calculate the cross-sectional area, the strength will be calculated as it follows:

$$\sigma = \frac{P}{A} \qquad (8)$$

Where:

σ: Compressive strength [Pa]

P: Maximum load [N]

A: Cross-sectional area [m^2].

2.1.2.2   Triaxial compressive test

Triaxial tests are highly important tests in the field of geotechnical engineering, they are applied for both soil and rock materials. These tests consist in applying axial loads to samples until failure while maintaining a constant surrounding pressure. This method allows to determine how different is the behave of the materials under stress in the three principal axes. In these experiments, there are three main types of stresses: the maximum, intermediate, and minimum normal stresses, denoted as σ_1, σ_2, and σ_3 respectively, with σ_1 being the highest. While real-world scenarios may have varying stress combinations, in typical laboratory triaxial tests, the intermediate stress (σ_2) is equal to the minimum stress (σ_3). The confining pressure is determined and it's constant during the test. Initially, the sample is isotropically loaded until the principal stresses are equal to the defined confining pressure; then, the axial stress, σ_1, increases until failure of the specimen and the maximum σ_1 is recorded (International Journal of Rock Mechanics and Mining Sciences & Geomechanics Abstracts, 1983). This test provides the data to define the strength of the rock and its elastic properties such as: shearing resistance angle, shear strength at different lateral pressures, Young's modulus and cohesion.
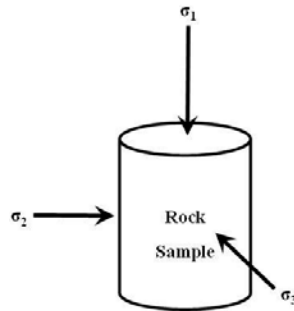
Figure 9: The principal stresses applied in a cylindrical rock sample in triaxial testing (σ1> σ2= σ3) (Geo Engineer, 2017)

This test followed the ASTM D2664-95a standard and the test apparatus is equipped with:

- Loading device: Same as it was described in uniaxial compression test.
- Pressure-maintaining device: A system (i.e., hydraulic pump or pressure intensifier) that allows to maintain constant a specific value of lateral pressure σ_3.
- Triaxial compression chamber: In this apparatus the test specimen must be surrounded by an impermeable membrane, at the same time that is placed between two platens equally set as in uniaxial compression test. This chamber must be subjected to a constant lateral pressure as the axial force increases up to the failure of the specimen. In addition to the platens and the chamber the apparatus must have a high-pressure cylinder with an overflow valve, this will ensure a correct variation of the lateral pressure in order to keep it constant.
- Flexible membrane: Made of a material that prevents the surrounding fluid from coming into contact with the rock specimen, this membrane must be sufficiently large to fit between the two plates and also match the diameter of the rock specimen without excessive stretching.

Figure 10: Triaxial compression chamber, plates and cylinder.

Figure 11: High pressure cylinder.

The test includes the following steps:

- Check that the spherical seating is free to rotate before placing the specimen.
- Place the lower plate in the base of the loading device and clean the surface.
- Fit the flexible membrane to the rock specimen and seal with O-rings, to keep aisled from the fluid.
- Place the cylinder over the specimen, it must be properly aligned to the base in order to be sealed with it.
- Position a deformation measuring device (if deformations are aimed to be measured in the test) and fill the chamber with the hydraulic fluid then apply a low axial load

of approximately 110 N to check if all the parts and the specimen are correctly placed and aligned.

- Take the initial reading of the deformation device (if applies) and start to raise, progressive and slowly, the lateral fluid pressure and the axial load to prevent deviated deformations until the predetermined fluid pressure is reached; record the axial load of the loading device.
- Apply the axial load in such mode that the strain rate is constant, do not let the strain rate deviate more than 10% from the determined one. The failure must be produced between 2 and 15 minutes from the initiation of the test.
- When the test is done the fluid must be taken out, the cylinder and the plates may be removed, then when the membrane is taken out of the specimen it must be checked that there is no fluid in the specimen, otherwise the test must be done again.

A graphic of stress difference versus axial strain must be plotted. Stress difference is defined as axial stress minus lateral pressure (σ_1- σ_3). It must be noted that if there is a difference between the piston and the specimen diameter, a correction must be applied to the measured load in order to consider the difference of these areas.

Draw the Mohr circles which is done by the plot of the normal stresses as abscissa and shear stresses as ordinates. At least three triaxial compression tests must be performed (varying each one the confining pressure) in order to draw the envelope to the Mohr stress circles.

Draw the tendency line (Mohr envelope) tangent to the three Mohr circles as it's indicated in Figure 12.
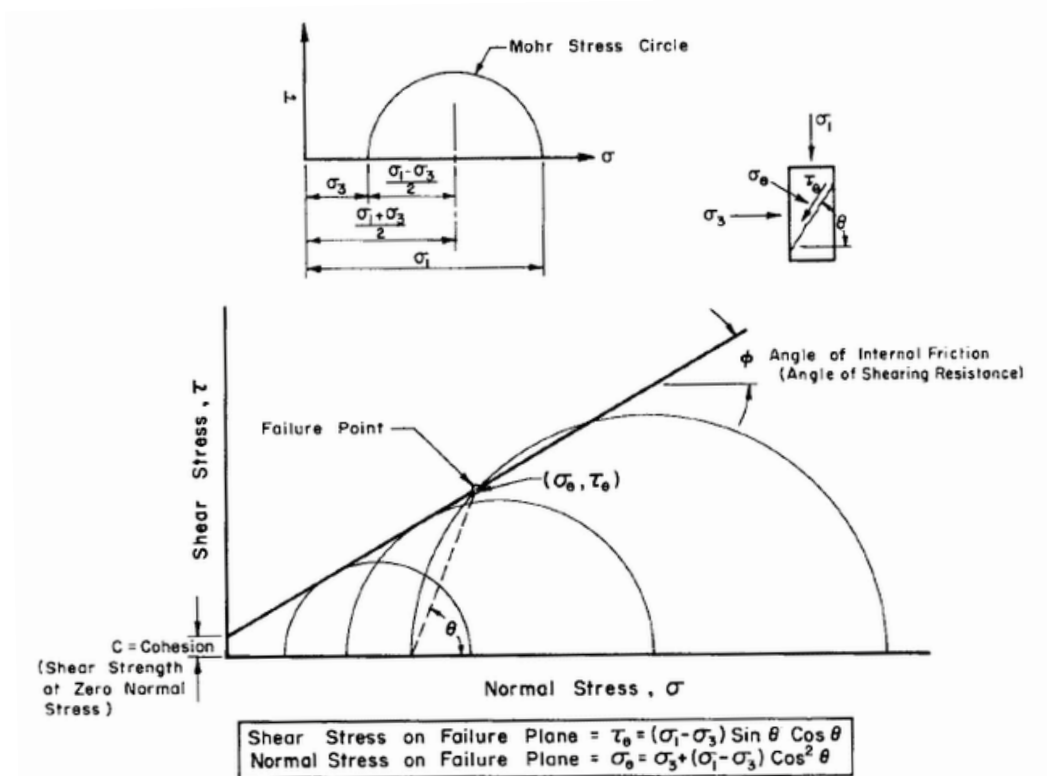
Figure 12: Typical Mohr Stress circles. (ASTM, 1995b)

2.1.2.3   Four-point bending test

The four-point bend test is used to determine the flexural strength of the specimen, flexural strength is defined as the material's ability to resist deformation under load. This test consists in a rectangular specimen, simply supported in 2 supports and loaded in 2 points, when the maximum stress is reached the specimen will experience a range of stresses across its depth, the maximum compressive value will be in the concave face of the specimen (point A) while the maximum value of tensile stress will be in the convex face (point B), as it can be seen in Figure 13 (Perelman, 2016).
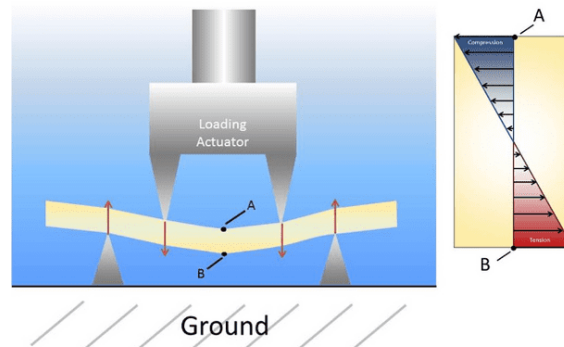
Figure 13: Range of stresses across specimen's depth at maximum load. (Perelman, 2016)

Flexural strength can be evaluated as failure under tensile stress occur before they reach the maximum compressive strength, it must be pointed that flexural strength is not the same value as tensile strength because no material is completely homogeneous, there is always a value of anisotropy in all materials. Most materials fail under tensile stress before they fail under compressive stress, thus the value that can be determined before the specimen fails is its flexural strength. The flexural strength would be the same as the tensile strength if the material were homogeneous; in general, this value is overestimated because the relationship between stress and strain behavior is considered linear (Mardalizad et al., 2017).

The execution of this test was in accordance with the ASTM D6272-17 standard, which defines the method to determine the flexural properties of the prismatic rock specimen by applying a four-point loading to a simply supported beam. Specimen is placed over two supports and is loaded at two points, each in an equal distance from the adjacent support point (the distance is one-third of the support span as it's shown in Figure 14).
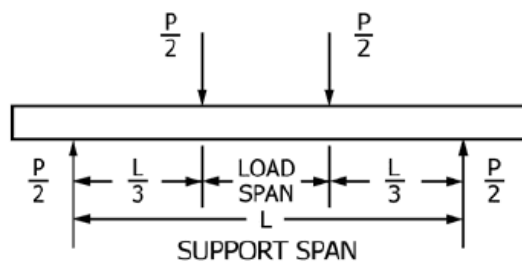
Figure 14: Loading diagram. (ASTM, 2017)

The test apparatus is equipped with:

- Testing machine: A calibrated machine that can operate in constant rates of crosshead motion over the range indicated that does not exceed more than 1% of the expected maximum load, it also should have a deflection measuring device.
- Loading noses and supports: These parts must have cylindrical surfaces, this in order to avoid stress concentrations and early failures. The radius must be 5.0±0.1 mm. The arc of the loading noses shall be large enough to prevent the contact between the specimen and the side of the noses.
- Deflection measuring devices: This device must be properly calibrated to continuously measure the deflection of the specimen during the whole test.

Figure 15: Testing machine.

At least five specimens per sample must be tested, in this case at least 20 specimens should be tested.

The test includes the following steps:

- Take the width and depth measures of the specimen to the nearest 0.03mm at the center of the support span.
- Set the support span
- Calculate the rate of the crosshead motion as it's shown in Figure 16, and set that value in the machine as near as possible to that value:

$$R = \frac{0.185 * Z * L^2}{d} \qquad (9)$$

Where:

R = rate of crosshead motion [mm /min].

L = support span [mm].

d = depth of beam [mm].

Z = rate of straining of the outer fibers [mm/mm.min]. Z shall equal 0.01.

- Align the loading noses and supports in mode that the axes of the cylindrical surfaces are parallel each other, be sure that the distance of the load span is one-third of the length. The loading nose assembly shall not rotate.
- Apply the load until failure at the specified crosshead rate, take the deflection data at the same time that the loading process start. The deflection device must be placed in a device under the specimen with common centers (do not take the deflections directly from the specimen).

Figure 16: Measuring device and deflection device placed in a plate under the actual specimen.

In this way, the Flexural Strength representing the maximum fiber stress occurring between the two central load points is calculated as:

$$fcd = \frac{P * L}{b * d^2}$$

(10)

Where:

fcd: Flexural resistance [Pa]

P: Maximum load [N]

L: Support span [mm]

b: width of the beam (specimen) [mm]

d: depth of the beam (specimen) [mm]

2.2 HOEK AND BROWN LINEARIZATION

The Hoek-Brown failure criterion characterizes the stress conditions that lead to failure in intact rock and rock masses. This criterion is a non-linear strength criterion expressed in the principal stress planes σ1 and σ3.

$$\sigma 1' = \sigma 3' + \sigma ci \left(m * \frac{\sigma 3'}{\sigma ci} + s \right)^{0.5} \tag{11}$$

Where:

σ1' and σ3' are the main effective stresses at failure.

σci is the uniaxial compressive strength of the intact rock (Co)

m and s are two constants' characteristics of the material, that are defined by the lithotype and the quality of the rock mass (s=1 for intact rocks) respectively.

2.3 MOHR COULOMB LINEARIZATION

The Mohr-Coulomb criterion is based on the concept that yielding in the material occurs on any plane when a critical combination of shear stress and mean normal stress is reached.

In order to linearize 8 values between 0 and 0.25* σ$_{ci}$ (from Hoek and Brown) must be chosen on equal range, then the relation between the principal stresses is given by:

$$\sigma 1' = \sigma 3' + \sigma ci \left(mb * \frac{\sigma 3'}{\sigma ci} + s \right)^{\alpha} \tag{12}$$

Where:

$$m_b = m_i \exp\left(\frac{GSI - 100}{28} \right)$$

GSI > 25

$$s = \exp\left(\frac{GSI - 100}{9} \right)$$
$$\alpha = 0.5$$

GSI < 25

$$\alpha = 0.65 - \left(\frac{GSI}{200} \right)$$
$$s = 0$$

Once the line given by the 8 values of σ_3 and equation 11 is drawn, the linearization to determine the parameters are:

$$\sigma_1' = \sigma_{ci} + \sigma_3 \left(\frac{1 + sin\phi}{1 - sin\phi}\right) \tag{13}$$

In this equation σ_{ci} represents the intercept of the tendency line of the graphic (obtained by equation (13) and $\left(\frac{1+sin\phi}{1-sin\phi}\right)$ represents the slope. This will allow to determine the parameters of the friction angle ϕ and the cohesion c'.

The value of the cohesion is obtained by:

$$\sigma_{ci} = \frac{2c' \cos\phi}{1 - \sin\phi} \tag{14}$$

2.4 DISCONTINUUM NUMERICAL MODEL (DEM)

The distinct element method (DEM) is a numerical solution utilized to simulate and describe the mechanical behavior of discontinuous bodies. This method was introduced in 1971 by Peter Cundall, DEM was initially created for applying in rock mechanics problems by using deformable polygonal blocks and later it extended to soils applications in 1979. (ITASCA, 2019)

In DEM, the modelled material is treated as an assembly of separate blocks. In order to find the solution, this method uses an explicit time-domain integration to solve the motion equations for both rigid and deformable discrete bodies with deformable contacts. (Li & Zhao, 2019)

In general, the DEM is applied (but not limited) to the next rock engineering problems:

- Large rock structures (rock slopes, faults, seismic instability).
- Underground opening stability (rock chambers, tunnels, rock reinforcement)
- Mine structures (underground mines, blast loading, open pits, pillars)
- Radioactive waste disposal (block tests, shaft sinking)
- Groundwater flow (dam foundation, pump testing geothermal energy)

In order to the correct application of the discrete modelling three properties must be well defined before constructing or running a computational model: geometry, boundary conditions and mechanical properties of the material(s), without the proper and justified definition of these three properties, the model may become too complicated and the results interpretation will become ineffective. (Jing & Stephansson, 2007)

To find a solution for a model a cycle is performed, which the propagation speed mainly depends on the physical properties of the system. The dynamic behavior of the system is numerically represented by a time-step algorithm that assumes the velocities and the acceleration of the system are constant within each time step. The time-step chosen must be sufficiently small that for a single step no disturbances are propagated from one block to the other ones in contact. One advantage of applying this type of interaction is that is possible to simulate a non-linear interaction of a large number of blocks without the need of a large memory in the computer system, this is called explicit numerical solution. The physical principles applied in the DEM are an alternation between Newton's second law and a force-displacement law in the block contacts; Newton's second law is used in order to determine each block's motion while the force-displacement law evaluates all the contact between the blocks on each time-step. Contacts that may exist between blocks are formed and broken automatically during the simulation; the time-step algorithm apply each cycle the law of motion to every block at the same time that the force-displacement law is applied to each block in contact, the software automatically update the blocks positions and each contact between them. (ITASCA, 2019)

The DEM code must detect quick whether two blocks are interacting or not. In addition to this the code must also determine the type of contact in order to apply the correct constitutive model, i.e., the response of a vertex pushing a face will be very different as two faces in contact. This classification is usually performed by analyzing the vertexes of the blocks and each position each respect other, for example if two blocks have x and y number of vertexes

respectively it will require x*y operations to determine the interaction of the blocks, this is the principle of how it works but it becomes more complex when the model is in 3D. (Morris et al., 2003)
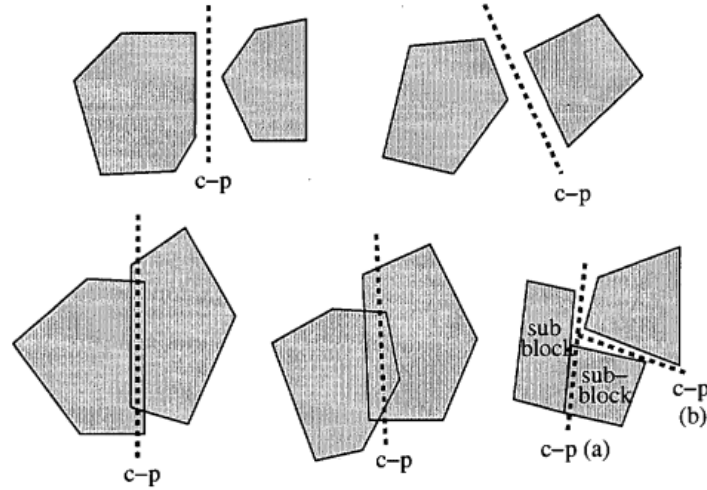
Figure 17: Type of contact and orientation between blocks.(Morris et al., 2003)

In the beginning of each time-increment, the interactions between blocks are updated using the known positions of blocks and walls. Subsequently, the force-displacement principle is applied to modify the contact forces for every interaction. Next, the law of motion is applied to each block to adjust their position and velocity; this adjustment is based on the resultant force and moment arising from the body and contact forces acting on each block. (ITASCA, 2019)
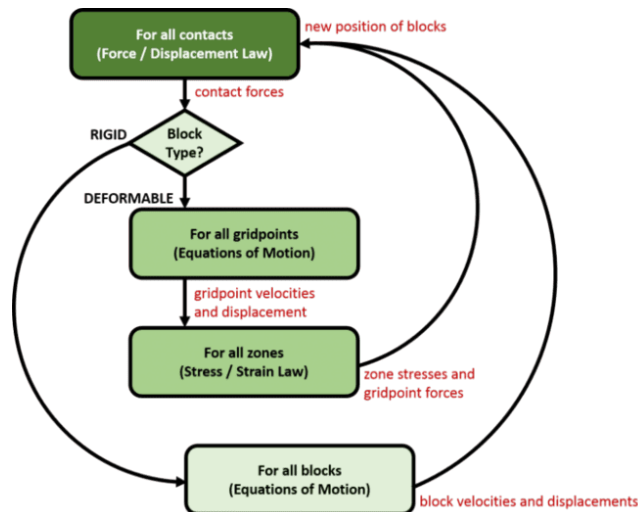
Figure 18: Solution Cycle in the DEM. (ITASCA, 2019)

2.4.1 UDEC

The Universal Distinct Element Code (UDEC) is a numerical software that works in two-dimensions, it simulates pseudo-static or dynamic response to applied loads in joint structures.

The Universal Distinct Element Code (UDEC) is a numerical software that works in two-dimensions, it simulates pseudo-static or dynamic response to applied loads to a media that contains intersecting joint structures. This discontinuous media (i.e., jointed rock masses), is represented as an assemble of discretized blocks (concave or convex corners) while the existing discontinuities are defined as boundary conditions between the blocks, models may contain a mix of rigid and deformable blocks; one of the advantages of UDEC is that is not limited to a specific initial condition or to a particular type of problem. (Itasca Consulting Group Inc., 2019)

In general, UDEC is applied for advanced geotechnical analysis of rocks, soil and structural support such as: stability analysis of jointed rock slopes or underground excavations, masonry structures, dams, and foundations, gas or fluid flow over jointed rock, blasting processes, earthquakes, micro-seismicity, simulation of large displacements along discontinuous medium's surface (opening and slip), relative motion along discontinuities ruled by linear and non-linear force-displacement relationship in both shear and normal directions and many more. (Geotech Data, 2013)
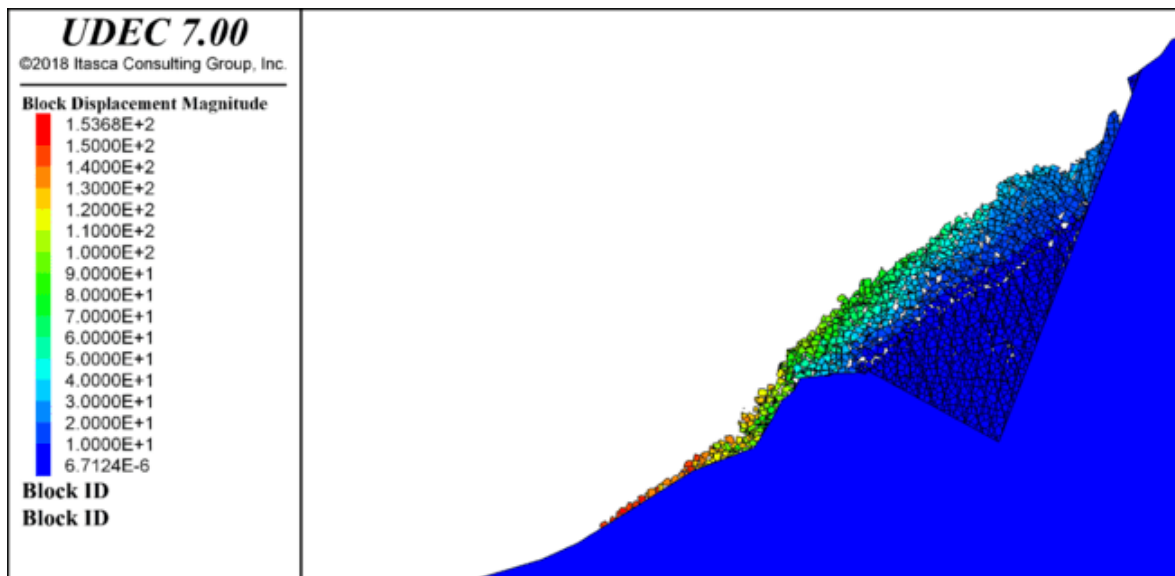
Figure 19: UDEC interface. (Itasca Consulting Group Inc., 2019)

UDEC features:

- Designed to perform any kind of analyzes of jointed, blocky systems.
- Simulates and tracks large displacements, slip and opening along a discontinuous medium.
- Mixed rigid and deformable blocks models.
- Simulation of soils or intact rock by means of deformable blocks consisting in a finite-difference mesh.
- Excavation, backfill simulation and "infinite domain" problems can be all modeled.
- Includes a built-in scripting language (FISH) and text-editor to customize or automatize all aspects of program operation, including user-defined properties and other model variables.

- Libraries of materials and constitutive models for deformable blocks and joints are included. (Itasca Consulting Group Inc., 2019)

There are three constitutive models provided in UDEC: null, elastic and plastic. These models can be applied into the model as commands, using graphical user interface (GUI) or by FISHING, controlled by the command window.

- Null model: A null material model is applied in order to represent material that is excavated or removed. Simply deleting the material when it's removed would make impossible to track any deformation around the extracted material, instead of this, the software replaces with a straight-forward material. Examples of applications include excavation holes, regions where material will be later added.

- Elastic model:
  - Isotropic: This is the simplest representation of a material, is valid for homogeneous and continuous materials that their stress-strain behavior is linear with no hysteresis or unloading phases.

  - Transversely Isotropic: This kind of model is applied when there is a layered system of isotropic materials and each one varies on their elastic moduli in the normal and parallel direction of the layers.

- Plastic model: There are plenty models that can represent different type of plastic materials, these models are referred in Table 1:

Model	Representative material	Application
Drucker-Pager	Soft clays with low friction.	Comparison to implicit finite-element programs.
Mohr-Coulomb	Soils, rocks, concrete in loose or cemented condition.	General soil/rock mechanics, slope stability, underground excavation.
Ubiquitous-Joint	Laminated material exhibiting strength anisotropy.	Excavation in closely bedded strata.
Strain-Hardening/Softening	Granular materials that show non-linear behavior hardening or softening.	Studies in post-failure, progressive collapse, yielding, caving.
Bilinear Strain-Hardening/Softening Ubiquitous-Joint	Laminated materials that show non-linear behavior hardening or softening.	Studies in post-failure for laminated materials.
Double-Yield	Lightly cemented granular material in which pressure causes permanent volume decreases.	Hydraulically placed backfill.
Modified Cam-clay	Materials which their deformability and shear strength depend mainly in function of the volume change.	Geotechnical construction on clay.

Hoek & Brown	Isotropic rock material.	Geotechnical construction on rock.
Modified Hoek & Brown	Isotropic rock material.	Geotechnical construction on rock including factor-of-safety calculations.
Cysoil (cap-yield)	Soils that decrease stiffness as plastic strains are developed.	Geotechnical constructions in soft-soil
Simplified Cysoil	Hyperbolic simulation of Cysoil stress-strain behavior.	Geotechnical constructions in soft-soil

Table 1: Plastic models included in UDEC. (Itasca Consulting Group Inc., 2019)

- Creep material models: There are several models that represent the response of the material through the time. (Itasca Consulting Group Inc., 2019)

Joint constitutive models:

There are four joint behavior models available on UDEC.

- Coulomb Slip: There are only two types of contacts: corner-to-corner and edge-to-edge contacts named as numerical contacts. In a physical sense, edge-to-edge contact is important because it represents a situation where a discontinuity is completely closed along its entire extent. This region follows the assumption that the joint extends between these two contacts and is evenly split, with each half-length supporting its own contact stress. For each contact point and its length, normal and shear displacements are calculated on each increment; the stress-displacement relation is assumed to be linear in normal direction. Contacts are assumed to be soft, meaning that blocks can overlap and may have a limiting tensile strength. In the shear response, the shear stress is limited by the combination of frictional and cohesive strength controlled by a constant shear stiffness. A behavior that can also occur is joint dilatation at the onset of slip of the joint, dilatation is governed by the dilatation angle (ψ), which usually is limited by either the accumulation of shear displacement or high normal stresses and is in function of the direction of the shearing. In UDEC, dilatation does not affect the shear strength by itself, it must be included in the effective friction angle for the joint and for each increment should be added if it's in the same direction of the total shear displacement and subtracted if the increment is on opposite direction of the shear displacement. (Itasca Consulting Group Inc., 2019)
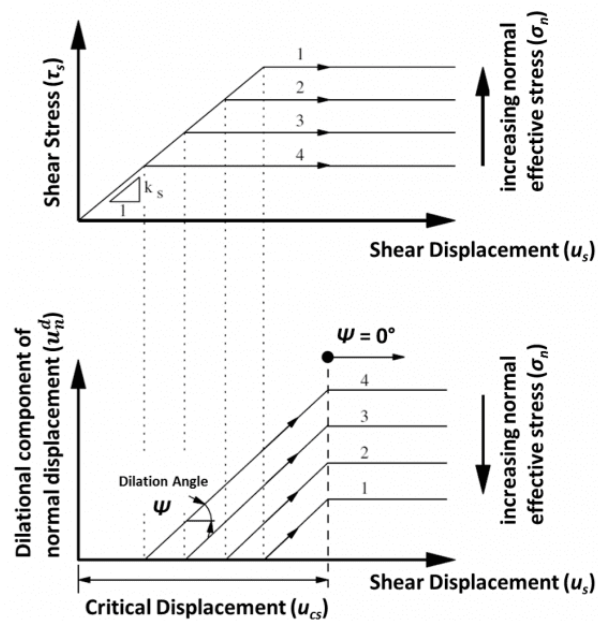
Figure 20: Shear stress and shear displacement considering dilatation angle. (Itasca Consulting Group Inc., 2019)

- Continuously yielding: This model proposed by Cundall and Hart, 1984 simulates the internal mechanisms of progressive damages of joints under shear actions. In dynamic simulations this model provides continuous hysteric damping by applying a bounding surface. This model is considered more realistic than the standard Mohr-Coulomb joint model in that the yielding model attempts to reach a non-linear behavior. The principal features of the continuously yielding are:
  - The shear stress-shear displacement curve always tends toward an aimed shear strength for the joint.
  - The aimed shear strength is continuously decreasing as it's a function of cumulated plastic displacements.
  - Dilatation angle is calculated as the difference between the apparent friction angle (which depends of the shear and normal stress) and the residual friction angle. (Itasca Consulting Group Inc., 2019)
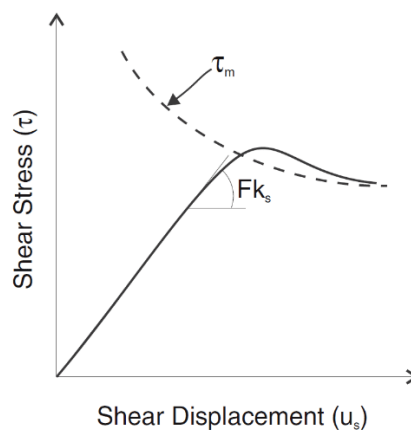
Figure 21: Shear stress-displacement curve and bounding shear strength (Itasca Consulting Group Inc., 2019)

- Barton-Bandis joint model: Dr. Nick Barton and Dr. Stavros Bandis have formulated a set of practical relationships that describe how surface roughness influences the deformation and strength of discontinuities. (Itasca Consulting Group Inc., 2019)
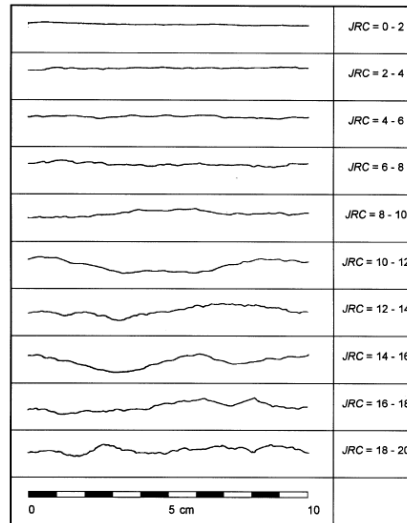
Figure 22: Roughness profiles and corresponding JRC values. (Itasca Consulting Group Inc., 2019)

- Jointed contacts: Discontinuities can be modeled as connected or bonded joints and are useful for geometric construction and incorporating joints into block. Joined contacts cannot slip or open. In UDEC, the grid-points from blocks on both sides of a contact are joined. In cases where there are no corresponding grid-points, a special contact constitutive model is applied, this special constitutive model is automatically determined by the software. The stiffness of the joined contacts is also calculated automatically but it can be modified if it's required. (Itasca Consulting Group Inc., 2019)
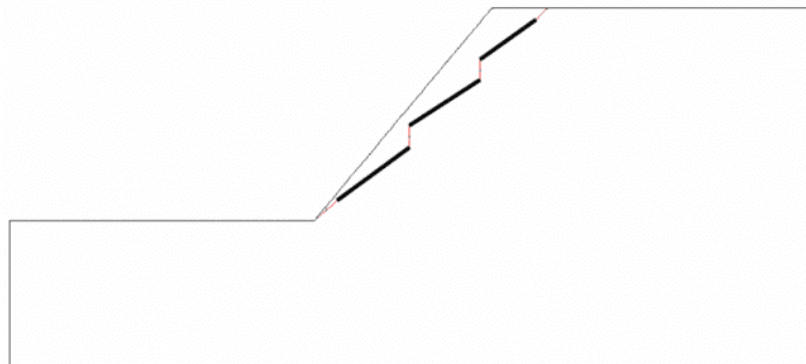
Figure 23: Slope included both joints (black) and joined contacts (red). (Itasca Consulting Group Inc., 2019)

Solving process in UDEC is a calculation cycle that repeats over and over until a steady state solution is achieved, for example when maximum unbalanced force or maximum nodal force vector is equal to zero, but for a numerical analysis a balanced force will never reach zero (exactly). In general, when the solution is found through iterations or cycles the equilibrium is reached when the difference between two consecutive iterations is relatively small compared to the total applied forces in the model.

In addition to cycling solving process UDEC features some solving tools that automatically detect the steady state solution for a mechanical problem, each solution is limited until a specific condition is reached or met:

- Solve ratio: Ratio between the maximum unbalance force to the total applied forces in the system is small (by default 0.00001).
- Solve Age: The cycle will be performed until the total time equals to a specified value.
- Solve Elastic: Joints and sets constitutive models are set to an infinite strength for the initial model equilibrium in order to avoid artificial plastic deformations due to numerical shock.
- Solve Relax: It slowly reduced the forces on the inside of an excavation in order to avoid large tensile stresses. Large tensile stresses may cause a dynamic failure in zones that normally would not fail under those stresses. This function also is used to reduce boundary forces on the internal boundary of an excavation, for example a tunnel advance.
- Solve FOS: The software slowly reduces the strength values of the materials to bring the slope to a state of limiting equilibrium, this process is known as the Strength Reduction Method (SRM). This method can be applied either to Mohr-Coulomb or Hoek and Brown models.
- Energy calculation: Energy changes due to an applied stress can be measure for a UDEC model. This calculation includes: potential energy, kinetic energy, damped energy, strain energy (stored in rock mass), plastic work and viscous boundary work. (Itasca Consulting Group Inc., 2019)

3 QUARRY DESCRIPTION

3.1 MARBLE

Marble is a metamorphic rock which is originated from the transformation of igneous or sedimentary rock by a combination of heat, pressure and chemical activity for long periods. This type of rock is characterized by the composition of recrystallized carbonate minerals. In general, marble is derived from the transformation of limestone or dolomite and it can be found in a variety of geological locations such as mountain ranges, sedimentary basins and fault zones. The most famous marble mines are located in Italy, Turkey and Greece and historically they have been characterized for their durability and beauty. Nowadays marble has a wide range of applications principally applied in the field of construction, design and decoration. (Geology Science, 2018)

In general, the physical properties of marble are:

Color	White, pink.
Grain size	Medium grained, fine grained.
Hardness	Hard, level 3 in Moh's scale of hardness.
Structure	Massive.
Texture	Granoblastic, granular.
Ability to polish	It can be polished to a high luster.
Major minerals composition	Calcite.

Table 2: Physical properties of marble (The Editors of Encyclopedia Britannica, n.d.).

Marble has a wide range of applications and it's been used during centuries, the most common areas where marble is used are:

- Building and architecture: It includes, façades, interior walls, floors and decoration (i.e., columns and arches).
- Sculpture: Fine grain marbles are useful when it's about detailing, many famous sculptures are made in marble.
- Countertops and tabletops: Not only because of its resistance to heat but also for its easiness to clean marble is a good choice for dinning and coffee tables and kitchen and bathroom countertops.
- Flooring: When luxury and elegance comes marble is the choice for residential and commercial applications. (Geology Science, 2018)

Italian marble is considered one of the bests among the world, historically it as used by renaissance artists such as Michelangelo and Donatello as well as architects in the design of their works. There are several types of marbles that are extracted in Italy, the next ones are the most famous:

- Calacatta marble: It is a fine-grained marble characterized by a bright white background and the presence of gray and black veins.
- Carrara marble: The most famous one, it has a dirty white background and light gray veins.

- Travertine marble: Very famous in construction, the variety of colors goes from white to walnut as well as yellow and red.
- Red Verona marble: It is considered the best red marble in the world and as its name says it is extracted from Verona, it is used in stairs, floors and interiors.

The most famous marble in the world comes from Carrara, located in the region of Tuscany, Italy. (Nexidia, 2021)

For this thesis work, the marble used came from the quarry of Lorgino di Crevoladossola; Crevoladossola is a commune in the Province of Verbano-Cusio-Ossola in the Italian region Piedmont. (Wikipedia, 2020)

Figure 24: Marble extraction in query of Crevoladossola. (Studio R.M., n.d.)

3.2 QUARRY

Marble extraction in Italy is a very ancient activity, it started in 180 B.C. when the Roman empire took possession of Carrara and the surroundings environments; Romans started to extract marble in order to imitate Greeks in the aspect of decoration of villas and monuments. (Lessiau, 2020)

The extraction techniques have been changing through the time. In the beginning, the use of percussion tools was essential to extract the blocks with the help of iron wedges inserted with hammers. To cut the block into slabs a large handsaw with an iron blade was used by two workers, this type of tool allowed to cut 7 to 8cm per day and it had to be constantly poured with a mixture of water and silica in order to preserve the blade. A single piece of marble could take up to 2 years just to be extracted, after that the path to transport the marble from the quarry to the base of the mountain was extremely dangerous, the technique consisted in put the 25-30 tons block over wooden beams, the 70-80% mountain slope made this process extremely dangerous, the wooden beams were greased with soap and dozens of men hemp the rope to control the block and to move the beams from back to front as it kept advancing, often the men located in the front got killed or lost a limb. (Lessiau, 2020).

In the end of 18th century, explosives were introduced in the process of extraction, but the damage they caused to the marble made them impractical, in the end explosives were used only to open new quarries. With industrial revolution new mechanical techniques were introduced in the extraction of marble. From 1966, synthetic diamond wires are used, these kinds of tools let to cut the massive 350 ton. marble block into 35 ton. block to load in the trucks in just 45-60 minutes, saving a big amount of time. It takes about 6-7 days to extract a 350 ton. block. First a big chainsaw cut the bottom of the block, it takes about one day, then two holes are drilled into the block to form a L-shape where the diamond wire will be inserted and make the cut, it takes about 2 days to each side of the block to complete this process. (SIMOADMIN, 2018)

To summarize the whole process can be describes in four main work phases as it's shown in Table 3:

WORK PHASE	SUB-PHASE	DESCRIPTION
1. Quarry front cutting.	Preliminary operations	Inspection of working area and delimitation of the blocks.
	Hole drilling	Assembling and starting the drilling machine
	Chain saw cutting	Positioning of the machine and cutting
	Diamond cutting	Positioning the diamond wire saw, positioning of protections, periodic checks.
2. Overturning of the bench.	Preparation	Use of pneumatic hammer to drill holes.
	Preparation of rubble bed	Deposing waste material in the base of quarry bench.
	Movement with jacks	Manual insertion of piston jacks and cushions
	Pushing with excavator	Pushing bench by inflation of the cushions and jacks, driving excavator to the top of the bench and pushing with bucket.
3. Handling of work material in quarry.	Transport of blocks to deposits	Lifting and transporting with loader.
	Transport of waste material	Using shovel and loader to pick waste material and transfer to loading area.
4. Transport of the blocks to the destination.	Driving truck inside the quarry	Driving the vehicle along the steep and narrow roads, often forwards and backwards maneuvers are made.
	Driving the truck on normal roads	Driving the vehicle around the mountainous roads, the use of brakes is frequently high.

Table 3: Work phases on marble extraction. (Angotzi et al., 2005)

Marble quarries involve hundreds of in-site workers and also several risks for them, that's why safety is a mandatory and serious factor considered in all the processes performed. One of these risks (and the one that is going to be considered in this thesis) is the stability of the quarry. In general, the extension of a marble mountain wall is about 50 to 100 m. high, this involves thousands of cubic meters of marble that, in the case of a failure, may fall over the entire quarry, leaving hundreds of human loss and economical damages. (CUS.MAR Marble Import Export s.r.l., n.d.).

3.3 CAVA LORGINO

3.3.1 PROFILE OF ANALYSIS

Lorgino's quarry is located in the province of Crevoladossola, Italy. The average elevation of the quarry is 448 meters over the sea level, being the highest point at 453 m.a.s.l. and the lowest 417 m.a.s.l. This is an open-air quarry and the excavation process is descending vertically in different phases, where on each of them giant blocks of the material are extracted to later give them the desired shape for commercial purposes.

Figure 25: General location of the quarry. Source: Google maps

Figure 26: Coordinates of the quarry. Source: Google maps

Figure 27: Reconstruction of the quarry by photos taken by an UAV and processed.

Palissandro marble is a dolomitic marble with fine and homogeneous saccharoidal grain composed mainly of dolomite minerals. Inside the quarry the different concentration of opaque and mica phlogopite gives a polychrome characteristic which allows to differentiate the categories of materials that have different textural and mechanical characteristics.

From a petrographic point of view the materials can be classified as: dolomitic marble and phylladic mica schist.

In order to simplify the nomenclature, the materials were defined as marble and are: Classic, Blue, Brown and Black. The materials that correspond to the dolomitic marble are: Classic, Blue and Brown; while Black corresponds to the phylladic mica schist

The excavation area is defined in the next figures:

Figure 28: Analyzed excavation area.

The profile that will be modeled in the numerical software corresponds to cut A-A. The green arrow located in the down right corner specifies the real north with respect to the quarry, the inclination is 156°.
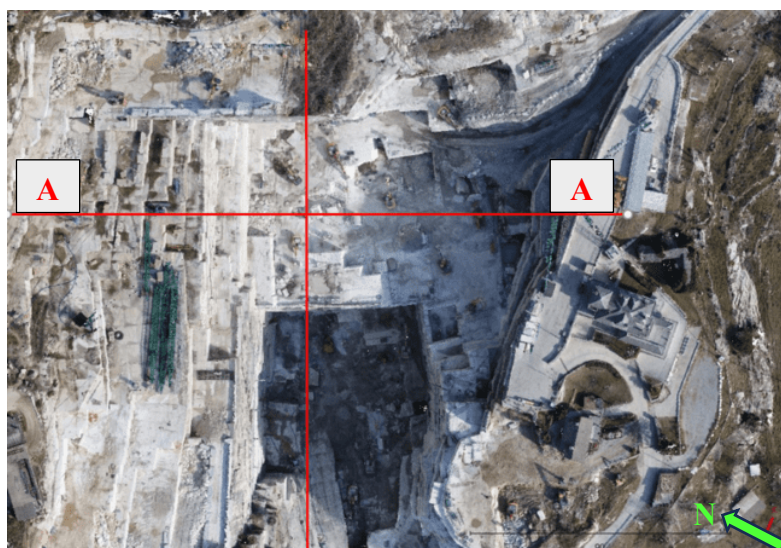
Figure 29: Cut of the excavation area.

From a visual analysis of the profile of the excavation area the different materials were determined in a petrographic card as follows:
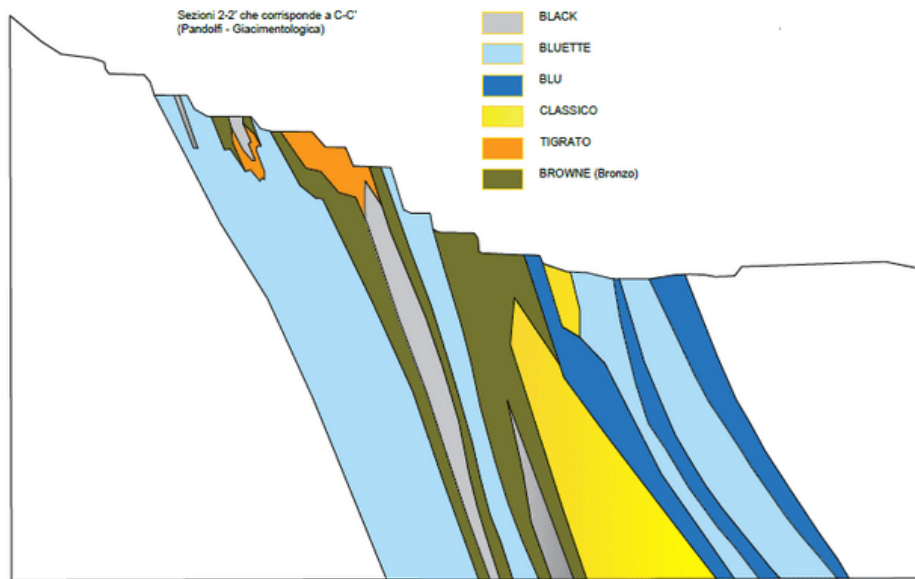
Figure 30: 2D Excavation profile and material distribution inside it.

.

3.3.2 DISCONTINUITY SYSTEMS:

In rock masses there are the presence of discontinuities, in this case there are two types: the discontinuities representing the separation between materials and the discontinuity system that represent the existent fractures on the rock. The discontinuities must be considered for the analysis of the stability of the rock because they lead to stability problems and large displacements.

To calculate the mechanical parameters of the diverse discontinuities there are diverse methods, in this work they were determined in different ways.

For the discontinuities that represent material separation, it started from the residual values of the intact rock parameters of each material and it was given a low value of GSI (Geological Strength Index) assuming that the discontinuity will have a low strength value.

The modulus of elasticity was calculated as:

$$E_d = \sqrt{\frac{\sigma_{ci}}{100}} \cdot 10^{\frac{GSI-10}{40}} \quad \sigma_{ci} < 100 \text{ MPa (Hoek \& Brown, 1997)}$$

Figure 31: Modulus of elasticity.

And the shear modulus:

$$G = \frac{Ed}{2\left(1+v\right)}$$

From there the values of the normal and shear stiffness are calculated as follows:

$$k_n = \frac{E_m \, E_r}{s\,(E_r - E_m)}$$

where E_m = rock mass Young's modulus;

E_r = intact rock Young's modulus;

k_n = joint normal stiffness; and

s = joint spacing.

$$k_s = \frac{G_m \, G_r}{s\,(G_r - G_m)}$$

where G_m = rock mass shear modulus;

G_r = intact rock shear modulus; and

k_s = joint shear stiffness.

Then the Hoek and Brown parameters α and s:

$$m_b = m_i \exp\left(\frac{GSI - 100}{28}\right)$$

GSI > 25

$$s = \exp\left(\frac{GSI - 100}{9}\right)$$

$$\alpha = 0.5$$

GSI < 25

$$\alpha = 0.65 - \left(\frac{GSI}{200}\right)$$

$$s = 0$$

Figure 32: Hoek and Brown parameters. (Hoek and Brown 1997)

And the linearization of Mohr-Coulomb was performed in the same way as it was defined in the previous chapter of this thesis, this, in order to obtain the friction angle and the cohesion value of each material interphase.

For the discontinuities that represent the fractures of the material, it started from the visual inspection of the rock.
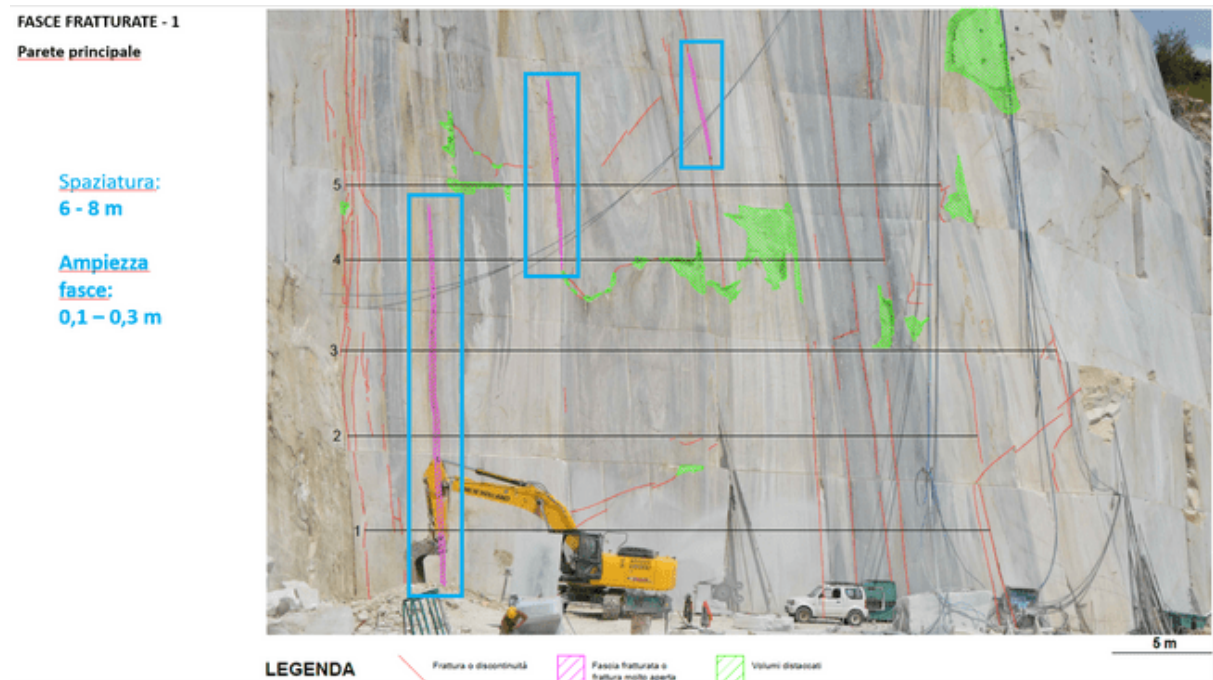
Figure 33: Existing fractures present in the rock mass.

From this photo the space and the trace of the discontinuities could be determined.

The orientation of the discontinuity system was performed by a geological analysis and the representation of 12 discontinuities in the stereogram.

FRONTI SETTORE NORD ED EST DI CAVA - ZONA STR_B

Località: Crevoladossola		Litotipo: marmo (dolomia ricristal.)		
Stendimento: lunghezza ml. 288 (48+54+25+33+45+58+25)		JCS medio roccia sana 48		

numero	Immers. [°]	Inclin. [°]	Sistema	Lungh. [sigla]	Apert. [sigla]	Rugos. [sigla]	Acqua [sigla]	R (JCS) discont.	JRC discont.	note
1	166	70	K_s	G	CH	LIS	A	44	8-10	
2	170	68	K_s	F	CH	LIS	A			
3	164	72	K_s	G	AC	LIS	A	42	8-10	
4	162	71	K_s	F	CH	LEV	A			
5	360	62	k_a	F	CH	LIS	A	40	8-10	
6	358	68	k_a	F	AC	LIS	A			
7	240	78	K_b	F	CH	LIS	A			
8	240	82	K_b	G	CH	LIS	A	40	8-10	
9	340	26	K_c	D	CH	LIS	A			
10	345	25	K_c	C	CH	LIS	A	38	6-8	
11	341	24	K_c	D	CH	LIS	A		8-10	
12	40	59	K_d	F	CH	RUG	A		6-8	

LUNGHEZZA (m)	A (<0,02)	B (<0,02-0,1)	C (0,1-0,5)	D (0,5-2)	E (2-5)	F (5-10)	G (>10)	
Apert. (mm)	CH (<2)		AC (2-5)		AP (>5)			
Scabrezza	LEV (levigata)		LIS (liscia)		RUG (rugosa)		SEG (segm.)	
Acqua	A (asciutta)		U (umida)		S (stillic)		V (venuta)	

Table 4: Discontinuity system to represent in the stereogram.
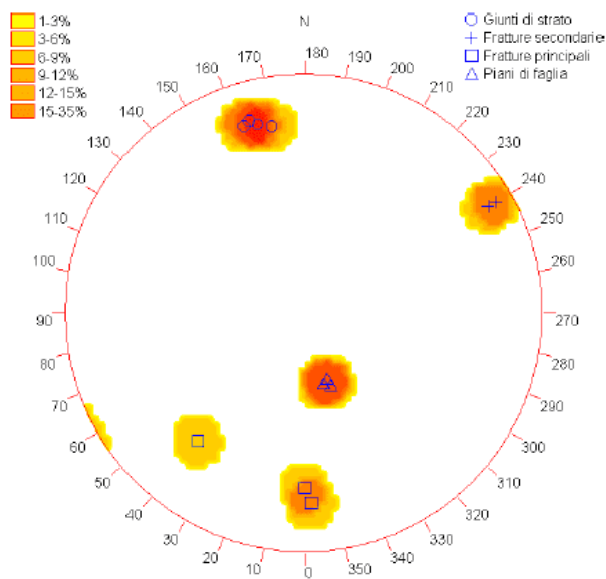
Figure 34: Representation of the discontinuities in the stereogram.

From this and according to the orientation of the excavation profile respect to the North, three sets of discontinuity were represented in the profile:
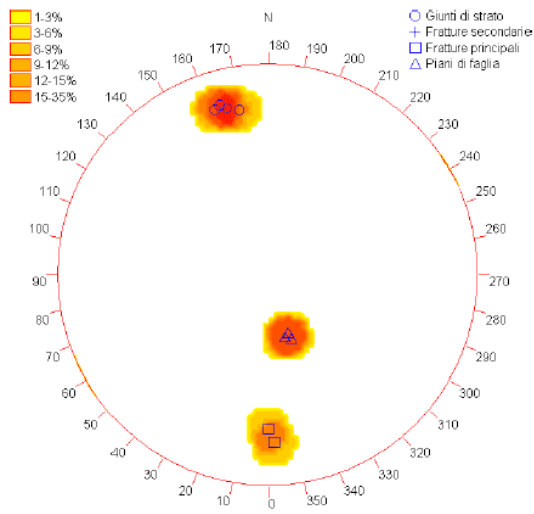
Figure 35: Discontinuity systems represented in the numerical model.

And the dip and dip direction of these three sets are:
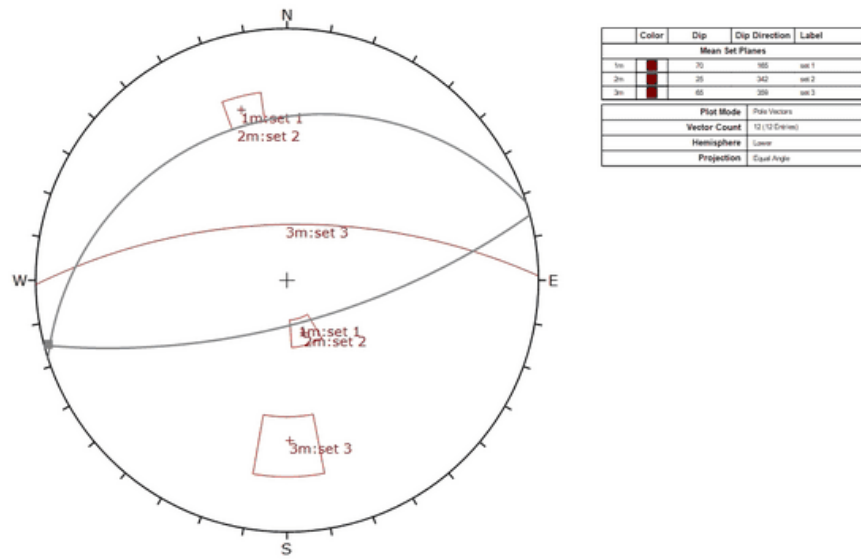
Figure 36: Dip and dip direction of the three sets of discontinuities.
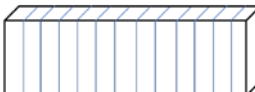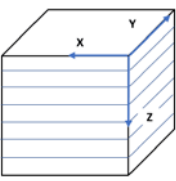
4 LABORATORY RESULTS

4.1 ROCK SPECIMENS

Four kinds of marble rock were extracted from the quarry of Lorgino, located in Crevoladossola, Province of Verbano-Cusio-Ossola, Italy, they were called according each product nomenclature in the market: black, blue, brown and classic. In total 178 specimens were analyzed their mineralogy and structural characteristics. There are also two different directions of the fibers with respect to the schistosity plane: one with the axis perpendicular to it (verso) and the other one parallel (contro), all these characteristics and quantities are specified in Table 5 and Table 6:

Direction: Perpendicular to schistosity plane (verso)			Direction: Parallel to schistosity plane (contro)		
Rock Type	Specimen type	Quantity	Rock Type	Specimen type	Quantity
Black	Cylinder	14	Black	Cylinder	3
	Prism	21		Prism	6
	Cube	-		Cube	1
Blue	Cylinder	11	Blue	Cylinder	4
	Prism	25		Prism	9
	Cube	-		Cube	2
Brown	Cylinder	12	Brown	Cylinder	4
	Prism	18		Prism	6
	Cube	-		Cube	2
Classic	Cylinder	13	Classic	Cylinder	3
	Prism	15		Prism	8
	Cube	-		Cube	1

Table 5: Rock specimens, types and quantities.

Cylinder		Prism		Cube		
Verso	Contro	Verso	Contro	X	Y	Z

Table 6: Type of specimens and direction of the fibers.

Codification of the rock specimens: All the specimens were codified in a way that specifies the type, the direction of the schistosity plane, number of specimen and the shape, all the codes and the acronyms are next:

Lithotype:

- BK: Black
- BL: Blue
- BR: Brown
- CL: Classic

Shape of the specimens:

- C: Cylinder
- B: Prism (barrette)
- CU: Cube

Direction of the schistosity plane:

Cylinders and Prisms

- V: Verso
- C: Contro

Cube

- X: Contro
- Y: Contro
- Z: Verso

For instance, a specimen called BK.V3.C, is a specimen type black, direction perpendicular to the schistosity plane, number 3 of this kind and with cubic shape.

4.2 DETERMINATION OF PULSE VELOCITIES

To determine the pulse velocities and ultrasonic elastic constants of rocks (which later will be defined in this chapter), all processes and calculations were conducted following the ASTM D 2485-00 standard. Evaluating the rock properties by means of pulse velocities is useful as an approach of the static properties of the rock, it should be emphasized that the quality of the results mainly depends on the personnel performing the test and the equipment's quality.

In accordance with the ASTM D2485 standard, there is no minimum dimensions of the specimens, however is specified in point 7.2 that the ratio between the length of pulse-travel distance and the minimum lateral dimension do not exceed 5. The overall dimensions for the specimens on this work are defined in Table 7: Specimens average dimension on each axis.Table 7:

Specimen type	Length (mm)	Width (mm)	Height (mm)
Cylinder	120.0	53.8 (diameter)	-
Prism	219.9	29.9	60.5
Cube	150.3	150.2	148.8

Table 7: Specimens average dimension on each axis.

The standard also specifies that the maximum tolerance between the length and the width must be 0.1mm for each 20mm which is satisfied for all the specimens performed in this work.

Figure 37: Prismatic rock specimen for type black.

Figure 38: Cylindric specimen for type blue.

Figure 39: Cubic specimen for type brown.

4.3 Pulse propagation of the prismatic specimens:

The measure of the pulse propagation was performed on all the samples in the different directions analyzed. In particular, for the cubic samples, the two components Vp and Vs were measured in three directions; for the cylindrical samples, the speeds Vp and Vs were measured along the axis of the samples (in contro and verso); for the prismatic specimen it was only possible to measure the velocity Vp along the maximum length. Tables 52 to 58 in Annexes chapter show all the measurements carried out, which are summarized in the figures below for the various samples and in the directions analyzed.
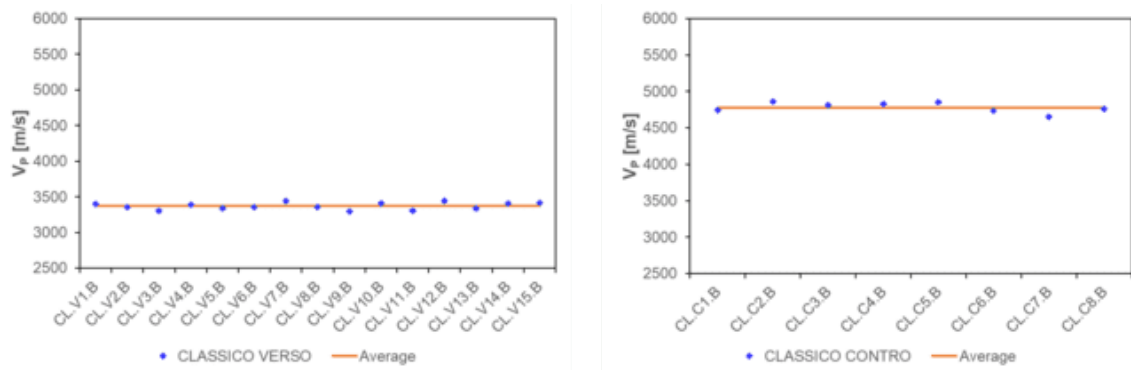
Figure 40: Pulse propagation of Classic Verso and Contro Prismatic Specimen.
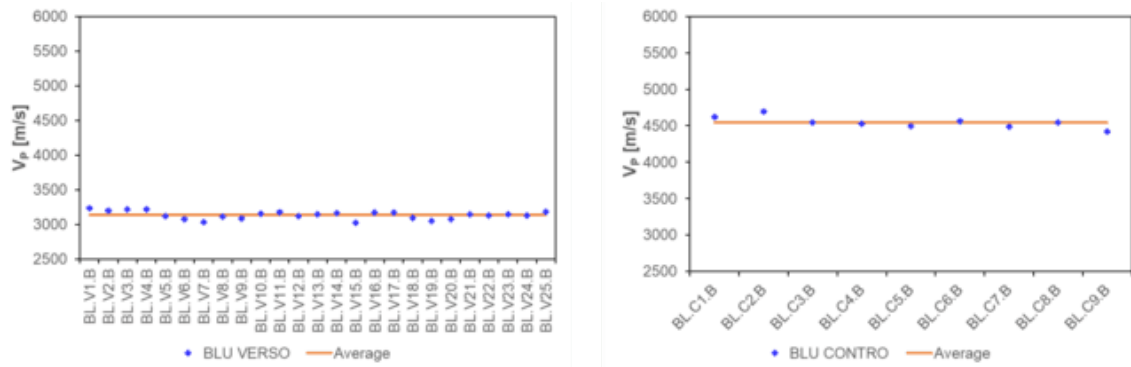
Figure 41: Pulse propagation of Blue Verso and Contro Prismatic Specimen.
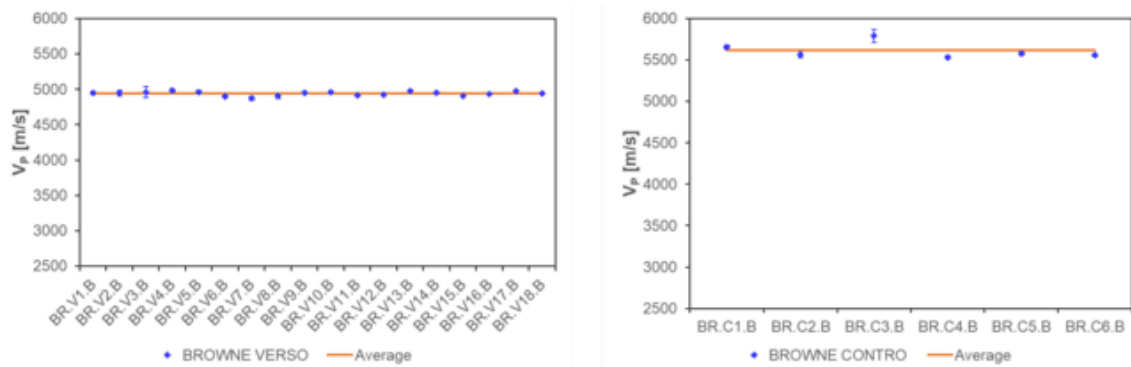
Figure 42: Pulse propagation of Brown Verso and Contro Prismatic Specimen.
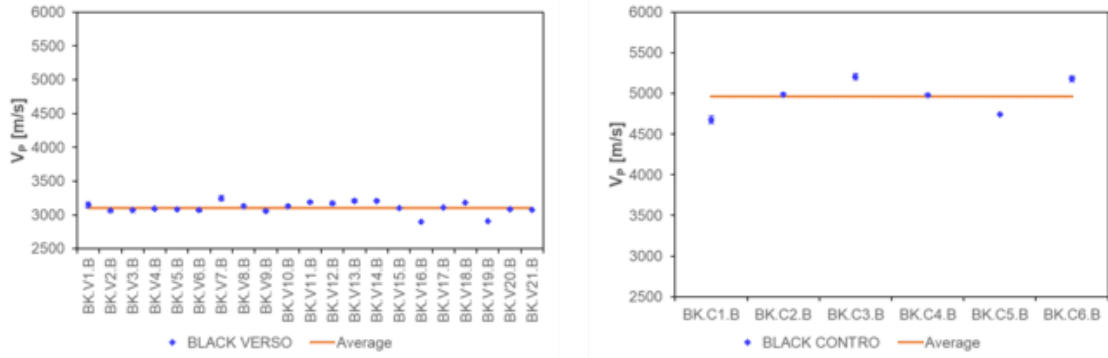
Figure 43: Pulse propagation of Black Verso and Contro Prismatic Specimen.

It can be evidenced that values of the measures taken are relatively close to each other, in other words the variation between measurements is very low. Therefore, the existent error in these data is very low.

By looking at the results it can be seen that the values of the verso, in all the cases, are lower than the values of the verso. This means that the presence of cracks and/or heterogeneities are less in contro than in verso, higher velocity means that the medium has a smooth path where waves are traveling in.

4.3.1 Pulse propagation of the prismatic specimens:
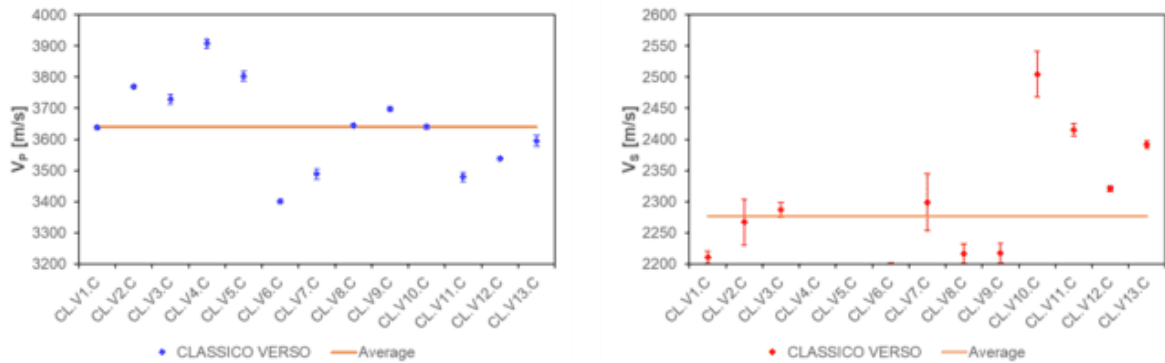
Figure 44:Vp and Vs of Classic Verso Cylindric Specimen.
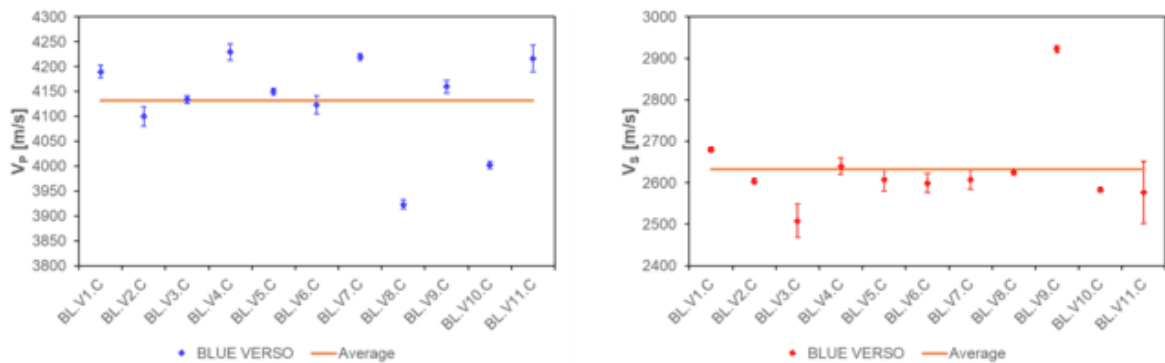
Figure 45: Vp and Vs of Blue Verso Cylindric Specimen.
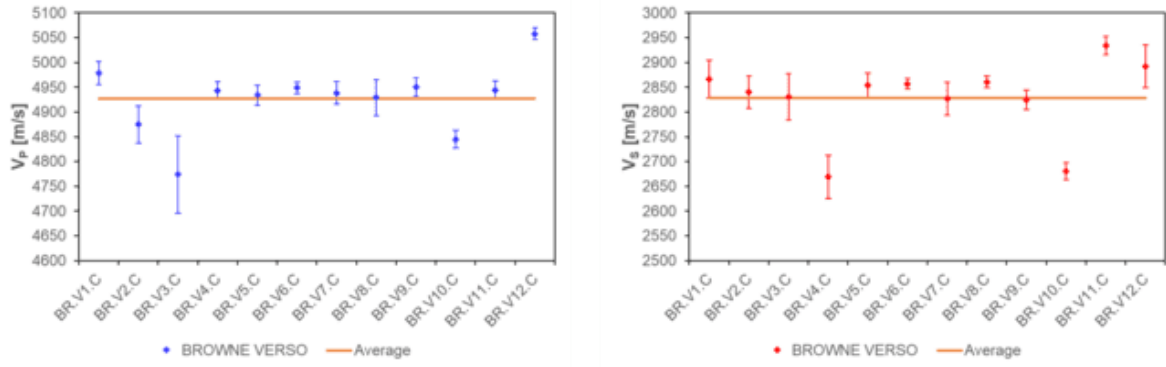
Figure 46: Vp and Vs of Brown Verso Cylindric Specimen.
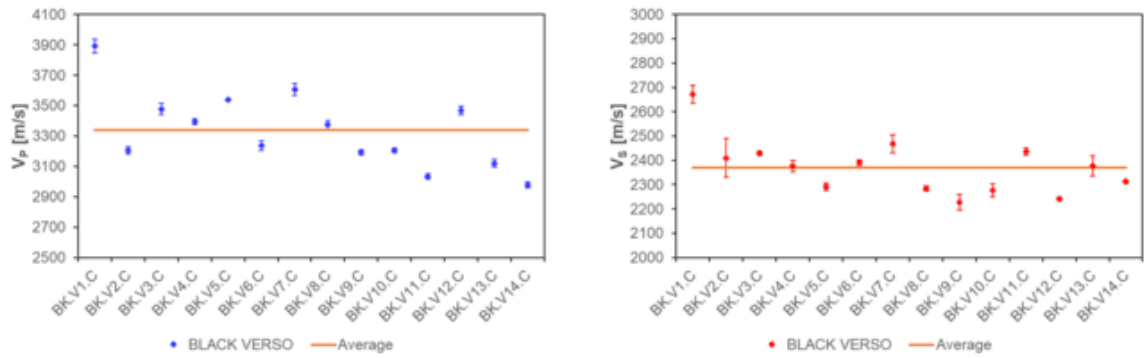
Figure 47: Vp and Vs of Black Verso Cylindric Specimen.
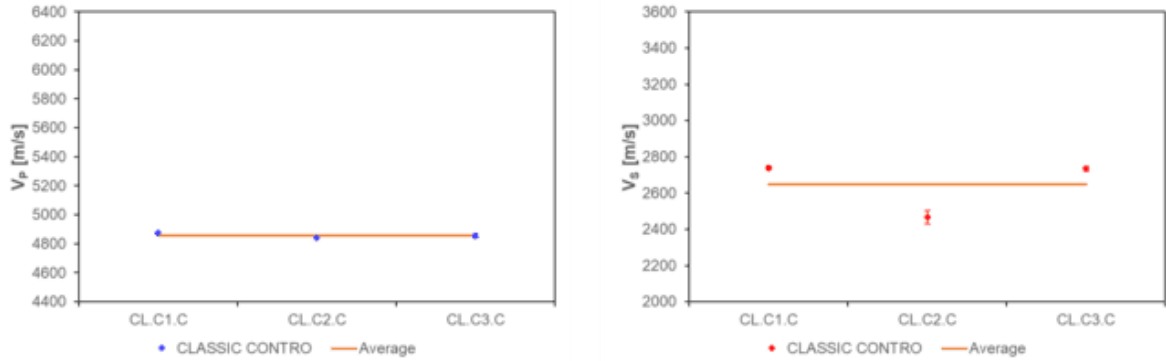
Table 8: Vp and Vs of Classic Contro Cylindric Specimen.
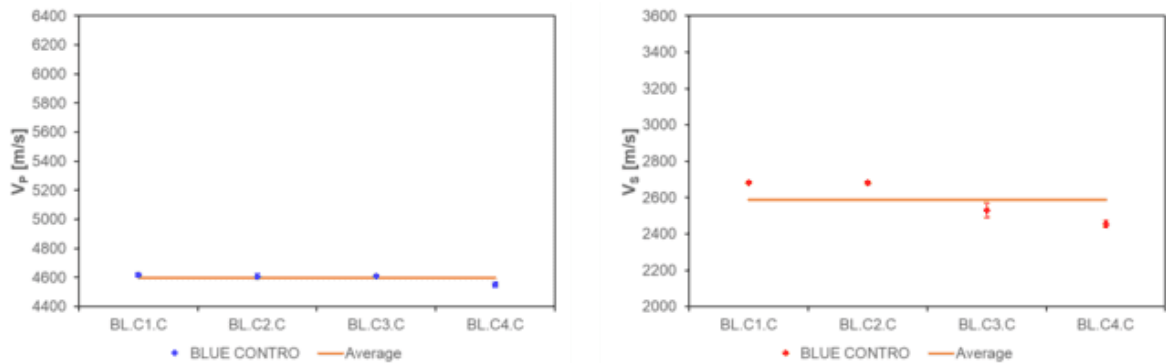
Table 9: Vp and Vs of Blue Contro Cylindric Specimen.
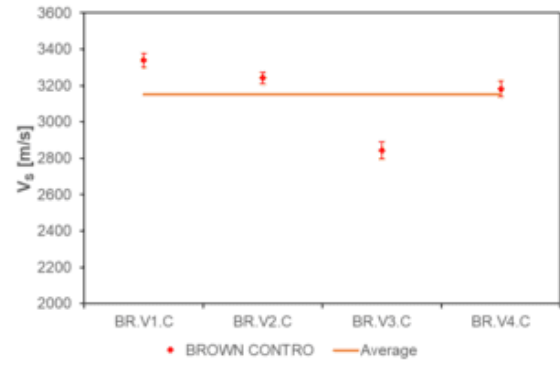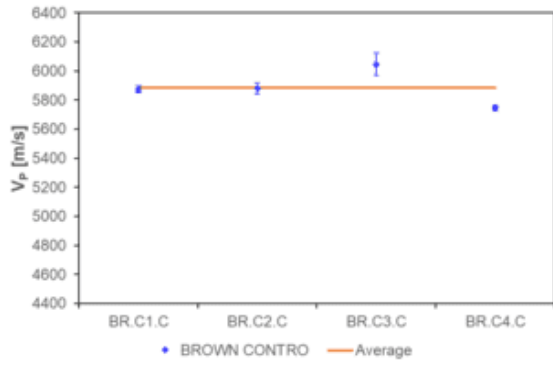
Table 10: Vp and Vs of Blue Contro Cylindric Specimen.
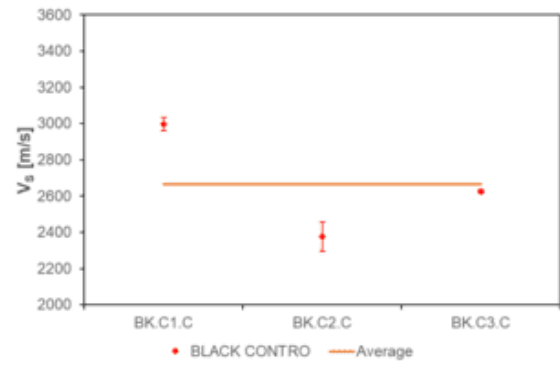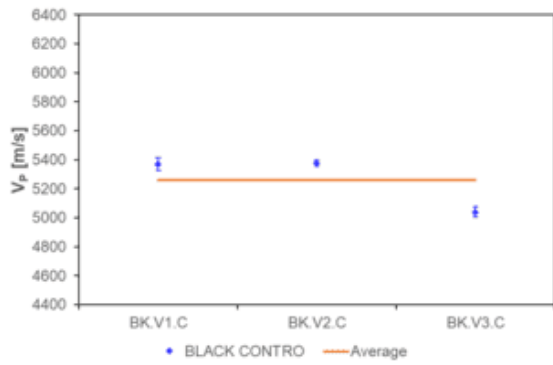
Table 11: Vp and Vs of Black Contro Cylindric Specimen.

From the previous figures it can be seen the variation between the measures of Vp and Vs on each specimen; compared with the measures of the prismatic specimens there are more variations, however in general the standard deviation of the values is relatively low, with 2 exceptions in the Vs measurements in the brown and black in the contro with values of 103 and 97 respectively.

4.4 Elastic parameters from the results of the cylindric specimens:

The values of the dynamic modules at small deformations obtained from Vp and Vs values reflect that in general the materials have good physical-mechanical characteristics, especially for the BROWN samples and in contrast clear heterogeneity for the BLACK samples

The average of the results is presented in the next table

Lithotype	Direction	Density ρ [kN/m³]	Pulse velocity					Elastic parameters			
			Compression Vp		Shear Vs		Vp/Vs [-]	Young's modulus E		Poisson's ratio ν	
			average [m/s]	d.s. [m/s]	average [m/s]	d.s. [m/s]	[m/s]	average [GPa]	d.s. [GPa]	average [---]	d.s. [---]
CLASSIC	VERSO	28.4	3641	143	2277	110	1.6	34.2	1.6	0.2	0.1
	CONTRO		4856	16	2647	155	1.8	51.2	4.2	0.3	0.0
BLUE	VERSO	28.3	4132	95	2632	105	1.6	45.2	3.7	0.2	0.1
	CONTRO		4598	31	2587	113	1.8	48.1	2.8	0.3	0.0
BROWN	VERSO	28.3	4927	70	2828	78	1.7	56.7	2.6	0.3	0.0
	CONTRO		5933	98	3141	263	1.9	73.0	12.3	0.3	0.1
BLACK	VERSO	28.8	3337	248	2371	116	1.4	31.1	4.1	0.0	0.2
	CONTRO		5263	194	2666	313	2.0	54.2	11.1	0.3	0.1

Table 12: Summary of the pulse velocities and elastic parameters of the cylindric specimens

4.5 Pulse propagation of cubical specimens:

In the next table that the results obtained from the measures in the cubical specimens are similar to the ones obtained in the cylindrical specimens, evidencing a correct performance of the measures of the pulse velocities.

Lithotype	Direction	Density ρ [kN/m³]	Pulse velocity					Elastic parameters			
			Compression Vp		Shear Vs		Vp/Vs	Young's modulus E		Poisson's ratio ν	
			average [m/s]	d.s. [m/s]	average [m/s]	d.s. [m/s]		average [GPa]	d.s. [GPa]	average [-]	d.s. [-]
CLASSIC	VERSO (z)	28.4	3527	-	2388	-	1.5	34.9	1.5	0.08	0.03
	CONTRO		4329	-	2584	-	1.7	46.5	-	0.22	-
BLUE	VERSO (z)	28.4	5050	-	3126	-	1.6	66.1	4.2	0.19	0.02
	CONTRO		5287	110	3269	124	1.6	72.3	4.3	0.19	0.00
BROWN	VERSO (z)	28.4	5133	-	3179	-	1.6	68.2	4.1	0.19	0.02
	CONTRO		5292	106	3272	122	1.6	72.4	0.3	0.19	0.00
BLACK	VERSO (z)	29.3	3192	-	2452	-	1.3	27.5	9.6	-0.22	0.32
	CONTRO		5178	-	4171	-	1.2	58.8	-	-0.42	-

Table 13: Summary of the pulse velocities

4.6 FLEXURAL STRENGTH

The results of the flexural strength, obtained by the four-point bending test are presented in the next tables.
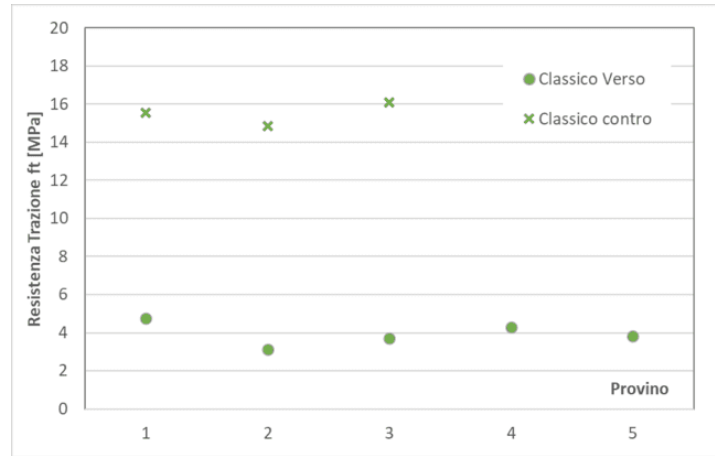
Figure 48: Flexural resistance of Classic specimens
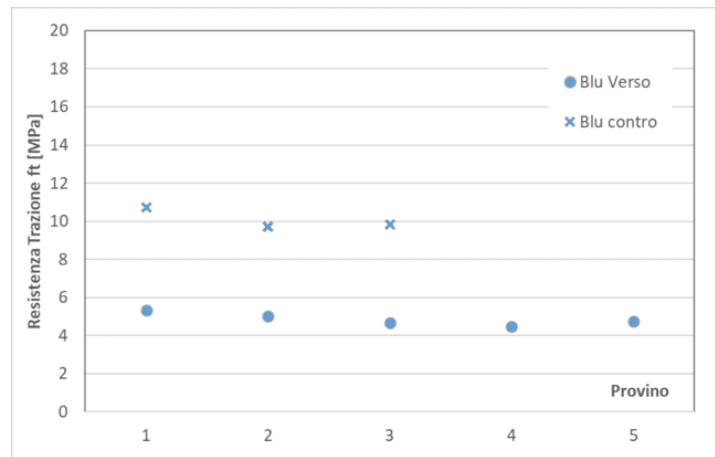
Figure 49: Flexural resistance of Blue specimens
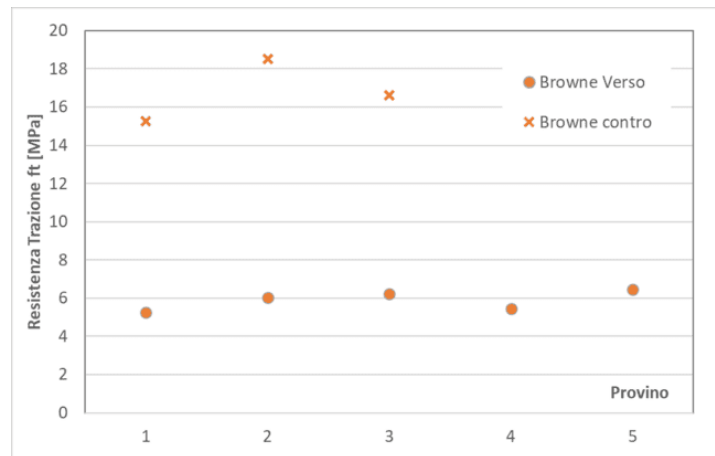
Figure 50: Flexural resistance of Brown specimens
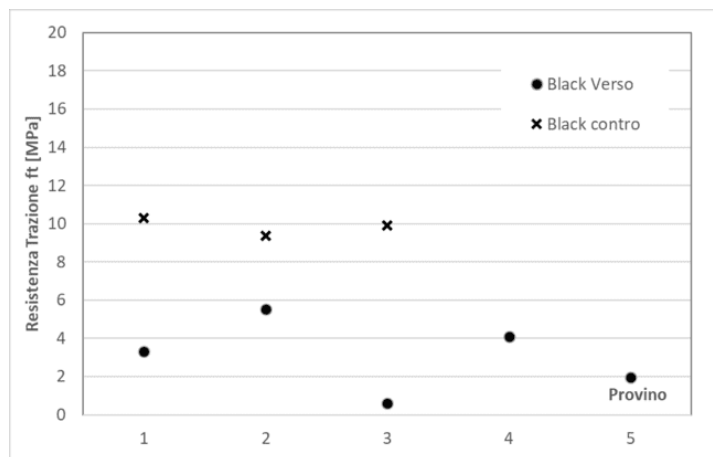
Figure 51: Flexural resistance of Black specimens
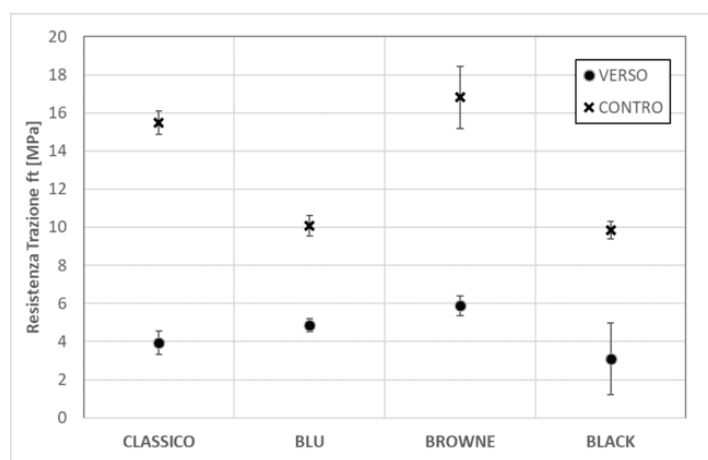
Figure 52: Average of the flexural resistance of each lithotype in each direction.

The results show, for all lithotypes, a greater resistance along the contro and lower in the verso, with a ratio of the two varying between 2.1 and 3.7. In one hand, the tensile strength along the contro varies between 3.1 (BLACK) and 5.9 (BROWN) MPa, on the other hand along the verso it varies between 9.9 (BLACK) and 16.8 (BROWN) MPa. In both directions, the lithotype called BLACK has the lowest resistance while the BROWN has the highest.

The results show a fairly contained dispersion varying between 4.0% and 15.6% except for the Black on the verso which showed a dispersion of 61.3%, as it can be seen in Figure 51.

4.7 Uniaxial Compression Test

The uniaxial compression tests were conducted on a total of 16 cylindrical samples: 2 for each lithotype and direction (towards and against). The tests were conducted by applying a load at a speed of approximately 2.5 kN/s.

The specimens were initially ground in order to make the bases perpendicular to their axis according to the requirements indicated in the ISRM recommendations (1979).

Each specimen was equipped with two pairs of diametrically opposed strain gauges: one pair arranged along the axial direction (BQ120-60 with grid length 57 mm and total length 67 mm) and the other along the circumference (BQ120-30 with length grid 30 mm and total length 36 mm).

The applied load, the deformations induced and the displacement of the plate measured with a LVDT were acquired with a frequency of 1 Hz.

The applied load and induced deformation values allowed to reconstruct the stress-deformation curves summarized in the following figures. In the annexes can be found the sheets of the specimens analyzed.
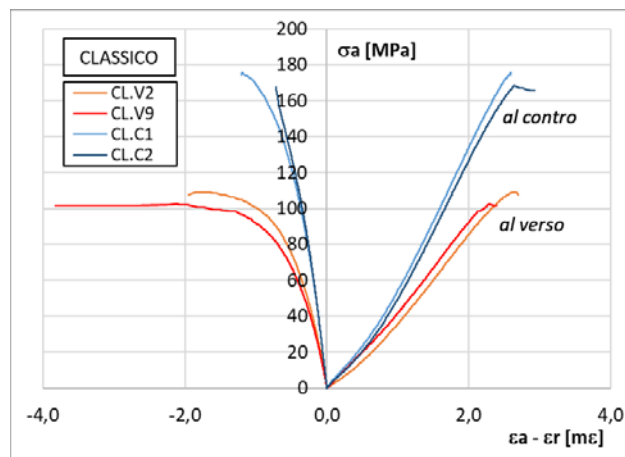
Figure 53: Curve tension-deformation from uniaxial compressive test for the lithotype CLASSIC.
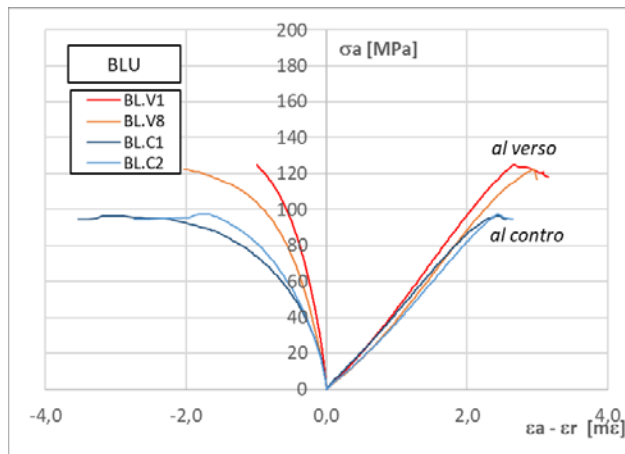
Figure 54: Curve tension-deformation from uniaxial compressive test for the lithotype BLUE.
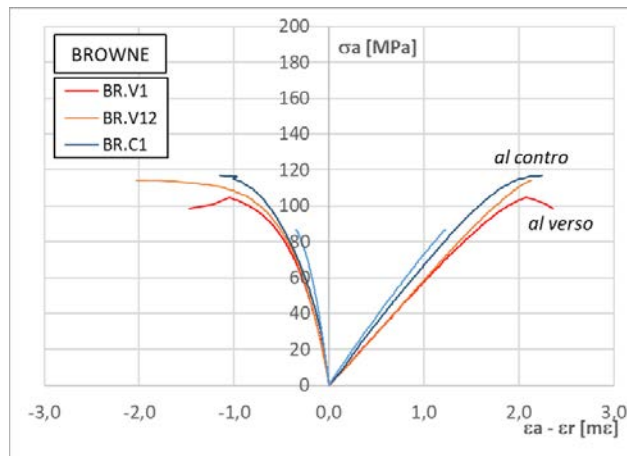
Figure 55: Curve tension-deformation from uniaxial compressive test for the lithotype BROWN.
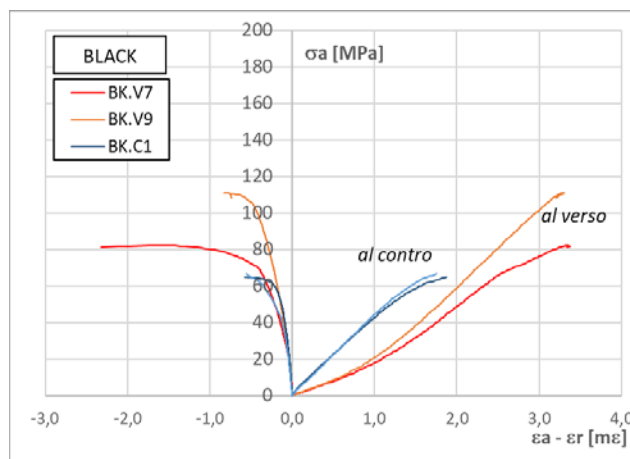
Figure 56: Curve tension-deformation from uniaxial compressive test for the lithotype BLACK.

In the figures showed previous for all the lithotypes it can be observed that the results of the uniaxial compressive strength show more similar resistance values in the contro and verso with ratios varying between 0.62 and 1.27.

The Classic shows the greatest anisotropy with an average resistance on the verso side of 172.0 (±3.3) MPa and on the contro of 109.2 (±3.7) MPa. For the other lithotypes the maximum resistance is in the verso and contro with average values equal to: Blue 123.8 (±1.4) – 97.1 (±0.5) MPa, Brown 109.4 (4.9) – 102.5 (± 15.7) MPa, Black 96.5 (±14.3) – 93.2 (±25.0) MPa. Black shows the lowest average values in both directions and a high dispersion of the measured values.

4.7.1 Elastic parameters

Lithotype	Specimen		Maximum strength UCS		Young's modulus				Poisson's ratio	
			UCS	average	Etan	average	Esec	average	v	average
			[N/mm²]	[N/mm²]	[GPa]	[GPa]	[GPa]	[GPa]	[--]	[--]
CLASSIC	Verso	CL.V2.C	109.2	105.9	47.2	47.1	39.2	41	0.22	0.25
		CL.V9.C	102.6		47		42.7		0.27	
	Contro	CL.C1.C	175.7	172	73.1	76.5	60.9	59.3	0.21	0.2
		CL.C2.C	168.3		80		57.7		0.19	
BLUE	Verso	BL.V1.C	125.1	123.8	60.3	56.2	46.6	44.3	0.19	0.22
		BL.V8.C	122.4		52.1		41.9		0.25	
	Contro	BL.C1.C	96.6	97.1	41.8	41.6	43.1	40.9	0.38	0.34
		BL.C2.C	97.6		41.3		38.6		0.31	
BROWN	Verso	BR.V1.C	104.5	109.4	56.4	57.5	58	58.5	0.26	0.26
		BR.V12.C	114.4		58.6		58.9		0.26	
	Contro	BR.C1.C	118.2	102.5	58.3	66.9	67.3	71.8	0.28	0.25
		BK.C3.C	86.8		75.5		76.3		0.21	
BLACK	Verso	BK.V7.C	82.2	96.5	33	37.5	23	26	0.08	0.08
		BK.V9.C	110.7		42		29		0.08	
	Contro	BK.C1.C	118.2	93.2	58.3	48.9	43.5	44	0.08	0.1
		BK.C3.C	68.1		39.6		44.5		0.12	

Table 14: Uniaxial Compressive strength, Young's modulus and Poisson's ratio values.
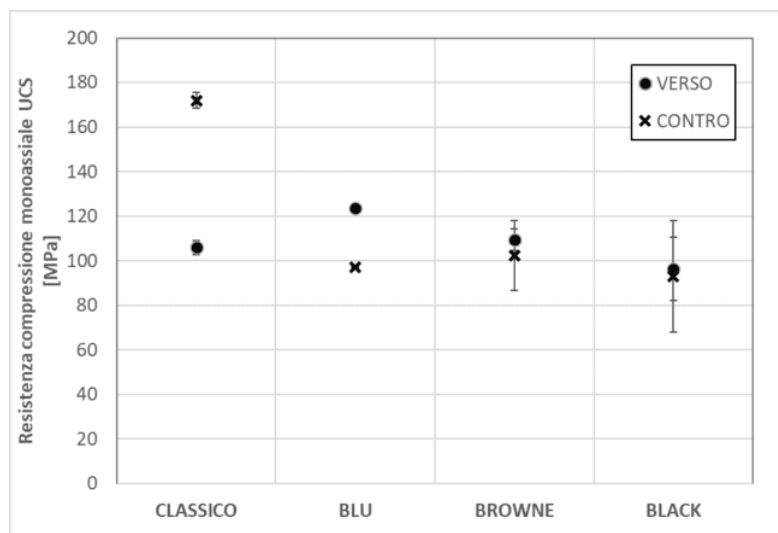
Figure 57: Average of the UCS of the specimens in each direction.
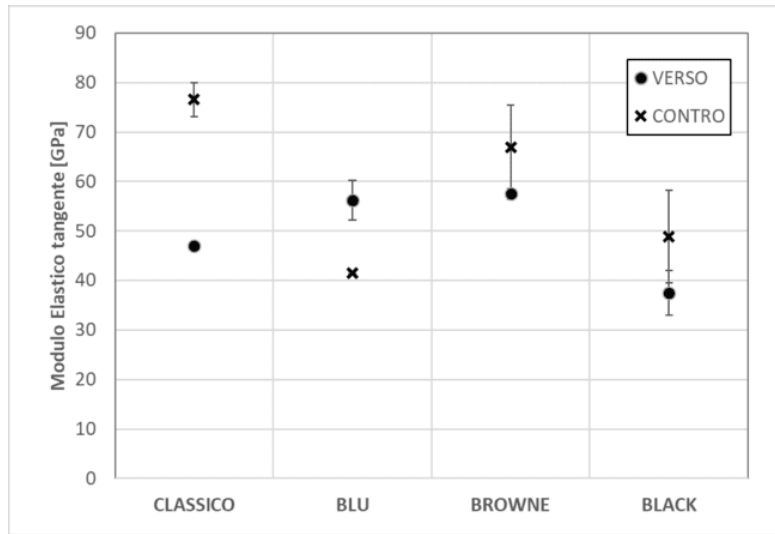
Figure 58: Average of the tangent Young's modulus of the specimens in each direction.
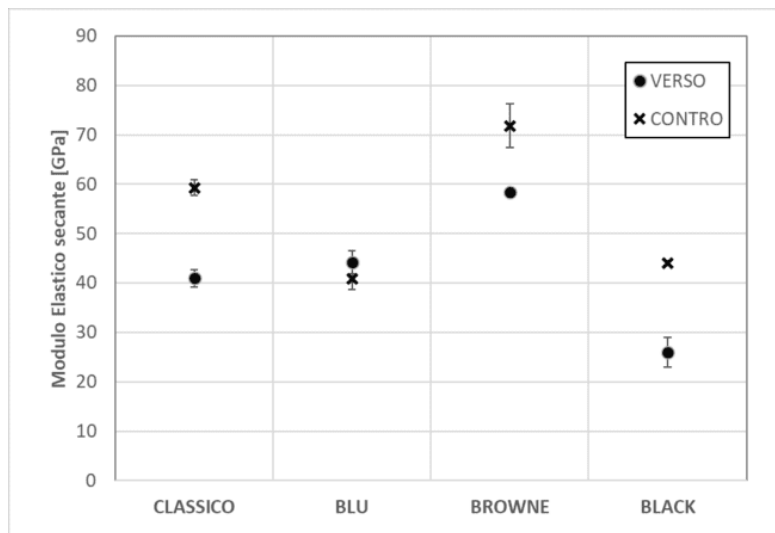
Figure 59: Average of the secant Young's modulus of the specimens in each direction.
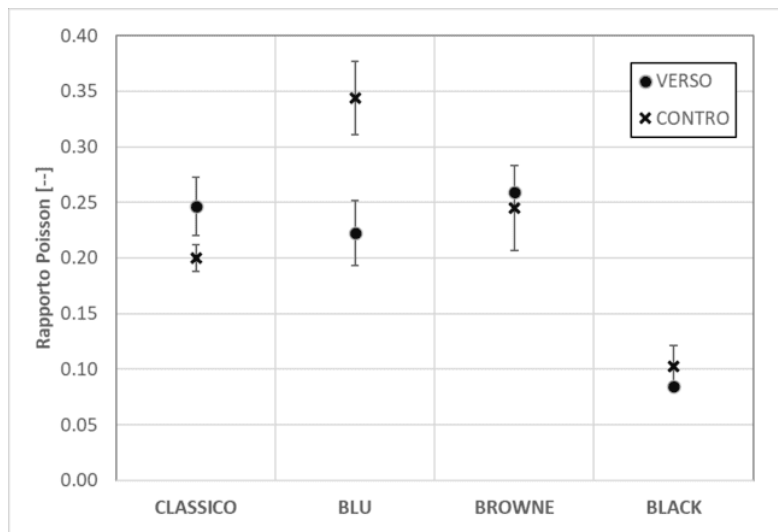
Figure 60: Average of the Poisson's ratio of the specimens in each direction.

The data were processed in order to determine from the Uniaxial Compressive Strength value (UCS), the tangent (E_t) and secant Elastic Modulus (E_s), both calculated at axial tension level equal to 50% UCS, and the Poisson's Ratio ν. The results are reported in Table 54 and represented in Figure 57. The values obtained for the tangent elastic modulus in the verso – contro are: Classic 47.1 (±0.1) – 76.5 (±3.4) GPa; Blue 56.2 (±4.1) – 41.6 (±0.3) GPa; Brown 57.5 (±1.1) – 66.9 (±8.6) GPa; Black 37.5 (±4.5) – 48.9 (±9.4) GPa. Same order of magnitude with slightly lower values for the secant elastic modules. The static Et values were compared with the dynamic values (from the pulse velocity tests) E_{dyn}, values, determined starting from the VP and VS values previously measured. Similarly, was done with Poisson ratios. Given the intrinsic inelasticity of the material, these values usually do not coincide; in this case the difference has a maximum ratio between static E_t and E_{dyn} equal to 2.35.

As regards the Poisson Ratio, it takes on a variable value between 0.1 and 0.35, assuming an average value of 0.25 for the Classic, Blue and Browne lithotypes while it is 0.1 for the Black.

4.8 Triaxial compression test:

The triaxial compression tests were conducted on a total of 14 cylindrical samples: 3 or 4 specimens for each lithotype carried out in the reverse direction. The tests were conducted in a Hoek cell, maintaining the cell pressure constant at 2, 4 and 8 MPa and applying the axial load with a speed of approximately 1 kN/s.

The specimens were initially capped in order to make the bases perpendicular to their axis and not to alter the measures performed by the strain gauges. Axial deformation was obtained from axial displacement measurements via lvdt measurements acquired during the tests. All load and displacement data were acquired with a frequency of 1 Hz.

Lithotype	Specimen		#GD TEST	Load speed [kN/s]	Peak σ3 [N/mm²]	Peak σ1 [N/mm²]	Residual σ1 [N/mm²]	Residual σ3 [N/mm²]
CLASSIC	Verso	CL.V1.C	17	2.25	2.00	127.9	2.0	26.4
CLASSIC	Verso	CL.V3.C	18	2.10	4.00	166.5	4.0	30.7
CLASSIC	Verso	CL.V12.C	19	2.40	8.00	189.4	8.0	55.5
BLUE	Verso	BL.V2.C	20	2.60	2.00	135.8	2.0	28.5
BLUE	Verso	BL.V6.C	21	2.60	4.00	159.2	4.0	30.3
BLUE	Verso	BL.V9.C	22	2.70	8.00	186.8	8.0	47.5
BROWN	Verso	BR.V2.C	29	2.80	12.00	125.6	12.0	57.6
BROWN	Verso	BR.V4.C	23	2.60	2.00	107.0	2.0	25.4
BROWN	Verso	BR.V5.C	24	3.00	4.00	123.4	4.0	35.5
BROWN	Verso	BR.V5.C	24	3.00	8.00	121.1	8.0	44.5
BLACK	Verso	BK.V3.C	27	2.50	2.00	110.5	2.0	23.1
BLACK	Verso	BK.V4.C	21	2.50	4.00	96.3	4.0	33.2
BLACK	Verso	BK.V8.C	28	2.70	12.00	129.8	12.0	74.4

Table 15: Triaxial compression strength results, peak and residual values.

4.8.1 Graphical representation of the triaxial compression test results:
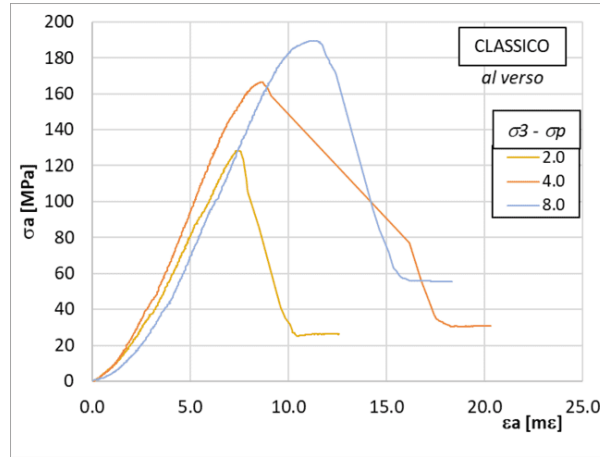
Figure 61: Load-deformation curve in Classic specimen in Verso direction.
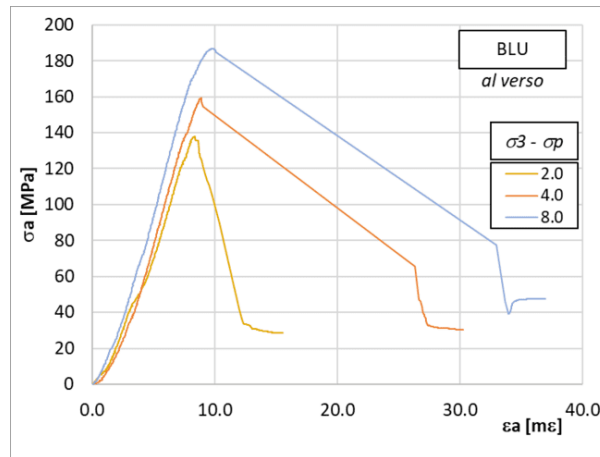
Figure 62: Load-deformation curve in blue specimen in Verso direction.
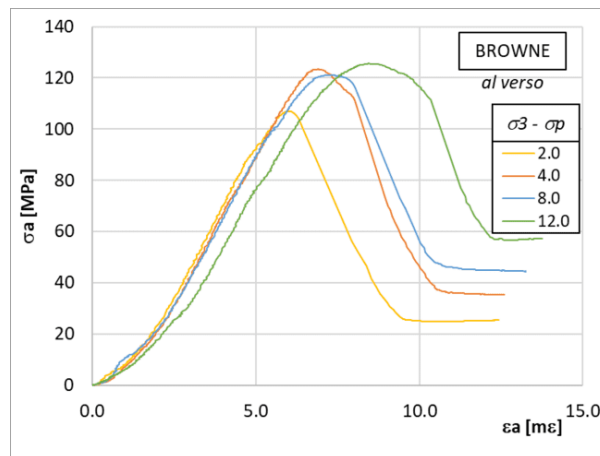
Figure 63: Load-deformation curve in Brown specimen in Verso direction.
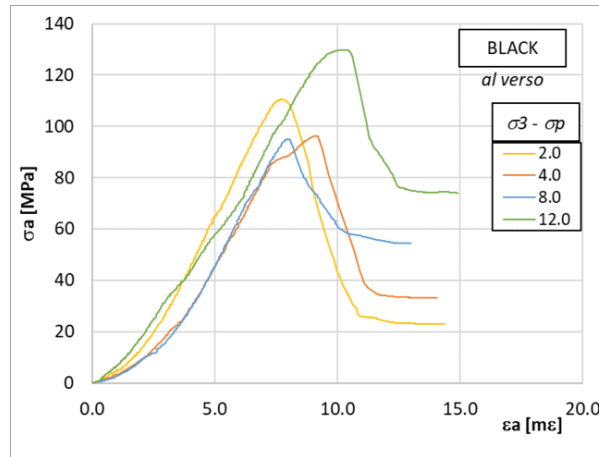
Figure 64: Load-deformation curve in Black specimen in Verso direction.

4.9 Strength Criteria

With the results obtained from the uniaxial and triaxial compression tests and the flexural test, the values of the principal stresses are listed and plotted in order to perform the linearization process of Hoek & Brown.

		CLASSIC		BLUE		BROWN		BLACK	
		$\sigma 1$ [MPa]	$\sigma 3$ [MPa]	$\sigma 1$ [MPa]	$\sigma 3$ [MPa]	$\sigma 1$ [MPa]	$\sigma 3$ [MPa]	$\sigma 1$ [MPa]	$\sigma 3$ [MPa]
FLEXURAL		0	-4.76	0	-5.35	0	-5.27	0	-5.51
		0	-3.72	0	-4.66	0	-6.04	0	-4.09
		0	-4.29	0	-4.49	0	-6.22	0	-1.94
				0	-4.75				
UNIAXIAL		109.2	0	125.1	0	104.5	0	82.2	0
		102.6	0	122.4	0	114.4	0	110.7	0
TRIAX	PEAK	127.9	2.0	135.8	2.0	107.0	2.0	110.5	2.0
		166.5	4.0	159.2	4.0	123.4	4.0	96.3	4.0
		189.4	8.0	186.8	8.0	121.1	8.0	129.8	12.0
						125.6	12.0	95.0	8.0
	RESIDUAL	26.4	2.0	28.5	2.0	57.6	12.0	23.1	2.0
		30.7	4.0	30.3	4.0	25.4	2.0	33.2	4.0
		55.5	8.0	47.5	8.0	35.5	4.0	74.4	12.0
						44.5	8.0	54.4	8.0

Table 16: Uniaxial and Triaxial compression test results.

From the flexural test, the maximum values are taken, these values correspond to the $\sigma 3$ axis, in $\sigma 1$ the values are zero since there are no axial stresses. From the uniaxial compression tests, the maximum strength values to compression correspond to $\sigma 1$ axis and since there are no confining pressure in the test the values of $\sigma 3$ are zero. From the triaxial test, the peak and residual values are obtained from the curve of the triaxial compressive test, being the peak

value, the highest axial stress reached by the material under the corresponding cell pressure of the test and the residual value is the value when the curve becomes constant after the peak value, in total 3 peak and 3 residual values are shown each one corresponding to the test at 2, 4 and 8 MPa, of confining pressure. These values are listed for each lithotype in Table 16.

From the equation obtained from every tendency line drawn, the Hoek & Brown parameters are obtained as it was stated in Equation (11), remember that σ_{ci} and m_i are parameters obtained from the linearization process previously performed. The principal stresses values and the H&B parameters for all the lithotypes are presented next.

Plotting the peak and residual values:
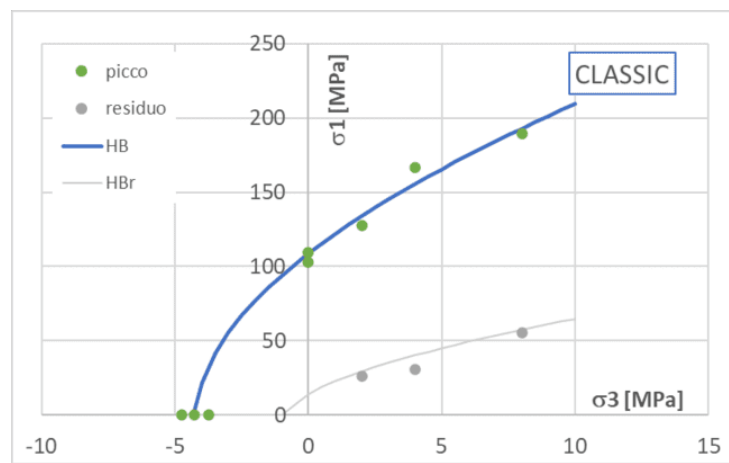
Figure 65: Peak and residual linearization of H&B for Classic marble.
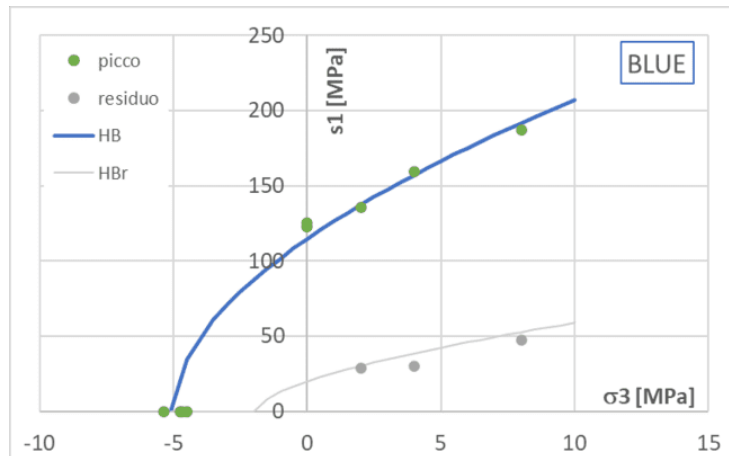
Figure 66: Peak and residual linearization of H&B for Blue marble.
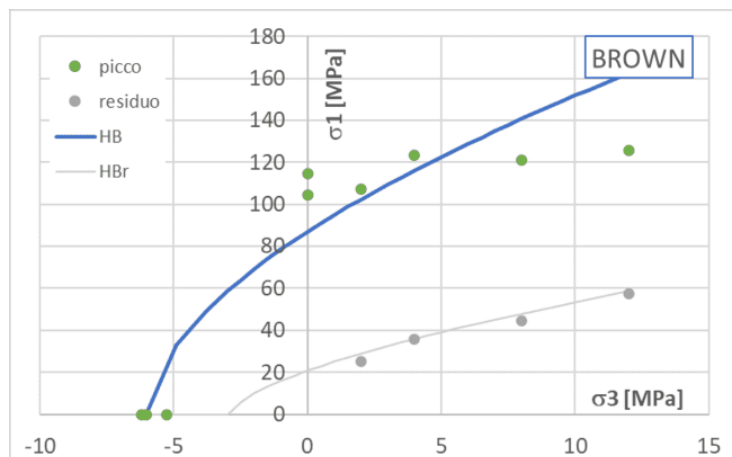
Figure 67: Peak and residual linearization of H&B for Brown marble.
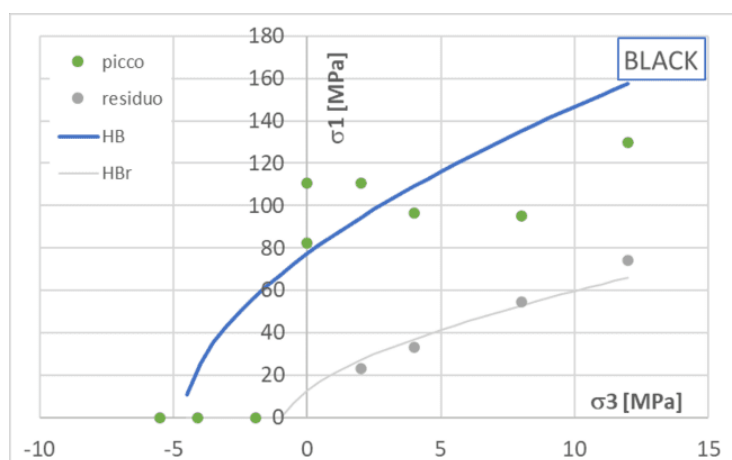
Figure 68: Peak and residual linearization of H&B for Black marble.
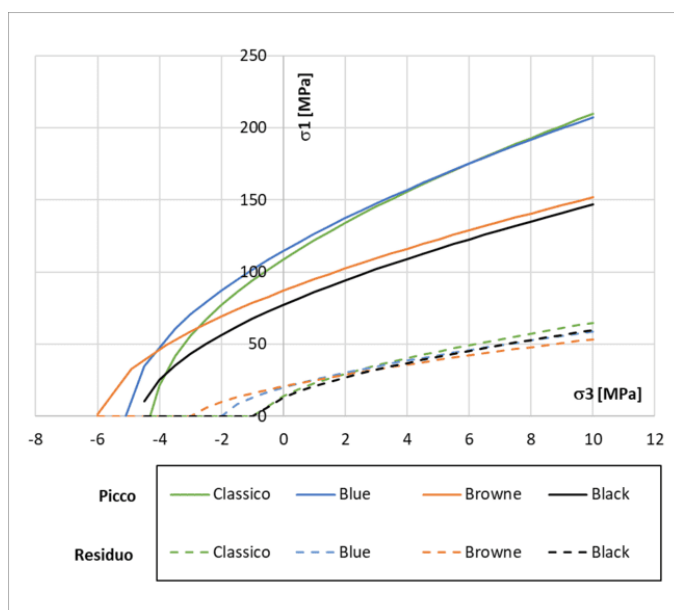
Figure 69: Summary of peak and residual H&B linearization for all the marble types.

It can be seen that the values are less dispersed in CLASSIC and BLUE while in BLACK and BROWN are very dispersed.

The value of the cohesion of the residual values is very low compared with the peak ones because cohesion is a component of the shear strength of the material, once it has undergone very large strains this value reduces drastically.

4.9.1 Mohr-Coulomb linearization

This criterion is also a linear strength criterion represented by equation (13), where the friction angle and the cohesion are calculated by substituting the known values of the slope and intercept in the equation. The substitution of these values in the equation are presented next figures.
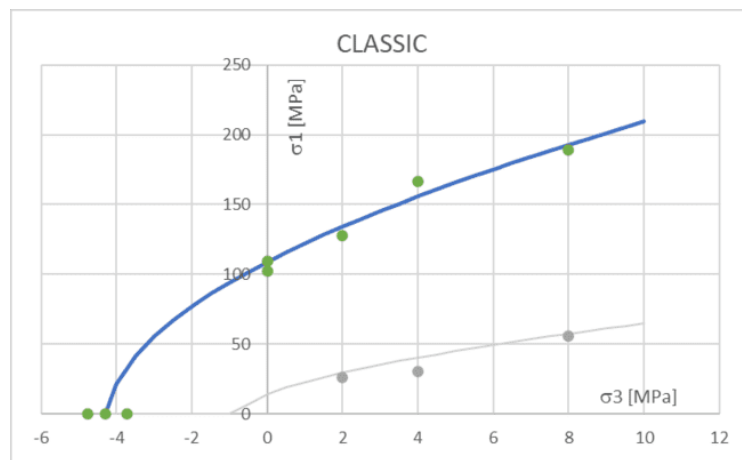
Figure 70: Mohr-Coulomb linearization for classic material.
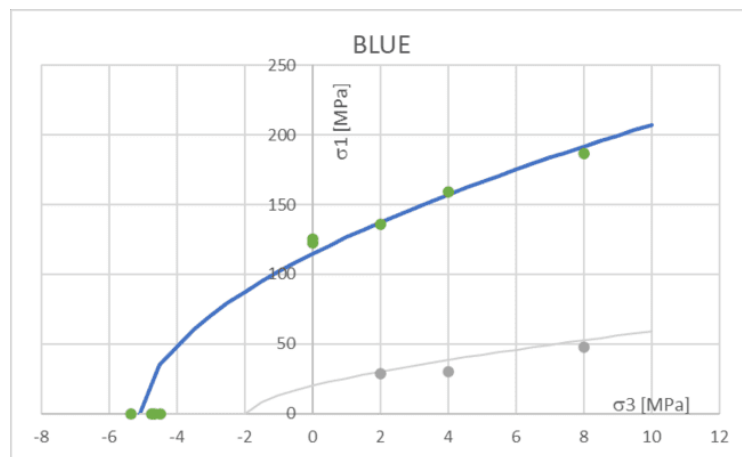
Figure 71: Mohr-Coulomb linearization for blue material.
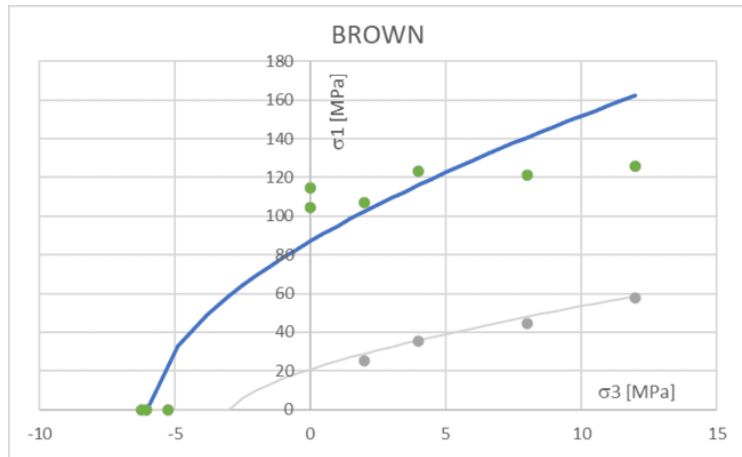
Figure 72: Mohr-Coulomb linearization for brown material.
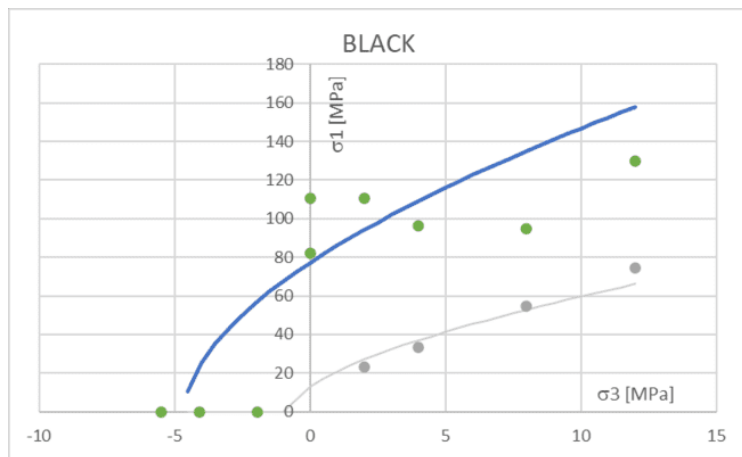
Figure 73: Mohr-Coulomb linearization for black material.

4.9.2 Summary of the mechanical values of the four materials:

In the context of pulse propagation in general can be said that the velocity values of pulse propagation for both compression and shear waves are greater in the contro than in the verso.

The lithotype BROWN has the greatest value of Vp and Vs, this means that is a very stiff material with low deformations.

The materials BLACK has the values most spread, as it was stated before this is because the great presence of heterogeneities in the material itself.

	Unit weight volume	UPV Compression				UPV Shear			
		contro		Verso		contro		Verso	
	γ	V_P	err.	V_P	err.	V_S	err.	V_S	err.
	[kN/m³]	[m/s]	[%]	[m/s]	[%]	[m/s]	[%]	[m/s]	[%]
Classic	28.3	4297	1%	3510	0%	2660	0%	2472	0%
Blue	28.3	4974	6%	3688	11%	2968	17%	2685	7%
Brown	28.3	5934	2%	5165	1%	3374	4%	3103	1%
Black	29	5564	3%	3332	1%	3107	0%	2196	1%

Table 17: Wave propagation

	Dynamic Young's modulus				Dynamic shear modulus				Dynamic Poisson's ratio				Bulk Modulus	
	contro		Verso		contro		Verso		contro		Verso		contro	Verso
	E_{dyn}	err.	E_{dyn}	err.	G_{dyn}	err.	G_{dyn}	err.	ν_{dyn}	err.	ν_{dyn}	err.	K_{dyn}	E_{dyn}
	[GPa]	[%]	[GPa]	[%]	[GPa]	[%]	[GPa]	[%]	[-]	[%]	[-]	[%]	GPa	GPa
Classic	48	1%	35	0%	20	1%	17	0%	0.19	5%	0.01	0%	40	18
Blue	61	25%	38	24%	25	35%	21	14%	0.22	45%	-0.08	-100%	35	22
Brown	81	5%	67	0%	32	8%	27	1%	0.26	15%	0.22	5%	62	39
Black	72	1%	32	0%	28	1%	14	0%	0.27	7%	0.12	0%	52	11

Table 18: Dynamic mechanical parameters.

The values of the tensile strength are the greater in contro than in verso, on contrary the values for the compression test are grater in verso than in contro with the exception of the classic specimen, being the less resistant the BLACK lithotype and BROWN and CLASSIC the highest values for tensile and compression strength respectively.

	Tensile strength				Compression strength			
	contro		Verso		contro		Verso	
	ft	d.s.	ft	d.s.	UCS	error	UCS	error
	[MPa]	[%]	[MPa]	[%]	[MPa]	[±MPa]	[MPa]	[±MPa]
Classic	15.5	4.0%	4.0	15.6%	172.0	3.7	105.9	3.3
Blue	10.1	5.4%	4.9	7.0%	97.1	0.5	123.8	1.4
Brown	16.8	9.8%	5.9	8.6%	102.5	15.7	109.4	4.9
Black	9.9	4.7%	3.7	40.1%	93.2	25.0	96.5	14.3

Table 19: Tensile and compressive strength.

Talking about statical mechanical parameters, static elastic modulus E is different depending on the direction of measurement. The values obtained for the tangent elastic modulus in verso – contro are: Classic 47.1 (±0.1) – 76.5 (±3.4) GPa; Blue 56.2 (±4.1) – 41.6 (±0.3) GPa; Browne 57.5 (±1.1) – 66.9 (±8.6) GPa; Black 37.5 (±4.5) – 48.9 (±9.4) GPa. Same order of magnitude with slightly lower values for the secant elastic modules.

	Tangent Young's modulus				Secant Young's modulus				Poisson's ratio			
	contro		Verso		contro		Verso		contro		Verso	
	E_{tan} [GPa]	error [±GPa]	E_{tan} [GPa]	error [±GPa]	E_{sec} [GPa]	error [±GPa]	E_{sec} [GPa]	error [±GPa]	ν [-]	error [±]	ν [-]	error [±]
Classic	76.5	3.4	47.1	0.1	59.3	1.6	41.0	1.8	0.2	0.01	0.25	0.03
Blue	41.6	0.3	56.2	4.1	40.9	2.2	44.3	2.3	0.34	0.03	0.22	0.03
Brown	66.9	8.6	57.5	1.1	71.8	4.5	58.5	0.4	0.25	0.04	0.26	0.04
Black	48.9	9.4	37.5	4.5	44	0.5	26.0	3.0	0.2	0.02	0.2	0.00

Table 20: Mechanical parameters.

	Tangent shear modulus		Shear modulus	Tangent bulk modulus	
	G contro [GPa]	G verso [GPa]	G [GPa]	K contro [GPa]	K verso [GPa]
Classic	32	19	23	43	31
Blue	16	23	19	43	33
Brown	27	23	24	45	40
Black	20	16	17	27	21

Table 21: Shear and bulk modulus.

In terms of the Hoek and Brown criterion, two classes of peak resistance are distinguished. CLASSIC and BLUE lithotypes belong to the first and have a σ_{ci} value of approximately 112 MPa and mi = 24, in average. BROWN and BLACK lithotypes belong to the second class with σ_{ci} of approximately 84 MPa and mi = 15.5 average. In residual conditions the situation changes being the highest values of the σ_{ci} BLUE and BROWN of 20.4 MPa, while CLASSIC and BLACK has the lowest values of 13.3 MPa.

	Hoek and Brown parameters				Mohr Coulomb parameters			
	Peak		Residual		Peak		Residual	
	σ_{ci} [MPa]	mi [--]	σ_{ci} [MPa]	mi [--]	c [MPa]	ϕ [°]	c [MPa]	ϕ [°]
Classic	108.8	25.7	14.0	20.0	15.4	57.1	4.4	40.7
Blue	114.6	22.5	19.9	10.0	13.6	68.4	5.1	37.0
Brown	87.0	14.4	20.8	7.0	11.9	66.4	5.4	33.7
Black	77.2	16.5	12.8	18.0	11.2	64.9	4.1	39.1

Table 22: Hoek and brown and Mohr-Coulomb parameters from linearization.

5 NUMERICAL MODEL

Once the mechanical parameters of all the materials are calculated the numerical model in UDEC can be made, the model's dimension is based from the information available of the topography of the place performed by a previous geological study. The coordinates of the profile were obtained from aerial photos processed and converted into an AutoCAD model where the values of the coordinates of each relevant point were extracted and given to UDEC. Then the material assignment was performed giving the corresponding values to the different areas existing in the profile. First it must be assigned the limits of the model as an entire geometric figure, these limits are called the block system, this block will contain different joints inside in order to build a model, and then it either can be meshed to simulate a series of deformable blocks or either rigid block.

5.1 Model setting

The stratigraphy of the model is shown in Figure 74. Previously defined materials, BLUETTE and TIGRATO have the same mechanical properties as BLUE and BROWN respectively, to build this numerical model they were assigned as it.
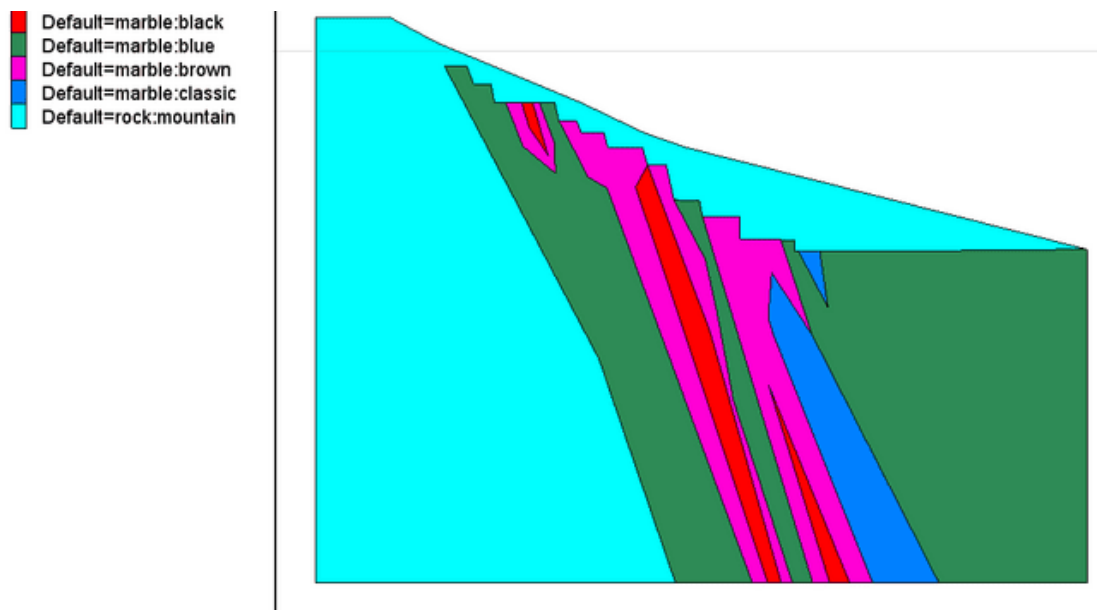
Figure 74: Profile numerical model

Since there were not the required tests to get the properties of the fractures, the mechanical parameters, assigned to this system, were obtained from literature and other projects with simile characteristics.

The fractures are not distributed equally, they were assigned randomly to the model by specifying the inclination, this last with no variation and the spacing, trace and gap by assigning an average value and applying a standard deviation, in this way it will not be a constant system and can be represented according to the reality. In the software the discontinuities are called joints, and the condition of a joint is to cross a block completely,

otherwise they will not be generated. The final model including the discontinuities looks like:
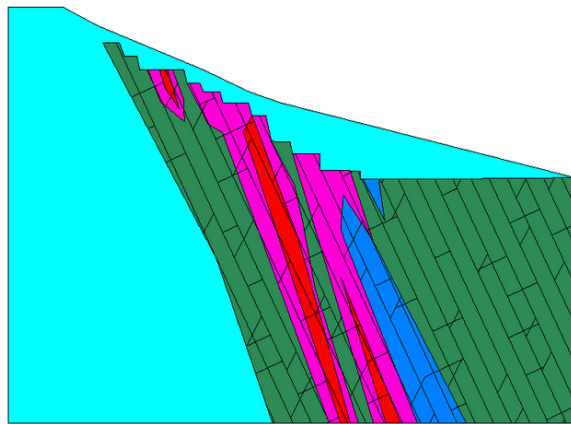
Figure 75: Profile of the marble materials and discontinuity systems.

It has a height of 201.5m and a total length of 254.3m

Since the model has a complex geometry, the lithotypes are mixed into the same block and there is presence of multiple discontinuities along all the block, a simplified model was performed by building all the existent blocks with a unique material, in this way the joints between the materials had not to be modeled and the formation of little blocks will not happen; in total 2 models were performed the best and the worst lithotype, talking about mechanical properties, CLASSIC and BLACK respectively.

In order to not have any problems with the boundaries the original model was extended in x and y direction in positive and negative direction respectively, the new model will look as it's shown in the next figure:
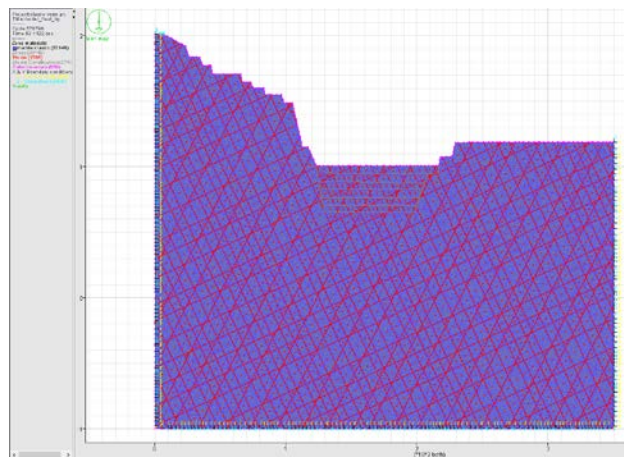
Figure 76: Simplified model.

This model has a total height of 301 m and a length of 350 m. As it can be seen there is only the presence of one material and the system of discontinuities assigned their respective parameters.

5.1.1 Excavation phases:

According to the projection of the maximum depth to reach, the excavation was represented in different phases close to a real depth that an excavation can be performed, they were represented in the model without any mechanical property in this way they are just representing the limits to perform the cut of the material on each phase and calculate the equilibrium state, these lines are represented as gray lines and in the model they are called construction joints as it can be seen in the next figure.
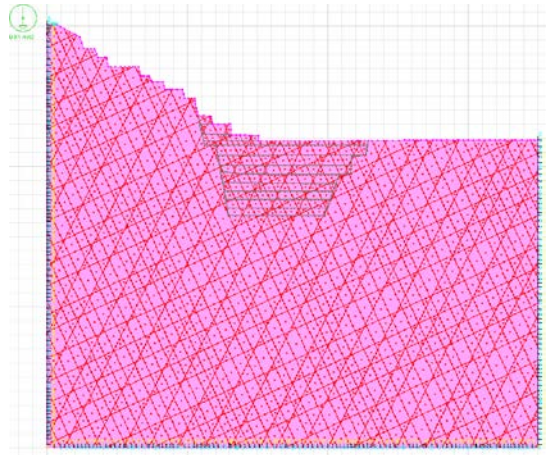
Figure 77: Excavation phases on the model.

5.1.2 Meshing:

In this case the model will be represented as a deformable block since the deformations and the state of stresses are going to be analyzed, therefore the mesh size must be defined. In the software the mesh represents a subdivision of the block of a specific size, the value defined for the mesh will mean the maximum size of a subdivided block in a specific zone, for example a mesh of 10 will create sub-blocks inside the first block, each one with a size of 10m in the borders. A little mesh (i.e.1.0) will give a best representation of the stress distribution and the displacements, but it will take much more time to perform the number of minimum cycles (by default 100.000) required to the software to reach the convergence in the system. A difference in the mesh can be seen in the next figures:
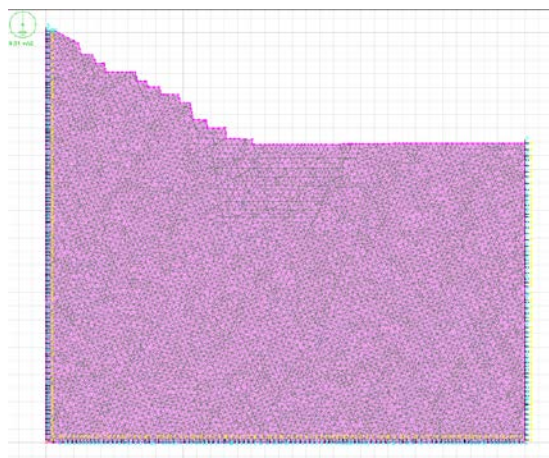
Figure 78: Block with a mesh of 3.0

5.1.3 Material assignment:

In order to assign the lithotype to a specific zone, the model of this must be specified. In this case the Mohr-Coulomb plastic model was chosen, it is the best, among the other options, that adjust to the type of behavior the analyzed material has.
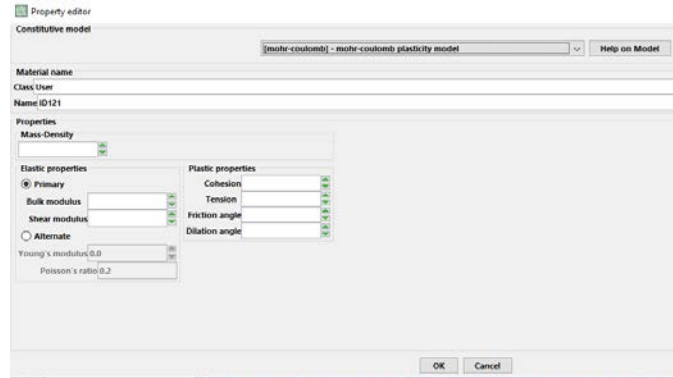
Figure 79: Mohr-Coulomb plasticity model availbale in the software.

5.1.4 Joints material assignment:

The mechanical parameters to the discontinuities and existing fractures are assigned to the model through this option. For this the Mohr-Coulomb model was available, since the values of cohesion and friction angle were already calculated they could be assigned for the discontinuities that separate the different lithotypes.
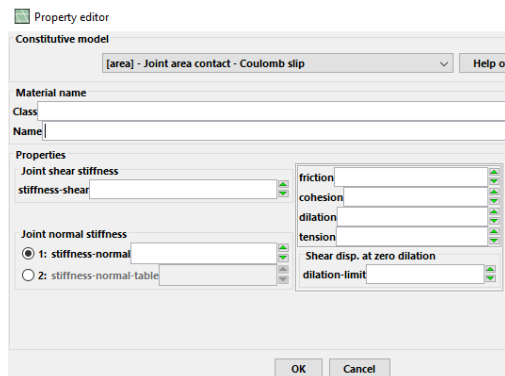
Figure 80: Joint's mechanical properties assignment.

In order to calculate the mechanical properties for the fractures an analysis of the trace and gap of the discontinuities was performed, from the fact that if the discontinuity has no gap the value of the cohesion will be the peak value of Mohr-Coulomb for the corresponding material, from Table 22.

To illustrate an example is shown for the case of a discontinuity in the Blue lithotype with a length of 30m and a gap of 15m:

If the gap will be 0 it means 30m is 100% in this case is 15 so it's a 50% of the total length, in this case the cohesion for that discontinuity will be 6.5 MPa.
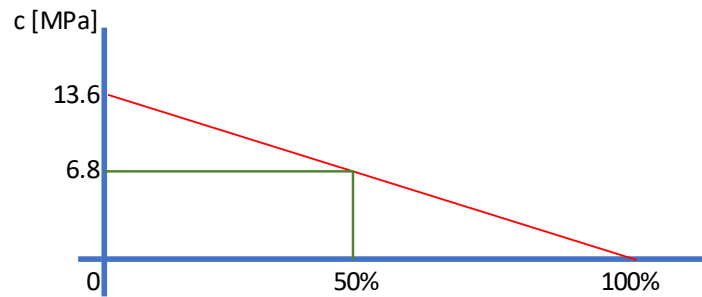
Figure 81: Criteria to calculate the cohesion for the discontinuities.

In the case of the values of kn and ks the criteria applied was already defined in Chapter 2 of this work in Equation (12). The values for each lithotype are presented next:

	Parameters H&B								Rock mass			
	Peak		Residual		Intact Rock							
	σci	mi	σci	mi	Er	Gr	Spacing	GSI	Em	Gm	kn	ks
	[MPa]	[--]	[MPa]	[--]	[MPa]	[MPa]	[m]	[-]	[MPa]	[MPa]	[MPa/m]	[MPa/m]
Classic	108.8	25.7	14.0	20.0	47100	19224	8	20	665	272	84	34
Blue	114.6	22.5	19.9	10.0	56200	21953	8	20	793	310	101	39
Browne	87.0	14.4	20.8	7.0	57500	22908	8	20	811	323	103	41
Black	77.2	16.5	12.8	18.0	37500	15625	8	20	636	265	81	34

Table 23: Values of kn and ks for the discontinuities.

5.1.5   Boundary conditions

Boundary conditions must be assigned to the model corresponding to the real conditions, in this case the vertical borders must be fixed in x direction, in this mode displacements can occur in the case they perform, for the contrary in the bottom border y direction is fixed in this way the model will not translate from the initial point, in UDEC instead of applying a support it is defined as velocity in the desired direction. They are represented with the letter F in the model.
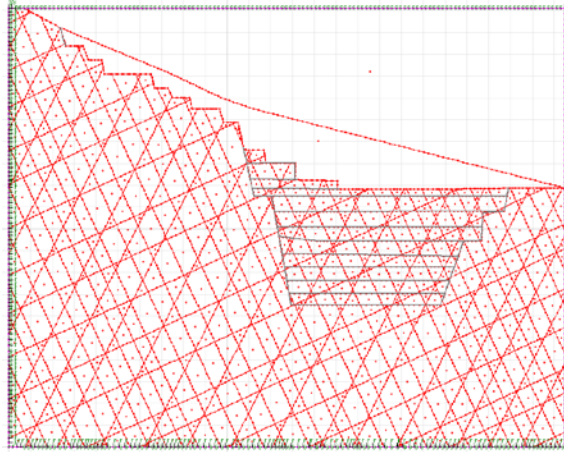
Figure 82: Boundary conditions applied on the corresponding edges of the block.

5.1.6   Initial state of stresses

Initial state of stresses must be assigned to the block, this model originally has a slope that is not regular, instead of analyzing the values of the slope corresponding to the change in the stresses in σ_x and σ_y direction a way to simplify the model is to construct and entire regular block (a rectangle in this case), apply the initial stresses:

$\sigma_y = \gamma*h*g$

$\sigma_x = \sigma_y *Ko$

Where:

σ_x and σ_y are the stresses in horizontal and vertical direction respectively.

γ= material density (2830 kg/m^3)

h= total height of the block (201.5m)

g= gravity (9.81 m/s^2)

Ko=anisotropy of the system

UDEC requires an equation with the initial values of stresses at point 0,0 and the variation in the x and y axis. Being a regular shape block there is no variation in x axis, only in y from the highest values of stresses at point 0,0 and arriving to 0 in all the upper contour of the block.
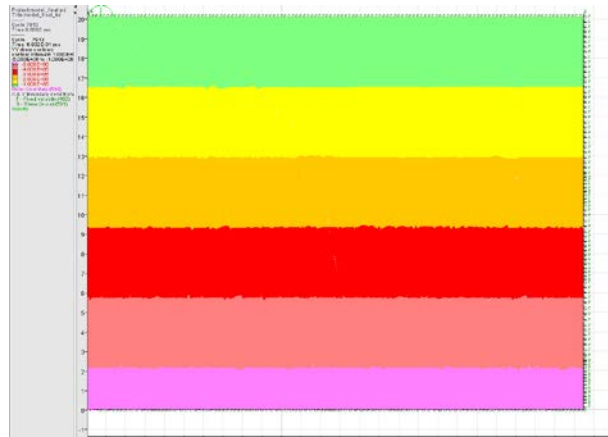
Figure 83: Stress distribution in σ_y.
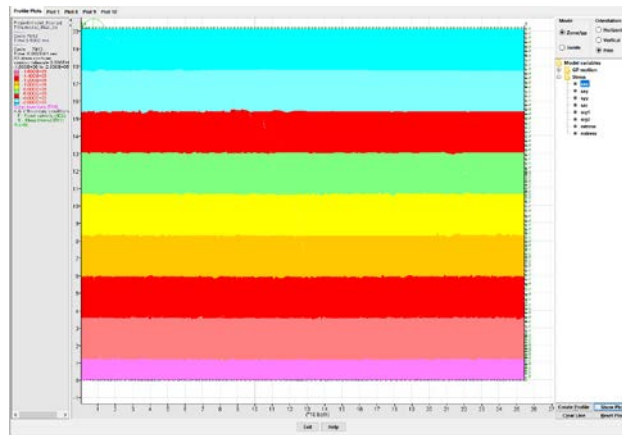
Figure 84: Stress distribution in σ_x.

A verification of the correct assignation of the stresses is to check if the stresses in the initial point are the same to the ones specified in the equation and if in the upper edge are zero.

5.1.7 Resetting displacements and excavation phases:

The phases of excavation until reach the deepest point was performed in 9 steps, being the first one the cutting of the block zone existing over the original slope and then the displacements resetting to zero, this last must be performed in order to analyze correctly the real displacements developed during the excavations without considering the ones developed when the model was altered and run for the first time.

Figure 85: Displacements reset to 0.

5.2 Final stage of the simplified model

The last stage of the quarry is when the last excavation is performed, the analysis will be performed about the left face of the excavation zone, since is desired to determine the state of stresses and maximum displacements developed in that zone, and if the case of developed plastic zones.

The next figure shows the state of the last stage:
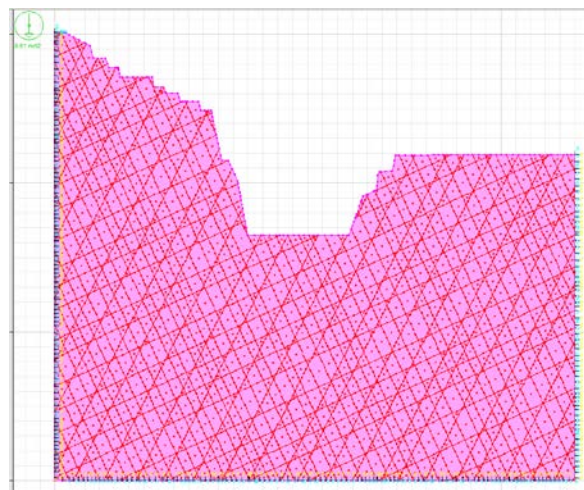
Figure 86: Last stage of excavation.

The state of stresses in the last stage will be:
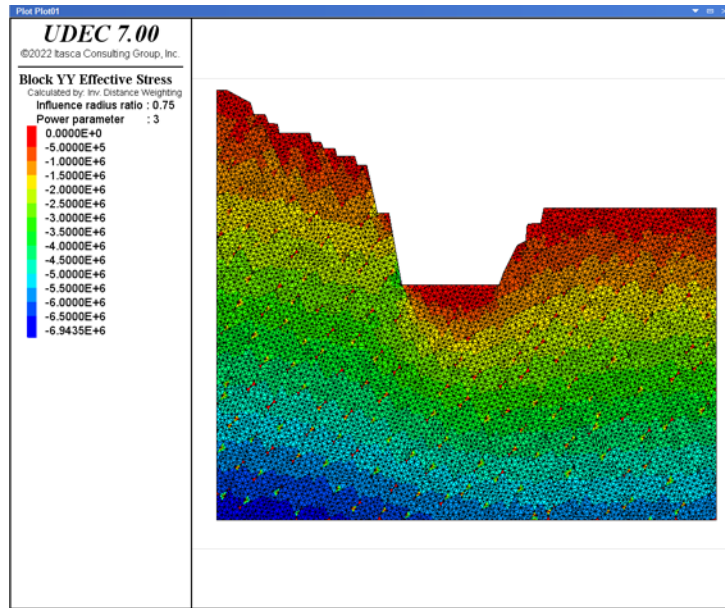
Figure 87: Vertical stress on last stage.
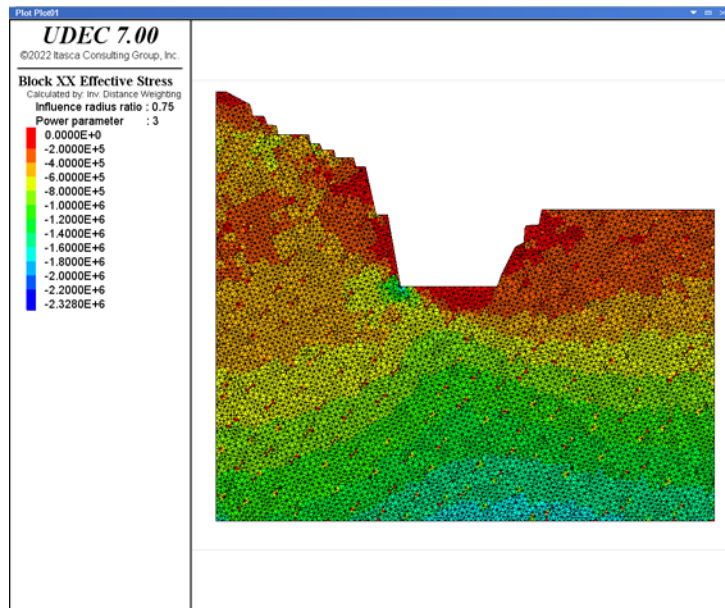
Figure 88: Horizontal stresses on last stage.

The stress distribution is similar as it was before performing the excavation, however there are zones where the stresses are distributed heterogeneously, this is because of the presence of discontinuities in the system.

The displacements in the last stage are:
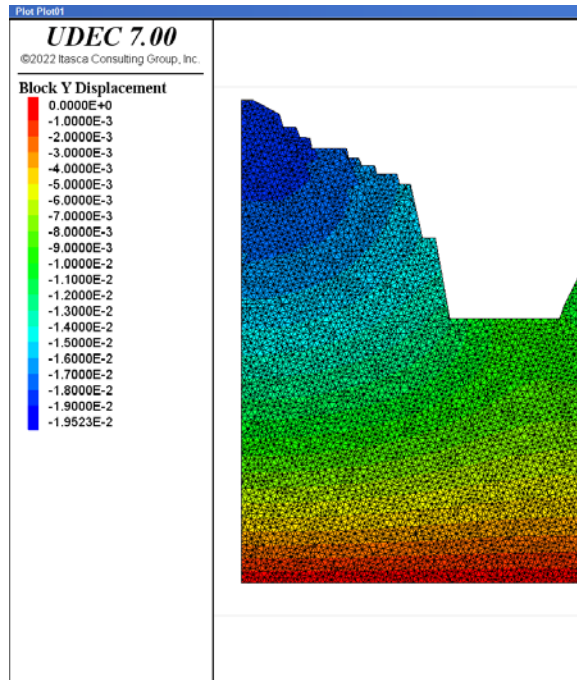
Figure 89: Vertical displacements on the last stage.
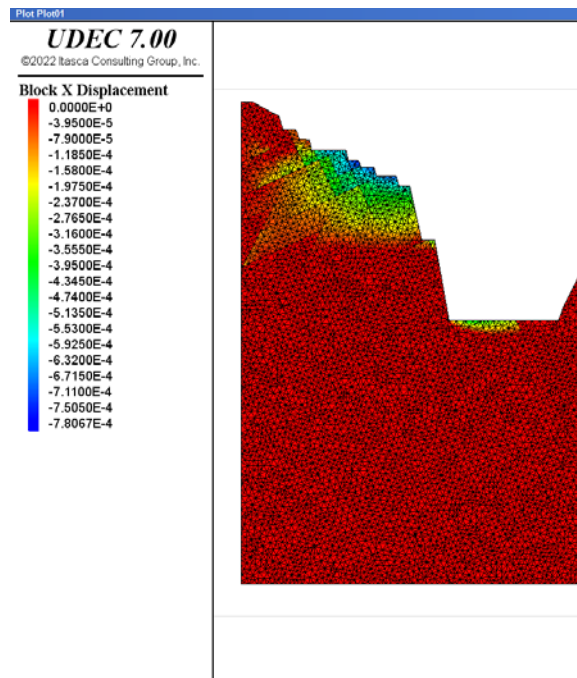
Figure 90: Horizontal displacements on the last stage.

In vertical direction the maximum displacement is about 2cm while in the horizontal direction the maximum displacement is less than 1mm.

The vectors of the displacements are:
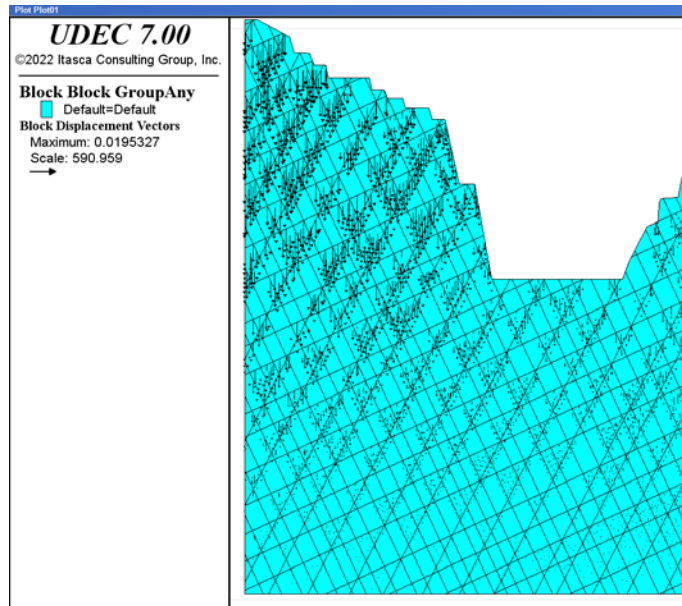
Figure 91: Vectors of the displacements.

Emphasizing the displacement in the analyzed zone:
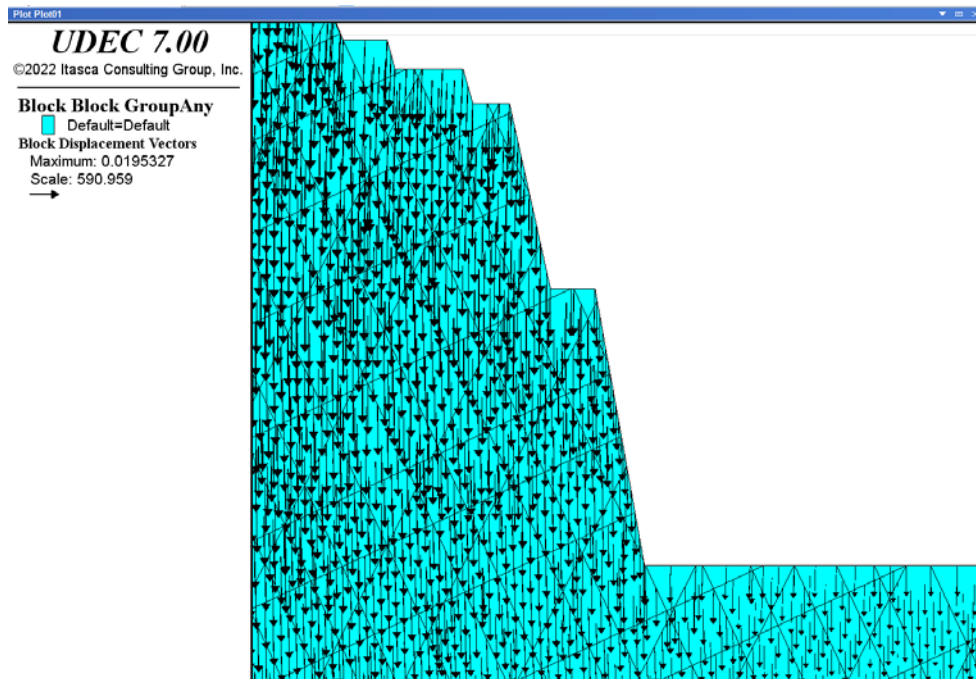
Figure 92: Vectors of displacements.

The direction of the rows indicates a predominance in the vertical direction, this makes sense with the results of the displacements previously showed.

6 CONCLUSIONS

In general, the results obtained for the physical and mechanical parameters of the studied specimens are in an expected range of values, this based on previous studies and scientific researches of the same lithotypes.

The weight of the unit volume is 28.3 kN/m3 for Classic, Blue and Brown and 29.0 kN/m3 for Black.

In the context of pulse propagation in general can be said that the velocity values of pulse propagation for both compression and shear waves are greater in the contro than in the verso.

By looking at the results it can be inferred that the presence of cracks and/or heterogeneities are less in contro than in verso, higher pulse velocity means that the medium has a smooth path where waves are traveling in.

In Uniaxial Compressive Strength context, the results show, for all lithotypes, a greater resistance along the contro and lower in the verso, with a ratio of the two varying between 2.1 and 3.7 respectively. In one hand, the tensile strength along the contro varies between 3.1 (BLACK) and 5.9 (BROWN) MPa, on the other hand along the verso it varies between 9.9 (BLACK) and 16.8 (BROWN) MPa.

The Classic lithotype shows the greatest anisotropy with an average resistance on the verso side of 172.0 (±3.3) MPa and on the contro of 109.2 (±3.7) MPa. For the other lithotypes the maximum resistance is in the verso and contro with average values equal to: Blue 123.8 (±1.4) – 97.1 (±0.5) MPa, Browne 109.4 (4.9) – 102.5 (± 15.7) MPa, Black 96.5 (±14.3) – 93.2 (±25.0) MPa.

Black lithotype shows the lowest average values in both directions and a high dispersion of the measured values.

The values obtained for the tangent elastic modulus in the verso – contro are: Classic 47.1 (±0.1) – 76.5 (±3.4) GPa; Blue 56.2 (±4.1) – 41.6 (±0.3) GPa; Brown 57.5 (±1.1) – 66.9 (±8.6) GPa; Black 37.5 (±4.5) – 48.9 (±9.4) GPa.

From Hoek and Brown linearization the values of lithotypes CLASSIC and BLUE are less dispersed than lithotypes BLACK and BROWN.

The stress distribution in the last stage is similar as it was before performing the excavation, however there are zones where the stresses are distributed heterogeneously, this is because of the presence of discontinuities in the system.

From the results of the numerical model the displacements performed in the last stage in the vertical direction are 2cm, this value compare with the block size (about 2m the smallest one) is acceptable to say that there is a stability of the system.

The complexity of this model made to represent it as a simplified model, however for future research works it can be better represented together with more laboratory tests, specially in the BROWN and BLACK lithotype, which had the most dispersion in the laboratory results and mechanical parameters.

7 ANNEXES

7.1 Pulse velocity in prismatic specimen

Lithotype	Specimen	Length [mm]	Height [mm]	Width [mm]	Area [mm²]	Volume [mm³]	Weight [g]	Density [g/mm³]	[kg/m³]	Vp [m/s]	ds [m/s]	Average [m/s]
CLASSIC VERSO	CL.V1.B	220.26	60.41	29.95	1808.83	398412.39	1128.20	0.002832	2831.74	3401.38	29.61	
	CL.V2.B	220.17	60.35	29.96	1807.63	397986.88	1127.60	0.002833	2833.26	3360.36	8.42	
	CL.V3.B	220.23	60.63	30.05	1821.78	401210.88	1136.70	0.002833	2833.17	3303.84	16.22	
	CL.V4.B	220.21	60.40	30.05	1814.57	399585.97	1129.50	0.002827	2826.68	3387.08	34.00	
	CL.V5.B	220.25	60.02	30.06	1804.20	397375.31	1108.70	0.002790	2790.06	3338.21	17.76	
	CL.V6.B	220.25	60.44	30.04	1815.32	399823.22	1132.90	0.002834	2833.50	3354.49	18.92	
	CL.V7.B	220.20	60.23	29.82	1796.06	395492.10	1121.10	0.002835	2834.70	3443.17	41.26	
	CL.V8.B	220.19	60.53	29.77	1801.53	396678.15	1123.70	0.002833	2832.78	3353.57	18.91	3369.91
	CL.V9.B	220.29	60.53	29.90	1809.70	398658.26	1124.80	0.002821	2821.46	3296.21	42.11	
	CL.V10.B	220.21	60.39	29.72	1794.34	395131.67	1122.30	0.002840	2840.32	3407.80	11.43	
	CL.V11.B	220.11	60.43	29.86	1804.44	397175.24	1126.20	0.002836	2835.52	3307.05	21.06	
	CL.V12.B	220.29	60.72	29.73	1805.06	397636.00	1125.90	0.002831	2831.48	3442.06	11.97	
	CL.V13.B	220.14	60.46	29.84	1803.82	397093.84	1124.40	0.002832	2831.57	3335.49	11.25	
	CL.V14.B	220.09	60.53	29.92	1810.91	398562.74	1129.10	0.002833	2832.93	3403.89	19.49	
	CL.V15.B	220.20	60.55	29.85	1807.42	397993.33	1128.50	0.002835	2835.47	3413.99	11.78	

Table 24: Pulse propagation of Classic Verso Prismatic Specimen.

Lithotype	Specimen	Length [mm]	Height [mm]	Width [mm]	Area [mm²]	Volume [mm³]	Weight [g]	Density [g/mm³]	[kg/m³]	Vp [m/s]	ds [m/s]	Average [m/s]
CLASSIC CONTRO	CL.C1.B	220.10	60.34	29.83	1799.79	396134.45	1123.10	0.002835	2835.15	4743.75	36.15	
	CL.C2.B	220.11	60.48	29.83	1803.82	397037.94	1126.50	0.002837	2837.26	4859.04	24.14	
	CL.C3.B	220.21	60.37	29.87	1802.80	396994.75	1125.00	0.002834	2833.79	4808.17	23.63	
	CL.C4.B	220.25	60.22	29.82	1795.76	395516.23	1121.80	0.002836	2836.29	4830.42	47.73	4780.28
	CL.C5.B	220.33	60.15	29.92	1799.24	396426.04	1119.90	0.002825	2824.99	4853.08	0.00	
	CL.C6.B	220.09	60.43	30.15	1821.96	400996.17	1137.90	0.002838	2837.68	4731.48	48.38	
	CL.C7.B	220.09	60.23	30.58	1841.83	405369.11	1142.10	0.002817	2817.43	4655.18	29.01	
	CL.C8.B	220.05	60.52	30.31	1834.06	403584.59	1143.90	0.002834	2834.35	4761.13	35.15	

Table 25: Pulse propagation of Classic Contro Prismatic Specimen.

Lithotype	Specimen	Length [mm]	Height [mm]	Width [mm]	Area [mm²]	Volume [mm³]	Weight [g]	Density [g/mm³]	[kg/m³]	Vp [m/s]	ds [m/s]	Average [m/s]
BLUE VERSO	BL.V1.B	219.49	60.42	29.95	1809.43	397151.63	1124.00	0.002830	2830.15	3237.34	10.72	
	BL.V2.B	219.35	60.44	30.07	1817.13	398587.16	1131.20	0.002838	2838.02	3201.38	22.23	
	BL.V3.B	219.40	60.53	30.11	1822.41	399836.26	1132.20	0.002832	2831.66	3218.97	17.49	
	BL.V4.B	219.34	60.46	29.88	1806.54	396247.54	1124.20	0.002837	2837.12	3220.89	12.93	
	BL.V5.B	219.40	60.48	29.92	1809.41	396984.99	1120.90	0.002824	2823.53	3120.94	9.97	
	BL.V6.B	219.39	60.38	29.83	1801.14	395151.10	1119.00	0.002832	2831.83	3076.21	17.37	
	BL.V7.B	219.42	60.21	30.05	1808.86	396899.89	1125.20	0.002835	2834.97	3030.66	0.00	
	BL.V8.B	219.41	60.50	29.78	1801.69	395308.80	1120.70	0.002835	2835.00	3116.62	0.00	
	BL.V9.B	219.41	60.56	30.00	1816.50	398557.65	1130.50	0.002836	2836.48	3090.31	9.69	
	BL.V10.B	219.31	60.57	29.76	1802.11	395221.09	1120.80	0.002836	2835.88	3155.62	7.25	
	BL.V11.B	219.39	60.59	30.02	1818.76	399018.13	1128.90	0.002829	2829.19	3170.42	12.57	
	BL.V12.B	219.39	60.47	29.95	1810.77	397265.74	1124.40	0.002830	2830.35	3120.79	9.97	
	BL.V13.B	219.40	60.27	29.98	1806.44	396333.68	1124.60	0.002838	2837.51	3149.66	16.75	3136.74
	BL.V14.B	219.40	60.53	29.93	1811.51	397446.01	1126.80	0.002835	2835.10	3167.84	16.04	
	BL.V15.B	219.42	60.00	29.77	1786.05	391895.34	1110.20	0.002833	2832.90	3022.35	11.39	
	BL.V16.B	219.41	60.50	29.80	1802.90	395574.29	1127.70	0.002851	2850.79	3172.57	16.99	
	BL.V17.B	219.40	60.23	29.90	1800.43	395013.55	1120.10	0.002836	2835.60	3174.25	15.96	
	BL.V18.B	219.40	60.12	30.04	1805.55	396138.55	1122.70	0.002834	2834.11	3094.50	0.00	
	BL.V19.B	219.39	60.25	29.77	1793.34	393441.14	1115.80	0.002836	2836.00	3054.76	12.56	
	BL.V20.B	219.38	60.29	30.02	1809.76	397024.21	1127.20	0.002839	2839.12	3081.22	11.87	
	BL.V21.B	219.37	60.23	30.01	1807.05	396412.81	1122.10	0.002831	2830.64	3144.66	9.90	
	BL.V22.B	219.40	60.31	29.56	1782.31	391039.75	1116.40	0.002855	2854.95	3133.43	11.95	
	BL.V23.B	219.39	60.23	29.94	1802.99	395556.89	1119.20	0.002829	2829.43	3144.09	16.60	
	BL.V24.B	219.41	60.33	29.98	1808.54	396812.53	1122.30	0.002828	2828.29	3134.45	9.97	
	BL.V25.B	219.41	60.67	29.83	1809.48	397018.61	1129.00	0.002844	2843.70	3184.47	0.00	

Table 26: Pulse propagation of Blue Verso Prismatic Specimen.

Lithotype	Specimen	Length [mm]	Height [mm]	Width [mm]	Area [mm²]	Volume [mm³]	Weight [g]	Density [g/mm³]	[kg/m³]	Vp [m/s]	ds [m/s]	Average [m/s]
BLUE CONTRO	BL.C1.B	220.30	59.76	29.98	1791.60	394690.54	1109.40	0.002811	2810.81	4616.82	42.25	
	BL.C2.B	220.29	60.59	29.74	1801.80	396918.06	1122.40	0.002828	2827.79	4697.01	0.00	
	BL.C3.B	220.29	59.92	29.26	1752.81	386127.25	1090.00	0.002823	2822.90	4545.84	12.54	
	BL.C4.B	220.28	62.35	29.62	1846.81	406814.65	1152.30	0.002832	2832.49	4527.13	34.41	
	BL.C5.B	220.29	60.27	29.53	1779.47	391999.83	1106.10	0.002822	2821.68	4495.79	20.39	4543.76
	BL.C6.B	220.30	60.39	28.65	1730.17	381157.22	1072.80	0.002815	2814.59	4561.16	21.25	
	BL.C7.B	220.30	60.34	29.44	1776.41	391343.03	1087.00	0.002778	2777.61	4485.60	61.29	
	BL.C8.B	220.29	61.53	29.78	1832.21	403618.53	1133.70	0.002809	2808.84	4545.99	31.75	
	BL.C9.B	220.30	60.71	29.91	1815.84	400028.69	1128.40	0.002821	2820.80	4418.49	25.62	

Table 27: Pulse propagation of Blue Contro Prismatic Specimen.

Lithotype	Specimen	Length [mm]	Height [mm]	Width [mm]	Area [mm²]	Volume [mm³]	Weight [g]	Density [g/mm³]	Density [kg/m³]	Vp [m/s]	ds [m/s]	Average [m/s]
BROWN VERSO	BR.V1.B	220.15	60.36	29.81	1798.88	396023.60	1123.60	0.002837	2837.20	4948.05	73.60	
	BR.V2.B	220.18	60.42	29.85	1803.39	397069.91	1124.90	0.002833	2833.00	4948.73	73.61	
	BR.V3.B	220.09	59.66	29.83	1779.51	391652.06	1111.40	0.002838	2837.72	4957.23	39.48	
	BR.V4.B	220.17	60.08	29.91	1796.99	395643.90	1118.50	0.002827	2827.04	4986.53	70.25	
	BR.V5.B	220.05	60.25	29.82	1796.35	395287.64	1121.50	0.002837	2837.17	4961.63	81.87	
	BR.V6.B	220.19	59.93	29.94	1794.30	395087.84	1118.70	0.002832	2831.52	4902.28	52.73	
	BR.V7.B	220.20	60.52	29.98	1814.09	399461.96	1128.70	0.002826	2825.55	4872.30	61.65	
	BR.V8.B	220.12	60.18	29.89	1798.63	395914.60	1119.80	0.002828	2828.39	4907.99	83.70	
	BR.V9.B	220.21	60.39	29.83	1801.43	396693.72	1123.10	0.002831	2831.15	4948.89	46.66	4940.51
	BR.V10.B	220.31	60.39	29.78	1798.27	396175.83	1123.60	0.002836	2836.11	4955.68	51.75	
	BR.V11.B	220.19	60.41	29.90	1806.26	397720.17	1127.00	0.002834	2833.65	4919.83	54.48	
	BR.V12.B	220.15	60.20	29.97	1803.89	397127.04	1123.00	0.002828	2827.81	4923.87	78.81	
	BR.V13.B	220.05	62.85	29.81	1873.56	412276.55	1167.40	0.002832	2831.59	4979.92	30.21	
	BR.V14.B	220.15	63.28	29.81	1885.91	415183.39	1173.60	0.002827	2826.70	4947.29	24.69	
	BR.V15.B	220.03	60.53	29.87	1807.88	397788.22	1124.90	0.002828	2827.89	4911.48	24.68	
	BR.V16.B	220.19	60.38	29.87	1803.40	397090.92	1125.50	0.002834	2834.36	4931.27	74.55	
	BR.V17.B	220.11	60.26	29.82	1796.95	395527.37	1123.20	0.002840	2839.75	4980.27	50.01	
	BR.V18.B	220.08	63.29	29.90	1892.05	416403.37	1173.40	0.002818	2817.94	4945.97	46.63	

Table 28: Pulse propagation of Brown Verso Prismatic Specimen.

Lithotype	Specimen	Length [mm]	Height [mm]	Width [mm]	Area [mm²]	Volume [mm³]	Weight [g]	Density [g/mm³]	Density [kg/m³]	Vp [m/s]	ds [m/s]	Average [m/s]
BROWN CONTRO	BR.C1.B	220.00	60.57	29.42	1781.82	392000.91	1109.00	0.002829	2829.08	5656.63	87.94	
	BR.C2.B	220.00	60.24	29.21	1759.31	387048.02	1089.80	0.002816	2815.67	5567.23	54.30	
	BR.C3.B	220.00	60.56	29.35	1776.99	390937.02	1101.70	0.002818	2818.10	5790.04	63.96	5613.85
	BR.C4.B	220.00	60.57	29.49	1786.06	392933.61	1106.70	0.002817	2816.51	5531.23	75.38	
	BR.C5.B	220.00	62.37	29.93	1866.42	410612.90	1155.80	0.002815	2814.82	5582.18	93.89	
	BR.C6.B	220.00	60.39	29.02	1752.52	385553.92	1082.40	0.002807	2807.39	5555.77	38.33	

Table 29: Pulse propagation of Brown Contro Prismatic Specimen.

Lithotype	Specimen	Length [mm]	Height [mm]	Width [mm]	Area [mm²]	Volume [mm³]	Weight [g]	Density [g/mm³]	Density [kg/m³]	Vp [m/s]	ds [m/s]	Average [m/s]
BLACK VERSO	BK.V1.B	219.14	60.41	30.11	1818.95	398603.63	1162.30	0.002916	2915.93	3145.03	17.88	
	BK.V2.B	218.93	60.63	30.17	1829.06	400435.28	1138.70	0.002844	2843.66	3066.25	0.00	
	BK.V3.B	219.00	60.45	30.14	1821.51	398910.71	1158.60	0.002904	2904.41	3071.55	9.67	
	BK.V4.B	220.00	60.59	30.34	1838.15	404392.76	1170.60	0.002895	2894.71	3089.92	11.90	
	BK.V5.B	218.80	60.39	29.97	1809.74	395970.77	1157.90	0.002924	2924.21	3080.92	19.28	
	BK.V6.B	219.71	60.88	30.16	1835.84	403351.62	1170.50	0.002902	2901.93	3078.94	12.46	
	BK.V7.B	220.00	60.55	30.33	1836.03	403925.97	1183.10	0.002929	2929.00	3244.94	19.98	
	BK.V8.B	220.00	60.49	30.08	1819.09	400199.00	1170.90	0.002926	2925.79	3129.53	18.59	
	BK.V9.B	220.00	61.06	29.96	1829.36	402458.67	1166.80	0.002899	2899.18	3059.86	15.05	
	BK.V10.B	218.70	60.59	29.88	1810.13	395874.61	1149.90	0.002905	2904.71	3128.82	15.83	
	BK.V11.B	220.01	60.29	29.97	1806.44	397434.87	1181.80	0.002974	2973.57	3185.81	10.60	3106.04
	BK.V12.B	219.38	60.46	30.07	1817.88	398806.92	1167.90	0.002928	2928.48	3174.86	12.56	
	BK.V13.B	219.68	60.33	30.35	1830.86	402204.15	1182.20	0.002939	2939.30	3207.03	10.42	
	BK.V14.B	219.21	60.30	30.15	1817.74	398467.55	1168.60	0.002933	2932.74	3209.61	19.62	
	BK.V15.B	219.59	60.39	30.36	1832.99	402505.54	1160.90	0.002884	2884.18	3101.58	9.84	
	BK.V16.B	218.31	60.57	29.96	1814.53	396129.48	1158.00	0.002923	2923.29	2899.38	25.17	
	BK.V17.B	218.34	60.71	30.29	1838.75	401473.65	1150.20	0.002865	2864.95	3107.83	29.57	
	BK.V18.B	219.42	60.38	30.10	1817.44	398782.25	1163.90	0.002919	2918.64	3181.96	21.46	
	BK.V19.B	218.41	60.78	30.06	1826.90	399012.46	1147.70	0.002876	2876.35	2906.20	61.12	
	BK.V20.B	219.02	60.45	30.08	1818.03	398185.75	1169.60	0.002937	2937.32	3084.81	9.67	
	BK.V21.B	219.33	60.52	30.10	1821.35	399476.56	1156.30	0.002895	2894.54	3071.91	15.21	

Table 30: Pulse propagation of Black Verso Prismatic Specimen.

Lithotype	Specimen	Length [mm]	Height [mm]	Width [mm]	Area [mm²]	Volume [mm³]	Weight [g]	Density [g/mm³]	Density [kg/m³]	Vp [m/s]	ds [m/s]	Average [m/s]
BLACK CONTRO	BK.C1.B	220.20	60.31	30.08	1813.97	399437.16	1154.70	0.002891	2890.82	4676.98	155.51	
	BK.C2.B	220.19	60.75	29.99	1821.59	401095.63	1154.60	0.002879	2878.62	4988.73	42.19	
	BK.C3.B	220.20	60.85	30.07	1829.46	402846.05	1182.80	0.002936	2936.11	5206.37	67.10	4963.54
	BK.C4.B	220.11	60.33	29.90	1803.42	396949.87	1130.40	0.002848	2847.71	4980.78	75.49	
	BK.C5.B	220.21	60.94	29.94	1824.54	401782.75	1178.20	0.002932	2932.43	4746.56	61.98	
	BK.C6.B	220.21	60.42	29.99	1811.54	398920.05	1165.70	0.002922	2922.14	5181.81	51.16	

Table 31: Pulse propagation of Black Contro Prismatic Specimen.

7.2 Pulse propagation of the cylindric specimens:

Lithotype	Specimen	Diameter [mm]	Height [mm]	Area [mm2]	Volume [mm³]	Weight [g]	Density [g/mm³]	[kg/m³]	Vp [m/s]	ds (each specimen)	Average [m/s]	ds (all specimens)	Vs [m/s]	ds (each specimen)	Average [m/s]	ds (all)	Vp/Vs [m/s]
CLASSIC VERSO	CL.V1.C	53.81	119.93	2274.13	272729.19	772.9	0.002834	2833.9	3639	6		143	2210	10		110	1.6
	CL.V2.C	53.80	120.33	2273.01	273518.41	773.7	0.002829	2828.7	3770	5		143	2267	37		110	1.7
	CL.V3.C	53.80	119.97	2273.01	272700.13	774.1	0.002839	2838.6	3728	15		143	2287	12		110	1.6
	CL.V4.C	53.80	120.05	2273.43	272917.54	774.6	0.002838	2838.2	3908	14		143	2112	9		110	1.9
	CL.V5.C	53.82	119.93	2274.84	272828.84	773.7	0.002836	2835.8	3803	16		143	2174	3		110	1.7
	CL.V6.C	53.82	119.97	2275.12	272953.64	775.0	0.002839	2839.3	3401	6		143	2180	21		110	1.6
	CL.V7.C	53.82	120.01	2274.84	272995.66	775.5	0.002841	2840.7	3489	16	3641	143	2299	46	2277	110	1.5
	CL.V8.C	53.77	119.99	2270.89	272477.01	772.6	0.002835	2835.5	3645	5		143	2216	16		110	1.6
	CL.V9.C	53.71	119.95	2265.83	271793.75	774.1	0.002848	2848.1	3698	6		143	2217	16		110	1.7
	CL.V10.C	53.83	119.92	2275.40	272866.10	773.4	0.002834	2834.4	3641	6		143	2505	37		110	1.5
	CL.V11.C	53.84	120.01	2276.81	273247.61	775.1	0.002837	2836.6	3479	14		143	2415	10		110	1.4
	CL.V12.C	53.80	120.02	2273.43	272856.91	775.0	0.002840	2840.3	3538	5		143	2321	4		110	1.5
	CL.V13.C	53.78	120.03	2271.60	272652.34	774.6	0.002841	2841.0	3596	18		143	2391	6		110	1.5

Table 32: Pulse propagation of Classic Verso Cylindric Specimen.

Lithotype	Specimen	Diameter [mm]	Height [mm]	Area [mm2]	Volume [mm³]	Weight [g]	Density [g/mm³]	[kg/m³]	Vp [m/s]	ds (each specimen)	Average [m/s]	ds (all specimens)	Vs [m/s]	ds (each specimen)	Average [m/s]	ds (all)	Vp/Vs [m/s]
CLASSIC CONTRO	CL.C1.C	53.77	120.17	2270.61	272851.94	775.9	0.002844	2843.7	4873	23		16	2737	12		155	1.8
	CL.C2.C	53.71	120.07	2265.41	271999.89	772.8	0.002841	2841.2	4841	14	4856	16	2468	15	2647	155	2.0
	CL.C3.C	53.84	120.09	2276.81	273429.75	775.2	0.002835	2835.1	4854	11		16	2734	6		155	1.8

Table 33: Pulse propagation of Classic Contro Cylindric Specimen.

Lithotype	Specimen	Diameter [mm]	Height [mm]	Area [mm2]	Volume [mm³]	Weight [g]	Density [g/mm³]	Density [kg/m³]	Vp [m/s]	ds (each specimen)	Average [m/s]	ds (all specimens)	Vs [m/s]	ds (each specimen)	Average [m/s]	ds (all)	Vp/Vs [m/s]
BLUE VERSO	BL.V1.C	53.82	119.99	2274.56	272931.52	772.7	0.002831	2831.1	4190	13		95	2680	5		105	1.6
	BL.V2.C	53.80	119.73	2273.15	272156.31	772.1	0.002837	2837.0	4100	20		95	2604	6		105	1.6
	BL.V3.C	53.78	120.05	2271.18	272647.06	771.2	0.002829	2828.6	4134	8		95	2508	41		105	1.6
	BL.V4.C	53.75	120.03	2269.35	272382.01	772.2	0.002835	2835.0	4229	16		95	2640	20		105	1.6
	BL.V5.C	53.78	120.01	2271.46	272605.15	772.4	0.002833	2833.4	4150	6	4132	95	2607	27	2632	105	1.6
	BL.V6.C	53.81	119.91	2273.71	272648.20	772.1	0.002832	2831.9	4124	18		95	2599	23		105	1.6
	BL.V7.C	53.79	119.92	2272.02	272460.69	772.4	0.002835	2834.9	4220	7		95	2608	23		105	1.6
	BL.V8.C	53.83	119.65	2275.96	272326.77	771.5	0.002833	2833.0	3923	9		95	2625	7		105	1.5
	BL.V9.C	53.81	119.96	2273.71	272754.30	772.5	0.002832	2832.2	4160	13		95	2922	8		105	1.4
	BL.V10.C	53.84	119.81	2276.39	272741.58	771.8	0.002830	2829.8	4002	7		95	2583	5		105	1.5
	BL.V11.C	53.81	119.81	2274.13	272471.46	772.2	0.002834	2834.1	4216	27		95	2577	75		105	1.6

Table 34: Pulse propagation of Blue Verso Cylindric Specimen.

Lithotype	Specimen	Diameter [mm]	Height [mm]	Area [mm2]	Volume [mm³]	Weight [g]	Density [g/mm³]	Density [kg/m³]	Vp [m/s]	ds (each specimen)	Average [m/s]	ds (all specimens)	Vs [m/s]	ds (each specimen)	Average [m/s]	ds (all)	Vp/Vs [m/s]
BLUE CONTRO	BL.C1.C	53.78	120.39	2271.46	273453.16	775.3	0.002835	2835.2	4620	20		31	2682	7		113	1.7
	BL.C2.C	53.81	120.43	2274.27	273883.23	775.7	0.002832	2832.2	4607	20	4598	31	2681	7	2587	113	1.7
	BL.C3.C	53.72	120.19	2266.67	272438.96	774.3	0.002842	2842.1	4612	27		31	2531	21		113	1.8
	BL.C4.C	53.81	120.15	2274.13	273229.50	775.6	0.002839	2838.6	4551	12		31	2455	16		113	1.9

Table 35: Pulse propagation of Blue Contro Cylindric Specimen.

Lithotype	Specimen	Diameter [mm]	Height [mm]	Area [mm2]	Volume [mm³]	Weight [g]	Density [g/mm³]	Density [kg/m³]	Vp [m/s]	ds (each specimen)	Average [m/s]	ds (all specimens)	Vs [m/s]	ds (each specimen)	Average [m/s]	ds (all)	Vp/Vs [m/s]
BROWN VERSO	BR.V1.C	53.70	118.39	2264.84	268142.53	760.7	0.002837	2836.9	4979	23	4927	70	2866	38	2828	78	1.7
	BR.V2.C	53.71	118.46	2265.55	268376.79	760.7	0.002834	2834.4	4875	37		70	2840	33		78	1.7
	BR.V3.C	53.70	118.46	2265.13	268326.83	758.4	0.002826	2826.4	4774	79		70	2831	47		78	1.7
	BR.V4.C	53.54	118.45	2251.37	266667.11	757.3	0.002840	2839.9	4944	18		70	2669	43		78	1.9
	BR.V5.C	53.65	118.41	2260.35	267655.38	758.9	0.002835	2835.4	4934	21		70	2854	24		78	1.7
	BR.V6.C	53.65	118.47	2260.63	267809.21	759.4	0.002836	2835.6	4949	11		70	2857	10		78	1.7
	BR.V7.C	53.74	118.43	2268.22	268617.75	760.1	0.002830	2829.7	4939	23		70	2827	34		78	1.7
	BR.V8.C	53.62	118.39	2257.82	267310.95	759.2	0.002840	2840.1	4929	37		70	2860	12		78	1.7
	BR.V9.C	53.68	118.51	2262.88	268181.10	760.4	0.002835	2835.4	4950	18		70	2825	20		78	1.8
	BR.V10.C	53.53	118.51	2250.67	266719.15	757.9	0.002842	2841.6	4845	18		70	2680	17		78	1.8
	BR.V11.C	53.70	121.33	2264.42	274750.00	758.9	0.002762	2762.1	4944	18		70	2934	19		78	1.7
	BR.V12.C	53.73	118.55	2267.38	268804.99	761.9	0.002834	2834.4	5058	12		70	2892	43		78	1.7

Table 36: Pulse propagation of Brown Verso Cylindric Specimen.

Lithotype	Specimen	Diameter [mm]	Height [mm]	Area [mm2]	Volume [mm³]	Weight [g]	Density [g/mm³]	Density [kg/m³]	Vp [m/s]	ds (each specimen)	Average [m/s]	ds (all specimens)	Vs [m/s]	ds (each specimen)	Average [m/s]	ds (all)	Vp/Vs [m/s]
BROWN CONTRO	BR.C1.C	53.64	120.17	2259.65	271534.14	772.6	0.002845	2845.3	5873	26	5886	123	3339	9	3151	216	1.8
	BR.C2.C	53.68	120.19	2262.74	271950.76	774.7	0.002849	2848.7	5880	16		123	3241	15		216	1.8
	BR.C3.C	53.67	120.19	2262.03	271881.40	770.1	0.002832	2832.5	6046	33		123	2843	103		216	2.1
	BR.C4.C	53.81	120.55	2274.27	274171.30	773	0.002819	2819.4	5745	12		123	3181	10		216	1.8

Table 37: Pulse propagation of Brown Contro Cylindric Specimen.

Lithotype	Specimen	Diameter [mm]	Height [mm]	Area [mm2]	Volume [mm³]	Weight [g]	Density [g/mm³]	Density [kg/m³]	Vp [m/s]	ds (each specimen)	Average [m/s]	ds (all specimens)	Vs [m/s]	ds (each specimen)	Average [m/s]	ds (all)	Vp/Vs [m/s]
BLACK VERSO	BK.V1.C	53.77	119.947	2270.47	272335.52	785.7	0.002885	2885.0	3892	45		248	2672	36		116	1.5
	BK.V2.C	53.76	120.037	2269.63	272438.49	779.5	0.002861	2861.2	3206	22		248	2410	80		116	1.3
	BK.V3.C	53.82	119.933	2274.70	272811.94	796.1	0.002918	2918.1	3479	36		248	2430	8		116	1.4
	BK.V4.C	53.73	119.977	2267.24	272015.35	785.6	0.002888	2888.1	3395	19		248	2376	24		116	1.4
	BK.V5.C	53.75	120.003	2269.35	272329.06	775.8	0.002849	2848.8	3538	5		248	2292	14		116	1.5
	BK.V6.C	53.81	119.907	2273.99	272666.82	789.6	0.002896	2895.8	3237	32		248	2391	11		116	1.4
	BK.V7.C	53.82	119.940	2275.12	272877.80	811.2	0.002973	2972.8	3607	41	3337	248	2469	37	2371	116	1.5
	BK.V8.C	53.80	120.033	2273.15	272853.41	778.5	0.002853	2853.2	3374	29		248	2284	10		116	1.5
	BK.V9.C	53.74	120.050	2268.08	272282.94	784.4	0.002881	2880.8	3193	17		248	2227	32		116	1.4
	BK.V10.C	53.76	120.000	2270.05	272405.94	781.2	0.002868	2867.8	3205	17		248	2276	28		116	1.4
	BK.V11.C	53.83	119.927	2275.96	272948.87	782.4	0.002866	2866.5	3033	18		248	2437	14		116	1.2
	BK.V12.C	53.79	120.010	2272.72	272749.67	779.1	0.002856	2856.5	3469	27		248	2242	6		116	1.5
	BK.V13.C	53.76	119.960	2270.19	272332.02	791.4	0.002906	2906.0	3121	26		248	2377	41		116	1.3
	BK.V14.C	53.80	119.997	2272.87	272736.26	797.5	0.002924	2924.1	2976	20		248	2313	7		116	1.3

Table 38: Pulse propagation of Black Verso Cylindric Specimen.

Lithotype	Specimen	Diameter [mm]	Height [mm]	Area [mm2]	Volume [mm³]	Weight [g]	Density [g/mm³]	Density [kg/m³]	Vp [m/s]	ds (each specimen)	Average [m/s]	ds (all specimens)	Vs [m/s]	ds (each specimen)	Average [m/s]	ds (all)	Vp/Vs [m/s]
BLACK CONTRO	BK.C1.C	53.59	120.427	2255.58	271631.46	787.6	0.002900	2899.5	5371	11		194	2997	19		313	1.8
	BK.C2.C	53.65	120.680	2260.91	272846.63	781.3	0.002864	2863.5	5378	13	5263	194	2375	29	2666	313	2.3
	BK.C3.C	53.75	120.620	2269.35	273728.49	780	0.002850	2849.5	5038	12		194	2626	97		313	1.9

Table 39: Pulse propagation of Black Contro Cylindric Specimen.

7.3 Elastic parameters results

Lithotype	Specimen	K [GPa]	E [GPa]	G [GPa]	λ [GPa]	ν [---]
CLASSICO VERSO	CL.V1.C	19.1	33.4	13.8	9.8	0.21
	CL.V2.C	20.8	35.4	14.5	11.1	0.22
	CL.V3.C	19.7	35.6	14.8	9.8	0.20
	CL.V4.C	26.5	32.8	12.7	18.0	0.29
	CL.V5.C	23.1	33.7	13.4	14.2	0.26
	CL.V6.C	14.9	31.1	13.5	5.9	0.15
	CL.V7.C	14.6	33.5	15.0	4.5	0.12
	CL.V8.C	19.1	33.6	13.9	9.8	0.21
	CL.V9.C	20.3	34.1	14.0	10.9	0.22
	CL.V10.C	13.9	37.4	17.8	2.0	0.05
	CL.V11.C	12.3	34.2	16.5	1.2	0.03
	CL.V12.C	15.2	34.3	15.3	5.0	0.12
	CL.V13.C	15.1	35.9	16.2	4.2	0.10

Table 40: Elastic parameters of the Classic Cylindric verso specimen

Lithotype	Specimen	K [GPa]	E [GPa]	G [GPa]	λ [GPa]	ν [---]
CLASSIC CONTRO	CL.C1.C	39.1	54.1	21.3	24.9	0.27
	CL.C2.C	43.5	45.8	17.3	32.0	0.32
	CL.C3.C	38.5	53.7	21.2	24.4	0.27

Table 41: Elastic parameters of the Classic Cylindric Contro Specimen

Lithotype	Specimen	K [GPa]	E [GPa]	G [GPa]	λ [GPa]	ν [---]
BLUE VERSO	BL.V1.C	22.6	46.9	20.3	9.0	0.15
	BL.V2.C	22.0	44.7	19.2	9.2	0.16
	BL.V3.C	24.6	43.0	17.8	12.7	0.21
	BL.V4.C	24.4	46.7	19.8	11.2	0.18
	BL.V5.C	23.1	45.2	19.3	10.3	0.17
	BL.V6.C	22.6	44.8	19.1	9.9	0.17
	BL.V7.C	24.8	45.9	19.3	11.9	0.19
	BL.V8.C	17.6	42.7	19.5	4.6	0.09
	BL.V9.C	16.8	49.0	24.2	0.6	0.01
	BL.V10.C	20.1	43.2	18.9	7.5	0.14
	BL.V11.C	25.3	45.2	18.8	12.7	0.20

Table 42: Elastic parameters of the Blue Cylindric Verso Specimen

Lithotype	Specimen	K [GPa]	E [GPa]	G [GPa]	λ [GPa]	ν [---]
BLUE CONTRO	BL.C1.C	33.3	50.8	20.4	19.7	0.25
	BL.C2.C	33.0	50.6	20.4	19.4	0.24
	BL.C3.C	36.2	46.8	18.2	24.0	0.28
	BL.C4.C	36.0	44.3	17.1	24.6	0.29

Table 43: Elastic parameters of the Blue Cylindric Contro Specimen

Lithotype	Specimen	K [GPa]	E [GPa]	G [GPa]	λ [GPa]	ν [---]
BROWNE VERSO	BR.V1.C	39.2	58.4	23.3	23.7	0.25
	BR.V2.C	36.9	56.9	22.9	21.6	0.24
	BR.V3.C	34.2	55.7	22.6	19.1	0.23
	BR.V4.C	42.4	52.4	20.2	28.9	0.29
	BR.V5.C	38.2	57.7	23.1	22.8	0.25
	BR.V6.C	38.6	57.9	23.1	23.2	0.25
	BR.V7.C	38.9	56.8	22.6	23.8	0.26
	BR.V8.C	38.0	57.9	23.2	22.5	0.25
	BR.V9.C	39.3	56.9	22.6	24.2	0.26
	BR.V10.C	39.5	52.2	20.4	25.9	0.28
	BR.V11.C	35.8	58.4	23.8	20.0	0.23
	BR.V12.C	40.9	59.6	23.7	25.1	0.26

Table 44: Elastic parameters of the Brown Cylindric Verso Specimen

Lithotype	Specimen	K [GPa]	E [GPa]	G [GPa]	λ [GPa]	ν [---]
BROWN CONTRO	BR.C1.C	55.9	80.0	31.7	34.7	0.26
	BR.C2.C	58.6	76.7	29.9	38.6	0.28
	BR.C3.C	73.0	62.2	22.9	57.8	0.36
	BR.C4.C	55.0	73.0	28.5	36.0	0.28

Table 45: Elastic parameters of the Brown Cylindric Contro Specimen

Lithotype	Specimen	K [GPa]	E [GPa]	G [GPa]	λ [GPa]	ν [---]
BLACK VERSO	BK.V1.C	16.2	43.4	20.6	2.5	0.05
	BK.V2.C	7.3	28.3	16.6	-3.8	-0.15
	BK.V3.C	12.3	35.3	17.2	0.9	0.02
	BK.V4.C	11.5	33.3	16.3	0.7	0.02
	BK.V5.C	15.7	34.1	15.0	5.7	0.14
	BK.V6.C	8.3	29.8	16.6	-2.8	-0.10
	BK.V7.C	14.5	38.4	18.1	2.4	0.06
	BK.V8.C	12.6	32.1	14.9	2.7	0.08
	BK.V9.C	10.3	29.3	14.3	0.8	0.03
	BK.V10.C	9.6	29.5	14.9	-0.3	-0.01
	BK.V11.C	3.7	20.1	17.0	-7.7	-0.41
	BK.V12.C	15.2	32.8	14.4	5.7	0.14
	BK.V13.C	6.4	26.6	16.4	-4.5	-0.19
	BK.V14.C	5.1	23.1	15.6	-5.4	-0.26

Table 46: Elastic parameters of the Black Cylindric Verso Specimen

Lithotype	Specimen	K [GPa]	E [GPa]	G [GPa]	λ [GPa]	ν [---]
BLACK CONTRO	BK.C1.C	48.9	66.4	26.0	31.6	0.27
	BK.C2.C	61.3	44.6	16.2	50.5	0.38
	BK.C3.C	46.1	51.6	19.6	33.0	0.31

Table 47: Elastic parameters of the Black Cylindric Contro Specimen.

7.4 Pulse propagation if cubical specimens

Lithotype	Specimen	Direction [mm]	Height [mm]	Area [mm2]	Volume [mm³]	Weight [g]	Density [g/mm³]	[kg/m³]	Vp [m/s]	d.s.	Vs1 [m/s]	d.s. [m/s]	Vp/Vs	Vs1 [m/s]	d.s. [m/s]	Vs2 [m/s]	d.s. [m/s]
CLASSIC	CL.CU1.X	Contro	150.22	22577.30	3391450	9645.1	0.002844	2843.9	4304	0	2639	18	1.6	2632	13	2646	21
	CL.CU1.Y	Contro	150.15	22587.83	3391450	9645.1	0.002844	2843.9	4355	6	2529	136	1.7	2401	11	2657	12
	CL.CU1.Z	Verso	150.37	22554.03	3391450	9645.1	0.002844	2843.9	3527	27	2388	9	1.5	2385	10	2391	8

Table 48: Pulse propagation of Classic Cylindric Specimen.

Lithotype	Specimen	Direction [mm]	Height [mm]	Area [mm2]	Volume [mm³]	Weight [g]	Density [g/mm³]	[kg/m³]	Vp [m/s]	d.s.	Vs1 [m/s]	d.s. [m/s]	Vp/Vs	Vs1 [m/s]	d.s. [m/s]	Vs2 [m/s]	d.s. [m/s]
BLUE	BL.CU1.X	Contro	150.33	22489.50	3380734.27	9621.5	0.002846	2846.0	5385	9	3364	13	1.6	3375	4	3352	4
	BL.CU1.Y	Contro	149.96	22544.24	3380734.27	9621.5	0.002846	2846.0	5185	8	3139	135	1.7	3011	4	3267	5
	BL.CU1.Z	Verso	149.97	22542.74	3380734.27	9621.5	0.002846	2846.0	5171	0	3192	90	1.6	3108	19	3276	3
	BL.CU2.X	Contro	150.29	21439.29	3222003.05	9151.5	0.002840	2840.3	5379	17	3367	40	1.6	3405	4	3329	4
	BL.CU2.Y	Contro	150.24	21446.42	3222003.05	9151.5	0.002840	2840.3	5198	0	3206	90	1.6	3121	6	3290	8
	BL.CU2.Z	Verso	142.71	22578.07	3222003.05	9151.5	0.002840	2840.3	4928	9	3060	62	1.6	3001	3	3119	4

Table 49: Pulse propagation of Blue Cylindric Specimen.

Lithotype	Specimen	Direction [mm]	Height [mm]	Area [mm2]	Volume [mm³]	Weight [g]	Density [g/mm³]	[kg/m³]	Vp [m/s]	d.s.	Vs1 [m/s]	d.s. [m/s]	Vp/Vs	Vs1 [m/s]	d.s. [m/s]	Vs2 [m/s]	d.s. [m/s]
BROWN	BR.CU1.X	Contro	150.36	22360.85	3362065.84	9552.4	0.002841	2841.2	5386	9	3364	13	1.6	3376	4	3353	4
	BR.CU1.Y	Contro	150.32	22366.06	3362065.84	9552.4	0.002841	2841.2	5198	8	3147	135	1.7	3018	4	3275	5
	BR.CU1.Z	Verso	148.76	22601.36	3362065.84	9552.4	0.002841	2841.2	5129	0	3169	86	1.6	3089	25	3249	3
	BR.CU2.X	Contro	150.36	22359.32	3361948.04	9541.7	0.002838	2838.1	5382	17	3369	40	1.6	3406	4	3331	4
	BR.CU2.Y	Contro	150.34	22363.04	3361948.04	9541.7	0.002838	2838.1	5202	0	3208	90	1.6	3123	6	3293	8
	BR.CU2.Z	Verso	148.73	22604.37	3361948.04	9541.7	0.002838	2838.1	5136	10	3189	65	1.6	3127	4	3250	4

Table 50: Pulse propagation of Brown Cylindric Specimen.

Lithotype	Specimen	Direction [mm]	Height [mm]	Area [mm2]	Volume [mm³]	Weight [g]	Density [g/mm³]	[kg/m³]	Vp [m/s]	d.s.	Vs1 [m/s]	d.s. [m/s]	Vp/Vs	Vs1 [m/s]	d.s. [m/s]	Vs2 [m/s]	d.s. [m/s]
BLACK	BK.CU1.X	Contro	150.180	22655.50	3402403.41	9981	0.002934	2933.5	5711	56	4583	101	1	4679	0	4488	18
	BK.CU1.Y	Contro	150.395	22623.12	3402403.41	9981	0.002934	2933.5	5457	30	3759	687	1	4410	0	3107	13
	BK.CU1.Z	Verso	150.640	22586.32	3402403.41	9981	0.002934	2933.5	3192	8	2452	42	1	2470	50	2435	26

Table 51: Pulse propagation of Black Cylindric Specimen.

7.5 Flexural strength

Lithotype	Specimen		#GD TEST	Force [N]	fcd [N/mm²]	load speed [kN/s]	support span [mm]	Length [mm]	Height [mm]	Width [mm]
CLASSICO	Verso	CL.V1.B	29	2.89	4.76	0.019	180	220.3	60.4	29.9
		CL.V9.B	--	1.90	3.12	0.018	180	220.29	60.5	29.9
		CL.V13.B	30	2.25	3.72	0.017	180	220.1	60.5	29.8
		CL.V14.B	31	2.61	4.29	0.012	180	220.1	60.5	29.9
		CL.V15.B	32	2.34	3.85	0.015	180	220.2	60.6	29.9
	Contro	CL.C3.B	33	9.40	15.55	0.017	180	220.2	60.4	29.9
		CL.C5.B	35	8.94	14.86	0.018	180	220.3	60.1	29.9
		CL.C6.B	34	9.84	16.09	0.016	180	220.1	60.4	30.2
BLUE	Verso	BL.V4.B	36	3.24	5.35	0.015	180	219.3	60.5	29.9
		BL.V6.B	--	3.04	5.04	0.021	180	219.4	60.4	29.8
		BL.V7.B	37	2.82	4.66	0.015	180	219.4	60.2	30.0
		BL.V8.B	38	2.72	4.49	0.015	180	219.4	60.5	29.8
		BL.V9.B	39	2.90	4.75	0.016	180	219.4	60.6	30.0
	Contro	BL.C6.B	40	6.22	10.71	0.017	180	220.3	60.4	28.7
		BL.C7.B	41	5.78	9.71	0.015	180	220.3	60.3	29.4
		BL.C9.B	42	6.03	9.84	0.018	180	220.3	60.7	29.9
BROWN	Verso	BR.V13.B	43	3.45	5.27	0.016	180	220.1	62.9	29.8
		BR.V14.B	44	4.00	6.04	0.018	180	220.2	63.3	29.8
		BR.V15.B	45	3.78	6.22	0.018	180	220.0	60.5	29.9
		BR.V16.B	46	3.29	5.44	0.017	180	220.2	60.4	29.9
		BR.V17.B	--	3.93	6.45	0.015	180	220.1	60.3	29.8
	Contro	BR.C1.B	47	8.99	15.26	0.019	180	220.0	60.2	29.2
		BR.C2.B	48	10.92	18.54	0.017	180	220.0	60.2	29.2
		BR.C3.B	49	9.95	16.64	0.019	180	220.0	60.6	29.3
BLACK	Verso	BK.V15.B	--	2.04	3.32	0.015	180	219.6	60.4	30.4
		BK.V18.B	50	3.36	5.51	0.013	180	219.4	60.4	30.1
		BK.V19.B	51	0.37	0.60	0.010	180	218.4	60.8	30.1
		BK.V20.B	52	2.50	4.09	0.014	180	219.0	60.5	30.1
		BK.V21.B	53	1.19	1.94	0.016	180	219.3	60.5	30.1
	Contro	BK.C4.B	54	6.22	10.29	0.019	180	220.1	60.3	29.9
		BK.C5.B	55	5.78	9.36	0.015	180	220.2	60.9	29.9
		BK.C6.B	56	6.03	9.92	0.017	180	220.2	60.4	30.0

Table 52: Results of the four-point bending test.

		Specimen		fcd	Average	d.s.		Relation
		Nomenclature	#	[N/mm²]	[N/mm²]	[N/mm²]	[%]	Contro/Verso
CLASSIC	Verso	CL.V9.B	1	4.76	3.95	0.62	15.6%	3.9
		CL.V1.B	2	3.12				
		CL.V13.B	3	3.72				
		CL.V14.B	4	4.29				
		CL.V15.B	5	3.85				
	Contro	CL.C3.B	1	15.55	15.50	0.62	4.0%	
		CL.C5.B	2	14.86				
		CL.C6.B	3	16.09				
BLUE	Verso	BL.V4.B	1	5.35	4.86	0.34	7.0%	2.1
		BL.V6.B	2	5.04				
		BL.V7.B	3	4.66				
		BL.V8.B	4	4.49				
		BL.V9.B	5	4.75				
	Contro	BL.C6.B	1	10.71	10.09	0.54	5.4%	
		BL.C7.B	2	9.71				
		BL.C9.B	3	9.84				
BROWN	Verso	BR.V13.B	1	5.27	5.88	0.51	8.6%	2.9
		BR.V14.B	2	6.04				
		BR.V15.B	3	6.22				
		BR.V16.B	4	5.44				
		BR.V17.B	5	6.45				
	Contro	BR.C1.B	1	15.26	16.81	1.65	9.8%	
		BR.C2.B	2	18.54				
		BR.C3.B	3	16.64				
BLACK	Verso	BK.V15.B	1	3.32	3.09	1.90	61.3%	3.2
		BK.V18.B	2	5.51				
		BK.V19.B	3	0.60				
		BK.V20.B	4	4.09				
		BK.V21.B	5	1.94				
	Contro	BK.C4.B	1	10.29	9.85	0.47	4.7%	
		BK.C5.B	2	9.36				
		BK.C6.B	3	9.92				

Table 53: Flexural resistance and standard deviation of the results.

7.6 Uniaxial compression test

| Lithotype | Specimen | | #GD TEST | Load speed | Uniaxial Compressive Strength | Young's Modulus | | Poisson's ratio | Height | Diameter | Area |
| | | | | | | Etan | Esec | υ | h | d | A |
				[kN/s]	[N/mm²]	[N/mm²]	[N/mm²]	[--]	[mm]	[mm]	[mm²]
Classico	Verso	CL.V2.C	1	2.25	109.2	47.2	39.2	0.22	118.9	53.7	2264.8
		CL.V9.C	2	2.10	102.6	47.0	42.7	0.27	118.7	53.7	2264.8
	Contro	CL.C1.C	3	2.40	175.7	73.1	60.9	0.21	118.1	53.7	2264.8
		CL.C2.C	4	2.80	168.3	80.0	57.7	0.19	118	53.7	2264.8
BLU	Verso	BL.V1.C	6	2.60	125.1	60.3	46.6	0.19	119.6	53.8	2273.3
		BL.V8.C	5	2.40	122.4	52.1	41.9	0.25	119.3	53.8	2273.3
	Contro	BL.C1.C	7	2.70	96.6	41.8	43.1	0.38	120.4	53.8	2273.3
		BL.C2.C	8	2.60	97.6	41.3	38.6	0.31	120.4	53.8	2273.3
BROWNE	Verso	BR.V1.C	9	2.80	104.5	56.4	58.0	0.26	117.3	53.7	2264.8
		BR.V12.C	10	2.60	114.4	58.6	58.9	0.26	117.7	53.7	2264.8
	Contro	BR.C1.C	11	3.00	118.2	58.3	67.3	0.28	119.7	53.7	2264.8
		BK.C3.C	12	2.50	86.8	75.5	76.3	0.21	119.8	53.7	2264.8
BLACK	Verso	BK.V7.C	13	2.60	82.2	33.0	23.0	0.08	119.6	53.8	2273.3
		BK.V9.C	14	2.50	110.7	42.0	29.0	0.08	118.7	53.8	2273.3
	Contro	BK.C1.C	15	2.50	118.2	58.3	43.5	0.08	120.3	53.8	2273.3
		BK.C3.C	16	2.70	68.1	39.6	44.5	0.12	119.9	53.8	2273.3

Table 54: Uniaxial compressive strength results.